



Universiteit  
Leiden  
The Netherlands

## Single-electrolyte isotachophoresis : on-chip analyte focusing and separation

Quist, J.W.

### Citation

Quist, J. W. (2014, March 20). *Single-electrolyte isotachophoresis : on-chip analyte focusing and separation*. Retrieved from <https://hdl.handle.net/1887/24857>

Version: Corrected Publisher's Version

License: [Licence agreement concerning inclusion of doctoral thesis in the Institutional Repository of the University of Leiden](#)

Downloaded from: <https://hdl.handle.net/1887/24857>

**Note:** To cite this publication please use the final published version (if applicable).

Cover Page



Universiteit Leiden



The handle <http://hdl.handle.net/1887/24857> holds various files of this Leiden University dissertation

**Author:** Quist, Johannis Willem

**Title:** Single-electrolyte isotachophoresis : on-chip analyte focusing and separation

**Issue Date:** 2014-03-20

# Single-Electrolyte Isotachophoresis

On-chip analyte focusing and separation

Proefschrift  
ter verkrijging van  
de graad van Doctor aan de Universiteit Leiden,  
op gezag van de Rector Magnificus prof.mr. C. J. J. M. Stolker,  
volgens besluit van het College voor Promoties  
te verdedigen op donderdag 20 maart 2014  
klokke 16:15 uur

door  
Johannis Willem Quist  
Geboren te Bergen op Zoom  
6 juli 1984

## **Promotiecomissie:**

### *Promotor:*

Prof. dr. Thomas Hankemeier

### *Co-promotores:*

Dr. Heiko van der Linden

Dr. Paul Vulto

### *Overige leden:*

Prof. dr. Juan Santiago (Stanford University)

Prof. dr. Hans Tanke (LUMC, Leiden)

Prof. dr. Ruud Berger (Universiteit Leiden)

Prof. dr. Meindert Danhof (Universiteit Leiden)

This study was financed by the research programme of the Netherlands Metabolomics Centre (NMC) which is a part of The Netherlands Genomics Initiative/Netherlands Organization for Scientific Research.

Single-electrolyte isotachophoresis: on-chip analyte focusing and separation

J.W. Quist

PhD thesis, Leiden University

ISBN/EAN: 978-90-74538-83-1

# Table of Contents

1.	General introduction	5
2.	Electric Field Gradient Focusing = Isotachophoresis: a Review	15
3.	Single-Electrolyte Isotachophoresis Using a Nanochannel-Induced Depletion Zone	53
4.	Tunable Ionic Mobility Filter for Depletion Zone Isotachophoresis	73
5.	PDMS Valves as Tunable Nanochannels for Concentration Polarization	95
6.	Conclusions and Perspectives	113
	Nederlandstalige samenvatting	117
	Dankwoord	123
	Curriculum Vitae	127
	Publicatielijst	128



# 1

## General Introduction

### **Challenges in metabolomics and the analysis of small samples**

The field of metabolomics aims at the comprehensive analyses of classes of metabolites and the understanding how these small molecules interact within biological systems. Two major goals of metabolomics research are 1) the discovery of novel biomarkers which are indicative for health and disease states and 2) obtaining insights into disease mechanisms and identification of possible pharmacological interventions. It can be expected that as a result of the biomarker research, metabolite fingerprints will serve as diagnostic assays for diagnosis, prognosis and choice of pharmacological interventions. The central paradigm of metabolomics in disease research is that certain metabolites or metabolite profiles are indicative for the progress of diseases like cancer. The discovery of such biomarkers and the development of clinically applicable assays would enable early diagnosis and treatment of such life-threatening diseases, significantly ameliorating the prospects for recovery.

Both for biomarker discovery and assay development, proper analytical methods are of crucial importance. Biomolecules and metabolites in particular have highly differing chemical structures, posing major challenges to analytical chemists. Especially when small sample volumes are used, conventional methods may have insufficient dynamic range, sensitivity, and/or separation power. Therefore new concepts in sample preparation and

separation are required. These issues appear to be most urgent in metabolomics because there are generally no amplification methods available (like PCR for genomics and transcriptomics research) nor common chemical structures (like peptide bonds, which are a common factor in all peptidomics and proteomics analyses). Nevertheless these -omics fields will also greatly benefit from novel analytical concepts as answer to these challenges.

The workhorses of bioanalytical laboratories usually include solid phase extraction (SPE), high performance liquid chromatography (HPLC) and gas chromatography (GC) instruments, often combined with mass spectrometry (MS). These techniques are extremely useful for the separation and detection of analytes in ultracomplex samples. However, they typically require microliters of sample, or a few hundred nanoliters at best. When dealing with small sample volumes, such as from a limited number of primary cells, small cells populations isolated from biopsies, only a single or a few analyses can be done with a single sample, forbidding repeated analysis and preventing the use of the sample for multiple tests. And in many cases the sensitivity will be not sufficient at all, as actually is currently for most methods for the analysis of individual cells.

A second disadvantage of these techniques is that they have only limited preconcentration capabilities. For example, in SPE preconcentration factors are in the order of 10-100, while biological concentrations of metabolites differ many orders of magnitude more. This limits the detectability of low-abundant compounds. It is very probable that currently many interesting biomarkers are going unnoticed through conventional analytical procedures, simply because detection limits may be orders of magnitude above biologically relevant concentrations and cannot be sufficiently improved.



## **The potential of electrokinetic methods**

With electrokinetic methods, it is possible to obtain enormous improvements with regard to these two limitations. When it concerns small sample volumes, capillary zone electrophoresis (CZE) and related methods are well-known to be able to handle sub-nanoliter volumes, especially when using narrow-bore capillaries or microfluidic channels. An impressive example is the analysis of the contents of a single cell<sup>1</sup>. In such picoliter-sized samples low numbers of copies of molecules are present and usually only the most abundant species are detected. With nanochannel CZE, femtoliter volumes of samples can be analyzed<sup>2, 3</sup>, though in practice such small volumes are only realistic if combined with inline sampling if one want to prevent significant; and maybe, the biggest problem one may encounter in such a case is adsorption at the surface of devices.

CZE is not as popular as HPLC, allegedly because it has inferior reproducibility and robustness. However, with proper expertise, CZE can be made as reproducible and robust as HPLC. Moreover, with CZE superior separation efficiency can be obtained, with plate numbers typically being around an order of magnitude higher than in HPLC.

An obvious limitation of CZE and other electrokinetic methods is that they can only separate charged compounds. Fortunately, the majority of metabolites and all peptides are or can be charged dependent on the pH, because acidic or basic groups are very common in biomolecules. For example, fatty acids, citric acid cycle products, molecules containing phosphate groups such as energy metabolism products and nucleic acids (including DNA and RNA), amino acids, peptides and proteins all include negatively charged moieties. Small ions also can be analyzed, as well as

positively charged molecules such as amines. A few classes of compounds remain which are not charged, including many sugars and sterols, but even for these neutral analytes there are interesting electrokinetic approaches, including micellar methods.

Concerning the detection of low-abundant compounds, CZE itself is not capable of preconcentration. Nevertheless there are numerous electrokinetic concentration methods which can easily be combined with CZE and which are able to achieve very impressive concentration factors: over thousandfold or even over millionfold<sup>4-12</sup>. Moreover, many of these methods can be used for selective trapping, which is extremely valuable when analysing low-abundant compounds in the presence of interfering molecules with much higher concentrations. Highly abundant matrix compounds, for example salts or albumin proteins can be discarded while concentrating the analytes of interest selectively. Such steps might be done inline, without the need for time- and sample-consuming pretreatment steps.

The approaches which result in up to or even over millionfold analyte trapping seem to fall within two classes: they are either isotachophoretic (ITP) or electric field gradient focusing (EFGF) techniques. This similarity is no coincidence according to the research presented in this thesis. In the subsequent chapters it will be argued and demonstrated that EFGF and ITP share many principles and phenomena.

## **Concepts of isotachopheresis (ITP), electric field gradient focusing (EFGF) and concentration polarisation (CP).**

ITP and EFGF are two central concepts in this thesis. These concepts will be introduced extensively in chapter 2, but for the reader unfamiliar with these methods a brief overview will be given here.

In EFGF, analytes are focused and separated along an electric field gradient. An electric field is expressed as a quantity  $E$  in volts per meter (V/m). The strength of an electric field determines how fast ions migrate through a medium. This velocity is also dependent on ion-specific factors like size and charge of a molecule and these factors are summarized in a value known as the ionic mobility. In principle, each kind of ion has a own ionic mobility. There are many EFGF methods, but commonly all have 1) a conductivity gradient at a predefined position, which gives rise to the electric field gradient and 2) a bulk flow in opposite direction of analyte migration. An ion migrating through an electric field gradient will accelerate or slow down. Analytes of interest encounter a point where the velocity of electromigration becomes equal to the counterflow velocity. At these points, the analytes will be focused. On shallow gradients, the focusing position will be dependent on the ionic mobility of the analyte concerned, resulting in simultaneous trapping and separation.

In ITP, two zones containing different electrolytes are used: a trailing electrolyte (TE) with low ionic mobility and a leading electrolyte (TE) with high ionic mobility. Analytes of interest should have intermediate mobility and are then focused between these two zones. Analytes present in sufficient quantities are concentrated until they reach a plateau concentration. A typical sign of a completed ITP separation is therefore a stair-like profile of

contiguous plateau zones, each analyte having its own plateau. These plateau zones move with equal velocities. This situation is different from CZE, where each zone travels with a different velocity, leading to resolved peaks. Moreover, analytes are in principle not being focused in CZE separations, while with ITP high concentration factors can be achieved.

A third important concept in this thesis is concentration polarisation (CP). CP occurs across conduits which exclude anions and permit cations, or vice versa. Such a conduit may be a nanochannel, where the close proximity of surface charges makes the pore selective, or a nanoporous membrane. As a result, upon application of an external voltage, an ion-enriched zone will form at one entrance of a conduit, and an ion-depleted zone at the other entrance. These zones give rise to conductivity gradients on which EFGF can be performed. Indeed, several EFGF approaches are based on CP.

In the research presented in this thesis, we demonstrate that CP-induced ion-depleted zones can replace the TE typically used in ITP separations. Therefore the LE is the only electrolyte needed in such experiments. Hence the title of this thesis: single-electrolyte isotachopheresis, which might have seem a *contradictio in terminis* to someone familiar with isotachopheresis.

### **Scope of this thesis**

The aim of this thesis was to develop novel, and to improve, electrokinetic methods for sample pretreatment and separation of charged biomolecules. The work in this thesis has been inspired by research on isotachopheresis (ITP) and other electrokinetic methods with excellent preconcentration capabilities, particularly electric field gradient focusing (EFGF). The ability to concentrate and separate analytes simultaneously and selectively makes ITP a

technique with much potential, but the fact that it requires multiple electrolytes makes it not easy to use.

Based on our discovery of the insight that ITP phenomena can be produced by EFGF methods, we have aimed at combining the best of two worlds. Methods have been developed that are based on isotachophoretic principles but that are simpler to use. The unique versatility of EFGF methods has been incorporated in these methods.

In addition, the aim was to create a conceptual framework for how to position novel methods developed in this thesis with already existing research and literature. Overall, with this thesis we aim to provide the bioanalysis and metabolomics communities, and the life sciences in general, with new insights and approaches for the analysis of small complex biological samples.

## **Thesis outline**

ITP, EFGF and concentration polarization (CP) are complicated phenomena. Chapter 2 provides first an in-depth introduction to ITP and EFGF, as well as to CP devices. Next, evidence is presented for the argument that ITP and EFGF have identical properties; this argument is underpinned by theoretical and experimental evidence, both from previous literature and from the research presented in this thesis. The strengths of ITP and of the several EFGF methods, including the in Chapter 3 presented novel method, are compared and major challenges are identified. It is discussed that theoretical knowledge and practical tricks from ITP and EFGF may be combined and integrated.

In chapter 3 a novel electrokinetic separation and preconcentration method is presented which is called depletion zone isotachophoresis (dzITP). dzITP is performed in miniaturized EFGF devices based on CP. dzITP is investigated as

a single-electrolyte method which forms isotachophoretic zones at the border of a nanochannel-induced depletion zone. Actually, ITP is widely supposed to require a leading and a trailing electrolyte. Nevertheless, it is demonstrated that a single-electrolyte separation can have all main characteristics of ITP – the only condition is that an electric field gradient is present on which charged analytes can be focused. This fact is one of the most interesting consequences from the insight that EFGF has ITP nature. dzITP is developed based on glass chips containing a nanochannel, and concentration polarization leads to the formation of depletion zones, enabling dzITP. Discrete and continuous injections, long-term zone stability and voltage-actuated zone positioning is demonstrated, too.

In chapter 4, selective release of dzITP-separated compounds along a depletion zone is studied. dzITP is investigated as a tunable ionic mobility filter, which may be used in pulsed and in continuous mode. Selective enrichment of a low-concentration compound is demonstrated, as well as selective trapping of metabolites in diluted raw urine sample.

In chapter 5, the hypothesis is tested that an elastomeric microvalve in a PDMS chip forms a tunable reversible nanospace between the deflected valve membrane and the channel walls. The effect of valve pressure on valve electrical resistance is investigated, as well as the influence of different voltages and valve pressures on concentration polarization regimes. The PDMS valve was used to achieve efficient analyte preconcentration (over 1000-fold) before release of trapped analyte.

Finally, at the end of this thesis, an overview of the most important conclusions is given and the perspectives of the findings of this thesis are discussed.

## References

1. C. E. Sims and N. L. Allbritton, *Lab on a Chip* **7** (4), 423-440 (2007).
2. K. Mawatari, S. Kubota, Y. Xu, C. Priest, R. Sedev, J. Ralston and T. Kitamori, *Analytical Chemistry* **84** (24), 10812-10816 (2012).
3. S. Pennathur, F. Baldessari, J. G. Santiago, M. G. Kattah, J. B. Steinman and P. J. Utz, *Analytical Chemistry* **79** (21), 8316-8322 (2007).
4. B. Jung, R. Bharadwaj and J. G. Santiago, *Analytical Chemistry* **78** (7), 2319-2327 (2006).
5. D. Bottenus, T. Z. Jubery, Y. Ouyang, W.-J. Dong, P. Dutta and C. F. Ivory, *Lab on a Chip* **11** (5), 890-898 (2011).
6. J. Wang, Y. Zhang, M. R. Mohamadi, N. Kaji, M. Tokeshi and Y. Baba, *Electrophoresis* **30** (18), 3250-3256 (2009).
7. Y.-C. Wang, A. L. Stevens and J. Han, *Analytical Chemistry* **77** (14), 4293-4299 (2005).
8. S. M. Kim, M. A. Burns and E. F. Hasselbrink, *Analytical Chemistry* **78** (14), 4779-4785 (2006).
9. R. K. Anand, E. Sheridan, K. N. Knust and R. M. Crooks, *Analytical Chemistry* **83** (6), 2351-2358 (2011).
10. M. Kim, M. Jia and T. Kim, *Analyst* (2013).
11. P. H. Humble, R. T. Kelly, A. T. Woolley, H. D. Tolley and M. L. Lee, *Analytical Chemistry* **76** (19), 5641-5648 (2004).
12. D. Ross and L. E. Locascio, *Analytical Chemistry* **74** (11), 2556-2564 (2002).





## 2 Electric Field Gradient Focusing = Isotachophoresis: a Review

*A revised version of this chapter has been submitted as a Perspective article to the journal Analytical Chemistry*

Isotachophoresis (ITP) and electric field gradient focusing (EFGF) are two powerful approaches for simultaneous focusing and separation of charged compounds. In EFGF, ionic analytes are immobilized on an electric field gradient, implying that, as in ITP, all focused analytes migrate with the same velocity upon completion of the separation. Therefore we argue in this review that EFGF methods should be regarded as forms of ITP. This claim is supported by theoretical and experimental studies from literature where EFGF demonstrates isotachophoretic hallmarks, including observations of plateau concentrations and contiguous analyte bands. An important implication of this unification is that functionality and applications developed on one platform can be transferred to other platforms. Single-electrolyte isotachophoretic separations with tunable ionic mobility window can be performed, as is illustrated with the example of depletion zone isotachophoresis (dzITP). We foresee many interesting combinations of ITP and EFGF features, yielding powerful analytical platforms for biomarker discovery, molecular interaction assays, drug screening and clinical diagnostics.

Isotachophoresis (ITP) and electric field gradient focusing (EFGF) are two classes of methods which are capable of simultaneous analyte separation and

efficient focusing. Concentration factors often exceed thousandfold and sometimes even millionfold for both ITP<sup>1-3</sup> and EFGF methods<sup>4-9</sup>. We believe that these similarities between ITP and EFGF are no coincidence. This review aims to provide a conceptual framework and to discuss experimental support for the unification of ITP and EFGF. As ITP is one of the most difficult to understand among electrokinetic techniques, we will first discuss the basic principles of this powerful method. Next, EFGF and the many variants thereof will be introduced, including conductivity gradient focusing (CGF), temperature gradient focusing (TGF), dynamic field gradient focusing (DFGF), electrocapture (EC), bipolar electrode focusing (BEF) and micro/nanofluidic concentration polarization (CP) devices. We then present our arguments for regarding EFGF techniques as forms of ITP and vice versa and provide support from several previous studies. Finally, we discuss the opportunities for different application areas in the life sciences created by the synergism of integrated ITP/EFGF platforms.

This review aims at understanding rather than comprehensiveness. Since the year 2000, numerous general reviews on electrokinetic preconcentration methods have been published<sup>10-28</sup>. These reviews include stacking methods like field amplified sample stacking/injection (FASS, FASI) and micellar methods like sweeping and micellar affinity gradient focusing (MAGF), which will not be considered here. For ITP, several useful introductory reviews are available<sup>29-31</sup>, while updates on recent developments have been frequently given by Gebauer et al<sup>32-38</sup>. For EFGF technologies, the review by Shackmann and Ross provides an excellent introduction<sup>39</sup>, but several more reviews are available<sup>40-43</sup>.

## Isotachophoresis

### *The isotachophoretic condition*

The word “isotachophoresis” contains the Greek words isos (equal) and takhos (speed), capturing the essence of the method: an ITP separation is forced towards a dynamic equilibrium in which all co-ions migrate with the same velocity. The electrophoretic velocity  $v_i$  of an ion is determined by its ionic mobility  $\mu_i$  and by the local electric field  $E$ :

$$v_i = \mu_i E \quad (1)$$

Therefore, if ions with different ionic mobilities have the same velocity they must be in regions with different local electric fields. Under the isotachophoretic condition that all co-ions migrate with same velocity, each co-ion must be situated in its own zone in which the electric field exactly matches the ionic mobility of the co-ion. In other words, ions a, b and c with ionic mobilities  $\mu_a < \mu_b < \mu_c$  will appear in zones A, B and C in which

$$\mu_{a,A} E_A = \mu_{b,B} E_B = \mu_{c,C} E_C \quad (2)$$

Ionic mobilities are influenced by factors that may vary from zone to zone like pH and ionic strength, hence the zone subscripts A, B and C.

Disturbances of the isotachophoretic condition are subjected to a self-correcting mechanism (figure 1). If any ion with mobility  $\mu_b$  were transported to zone C (for example, by diffusion) the lower electric field would cause it to migrate with lower velocity than all the surrounding ions with higher mobility  $\mu_c$ , until it returns in zone B.

Inversely, if the same ion would be placed in zone A, it would encounter higher electric field and would move faster than the surrounding ions with lower mobility  $\mu_a$ , again bringing the ion back in zone B. This self-correcting mechanism makes that in isotachophoresis pure co-ion zones are formed with

sharply defined borders. The sharpness of these borders is determined by a balance of electromigration and dispersion: at lower electric fields diffusion is more dominant, while higher electric fields lead to sharper zones.

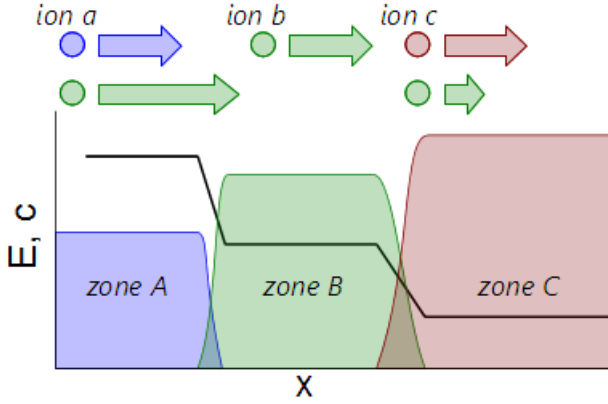


**Figure 1.** Self-correcting mechanism in ITP. Arrows represent electrophoretic velocities of ions. Profiles of electrical field and ion concentration profiles are indicated in the graph.

#### Plateau concentrations

Ion concentrations directly influence conductivity and local electric field. Therefore, each isotachophoretic zone must not only have its own electric field, but also must reach a corresponding plateau concentration (there is an exception for analytes in trace quantities, which will be discussed as “peak mode ITP” below). We assume monovalent strong ions, a common counterion  $x$ , and pure isotachophoretic zones. Under these conditions electroneutrality dictates:

$$c_{a,A} = c_{x,A} \quad (3)$$

$$c_{b,B} = c_{x,B} \quad (4)$$

For separations in linear channels, the current in all zones is equal ( $I_A = I_B$ ). Therefore, considering only zones A and B:

$$\sum_i c_{i,A} \mu_{i,A} E_A A_A = \sum_i c_{i,B} \mu_{i,B} E_B A_B \quad (5)$$

where A is the cross section of the channel. As we deal with pure zones, we only have to sum the co-ion and the common counterion  $x$ . Therefore, assuming uniform cross section we have

$$c_{a,A}\mu_{a,A}E_A + c_{x,A}\mu_{x,A}E_A = c_{b,B}\mu_{b,B}E_B + c_{x,B}\mu_{x,B}E_B \quad (6)$$

which using eq 3 and 4 simplifies to

$$c_{a,A}(\mu_{a,A} + \mu_{x,A})E_A = c_{b,B}(\mu_{b,B} + \mu_{x,B})E_B \quad (7)$$

Invoking the isotachophoretic condition in eq 2 results in

$$c_{b,B} = c_{a,A} \frac{(\mu_{a,A} + \mu_{x,A})\mu_{a,A}}{(\mu_{b,B} + \mu_{x,B})\mu_{b,B}} \quad (8)$$

This equation tells that the plateau concentration  $c_{b,B}$  of ion b in zone B is in principle solely dependent on the concentration  $c_{a,A}$  of ion a in zone A and on the mobilities of the ions involved. Eq 8 also may be derived from the Kohlrausch regulation function (KRF)<sup>44</sup>:

$$KRF = \sum_i \frac{z_i c_i}{\mu_i} \quad (9)$$

The KRF is a conservation law: at each position in any electrokinetic separation the value for KRF remains constant over time. If a bulk flow is present, KRF moves with the flow.

The importance for ITP is that the KRF remains the same even after an analyte or trailing electrolyte zone has replaced a leading electrolyte zone, dictating the concentrations in these zones. A clear and more extensive discussion of the KRF and its limitations, and of other conservation laws in electrophoresis has been provided by Hruška and Gaš<sup>45</sup>.

### *Leading and trailing electrolytes*

From the isotachophoretic condition we have deduced a number of important hallmarks of ITP separations: the formation of pure zones with sharply defined borders, a self-correcting mechanism, and plateau concentrations. This isotachophoretic condition can be imposed on a separation by introducing a discontinuous electrolyte system which contains at least a high-mobility leading electrolyte (LE) and a low-mobility trailing electrolyte (TE). The TE cannot move faster than the LE and overcome it, because the LE ions have higher mobility. The TE can neither move slower in the sense that an electrolyte-free zone would form between the TE and the LE, because such a region would be rapidly filled with TE ions by the increased electric field. The TE and LE zones therefore must move with equal velocity. Electric field in the TE becomes adjusted accordingly while the TE concentration is adjusted by Kohlrausch regulation.

### *Analytes, spacers and tracers*

Since ITP has a self-correcting mechanism, analyte injection can take place by dissolution in the TE or in the LE. Usually, TE injections are preferred because the higher electric field in the TE speeds up the ITP process. The TE and the LE define an ionic mobility window. Analytes within the ionic mobility window will migrate towards the LE/TE interface and will be focused there. Ions with higher mobilities than the LE or lower mobilities than the TE will be transported away from the LE/TE interface. Focused analytes migrate with the same velocity as the LE and TE ions, fulfilling the isotachophoretic condition. The analytes will form contiguous plateau zones that are ordered according to their ionic mobilities. The electric fields and the conductivities in the zones

will form a stair-like profile, the lowest electric field and highest conductivity being situated in the LE zone.

In order to achieve baseline separation between two adjacent analyte zones, spacers can be used. A spacer is an ion that has intermediate mobility between two analytes and therefore will insert between the two analyte zones and space them apart. For example, non-fluorescent spacers may be used to make two adjacent fluorescent zones discernable. Similarly, fluorescent spacers can be used for indirect detection and quantification of plateau zones of non-fluorescent analytes.<sup>46</sup>

Tracers aid in visualization of ITP zones. Tracer ions are continuously supplied in low concentrations to prevent significant alterations of the ITP process. While migrating through the ITP zones, tracer ions undergo stacking due to the differences in local electric field. In other words, the tracer concentration co-adjusts to the local conductivity. This enables visualization of different zones. Chambers et al. distinguished three kinds of tracer: so-called counterspeeders, underspeeders and overspeeders<sup>47</sup>. Counterspeeders are counterionic tracers, which migrate in opposite direction as the ITP zones. Underspeeders and overspeeders are co-ionic tracers which have respectively lower and higher mobility than all relevant analytes. As a tool for indirect detection, tracers are an interesting alternative to fluorescent labels and intercalating dyes.

#### *Peak mode and plateau mode*

ITP separations often can be readily recognized by a stairlike profile of contiguous plateau-shaped analyte zones. In simple cases, plateau concentrations can be predicted from the leading electrolyte concentration

and the mobilities of the analyte ion, the counterion and the leading ion (eq 8). However, in many cases analytes have insufficient quantities to reach plateau concentrations. Such analytes will form focused peaks between the zones of the ions with the nearest mobilities. This situation is often referred to as “peak mode ITP” and is contrasted to “plateau mode ITP”<sup>48</sup>. In principle, at the start of an ITP separation every analyte zone starts as a peak.

Overlap between adjacent ITP zones is always present due to diffusion. The concentration gradients in these overlap regions provide an electric field gradient on which analytes with intermediate mobilities find a focusing position. During the transition from peak mode to plateau mode, the focusing analytes replace co-ions at the same positions, gradually flattening the electric field gradient. When all co-ions are replaced, the focusing analyte has reached plateau concentration.

The overlap between zones, which is particularly strong in peak mode ITP, limits the capacities of ITP for separation purposes. For example, Kaniasky et al.<sup>49</sup> demonstrated an ITP separation of 14 small molecules, which is a fairly large number for an ITP separation. This is in contrast to zone electrophoresis, where electropherograms may show hundreds of peaks. To increase separation efficiency ITP is often combined with zone electrophoresis by means of transient ITP (see next section). Zone overlap also can be used very advantageously. Bercovici et al. showed that hybridization of two different DNA strands could be accelerated over 10 000 fold by means of peak mode ITP because of the ability to concentrate the DNA molecules in a very confined volume.<sup>50</sup>

The plateau concentrations resulting from Kohlrausch regulation impose a limit to analyte preconcentration. Nevertheless, if analytes have very low



starting concentrations and sufficient time is provided, peak mode ITP can be used to obtain extremely high concentration factors. Several articles report over 10000-fold protein preconcentration<sup>2, 3, 51</sup>, and in ideal conditions, millionfold concentration of a fluorophore has been achieved.<sup>1</sup>

### *Non-equilibrium ITP processes*

The isotachophoretic condition only holds for completed ITP separations. There are several situations in which the dynamic equilibrium, which is associated with the isotachophoretic condition, is never reached. Incomplete ITP separations are characterized by the presence of mixed zones, which contain multiple co-ions with different mobilities. For example, sample might be injected continuously, resulting in continuously broadening zones. A well-known non-equilibrium ITP process is transient ITP (tITP). Several tITP alternatives exist<sup>52</sup>. For example, analytes are dissolved in a TE plug which is sandwiched between LE zones. The analytes are focused at the front end of the TE plug, while the back of the TE plug is dissolved by the faster LE ions. When the TE becomes completely dissolved, ITP focusing ceases and analytes are separated by zone electrophoresis. tITP is widespread as a very useful method for inline sample preconcentration.

## **Electric field gradient focusing**

### *Concepts of EFGF*

Electric field gradient focusing (EFGF) methods use separation systems in which an electric field gradient is induced. Focusing occurs when analytes at opposite sides of the gradient migrate in opposite directions to a point where they have zero velocity on the gradient.

In some cases, the gradient may move as a whole, for example by electromigration. Therefore, it is more precise to define the analyte velocities relative to the gradient velocity  $v_{\text{gradient}}$ . The analyte focusing locations are the points on the gradient where the velocities of the analytes are equal to the velocity of the gradient ( $v_i = v_{\text{gradient}}$ ). The change of sign in ion velocity should then be regarded as being relative to the gradient velocity.

Moreover, we take the flow velocity as a frame of reference. The velocities of the ions and of the gradient therefore must be corrected for flow velocity. In many counterflow gradient focusing methods, the gradient has a constant position in the channel structure. In these situations, we take the gradient velocity as minus the flow velocity ( $v_{\text{gradient}} - v_{\text{flow}} = 0$ ). These considerations will make a direct comparison of EFGF and ITP more straightforward.

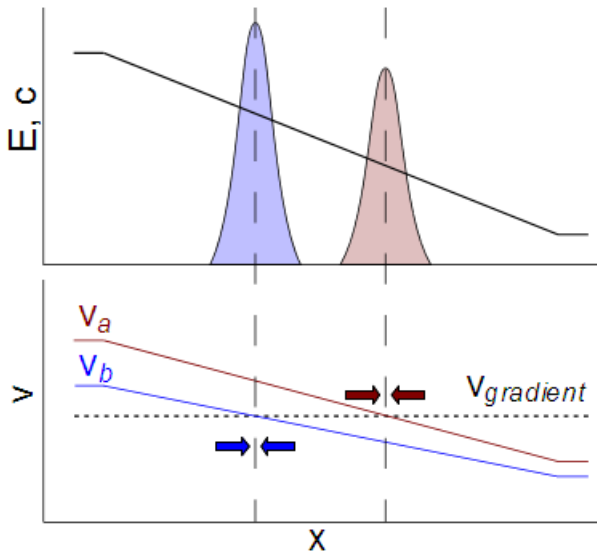


**Figure 2.** Common principle of EFGF methods. In the graphs, the electric field profile ( $E$ ) is sketched, as well as the concentration ( $c$ ) and velocity ( $v$ ) profiles for two analytes. Analytes focus at the point where the electrophoretic velocity is equal to the gradient velocity, these points are indicated by vertical dashed lines.

Figure 2 shows a schematic electric field gradient as might be used in EFGF, as well as the resulting velocities of ions  $a$  and  $b$  with ionic mobilities  $\mu_a > \mu_b$

versus the gradient velocity. The figure shows how the ions obtain different focusing positions dependent on their ionic mobility.

Analytes may have too low or too high ionic mobility to be focused on a gradient. These analytes are not trapped.

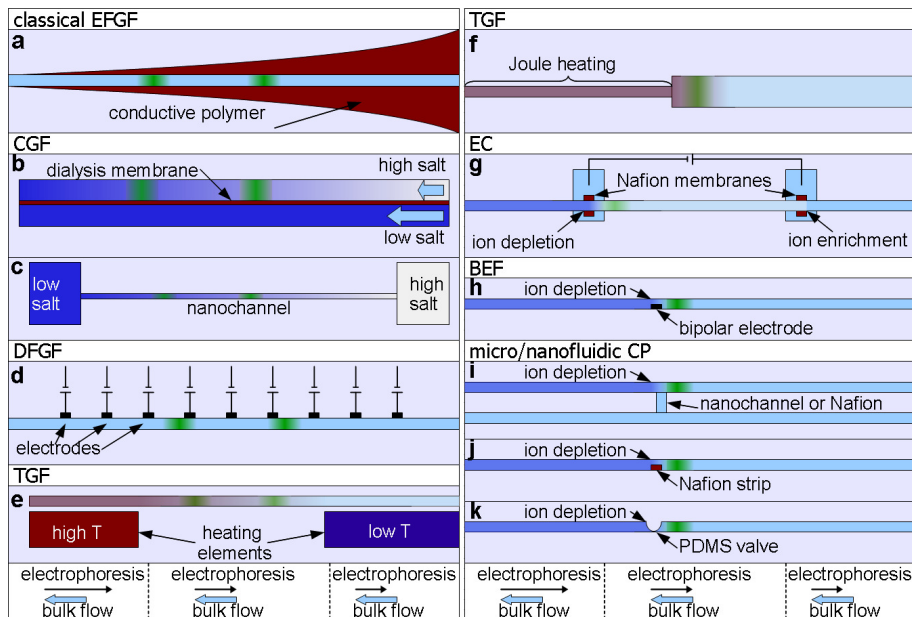


**Figure 3.** Overview of several EFGF methods and variants thereof. These methods are discussed in detail in the text. The green bands indicate analyte focusing positions, where electrophoretic velocity is equal to bulk flow velocity

We will proceed to discuss the numerous EFGF methods that have been published to date. EFGF methods are often compared to isoelectric focusing (IEF), which is one of the oldest and most well-known electrokinetic focusing methods. In IEF, amphoteric compounds are allowed to migrate through a pH gradient, resulting in adjustment of the net charge of the compounds, until they reach their isoelectric point (pI). IEF is particularly powerful for proteins, though precipitation often can be a limitation. In contrast to the EFGF methods discussed here, compounds obtain zero net mobility when focused

by IEF. Because this results in different physics, we do not regard IEF and related techniques like the dynamic pH junction method<sup>53</sup> as forms of EFGF, and therefore these methods will not be further considered in this review. The most important EFGF approaches are summarized in figure 3. These EFGF methods will be discussed in detail in the following sections.

### *Classical EFGF*

Electrical field gradient focusing (EFGF) was introduced by Koezler and Ivory<sup>54, 55</sup>, who focused and separated proteins in a dialysis tubing which was placed in a converging channel. The converging channel shaped the electric field while the dialysis tubing helped to maintain a pressure-driven counterflow with uniform velocity. We will call this and similar methods “classical EFGF”. For example, Humble et al used a miniaturized device in which they molded a linear channel into a converging area filled with conductive polymer (figure 3a), yielding an electric field gradient upon voltage application. With their device, they achieved separation of up to 5 proteins as well as 10 000 fold preconcentration.<sup>8</sup> Liu et al. also performed focusing and separation of protein mixtures and showed selective elution of protein peaks by increasing counterflow rate.<sup>56</sup> Changing the voltage drop also can result in selective elution, as was demonstrated by Wang et al.<sup>57</sup> Petsev et al. used a chip design in which the separation channel had several side channels in order to introduce step changes in the electric field<sup>58</sup>.

### *CGF*

In conductivity gradient focusing (CGF), an electric field gradient is formed by creating a gradient in electrolyte conductivity. CGF was introduced by

Greenlee and Ivory<sup>59</sup> who used a setup containing a separation channel and a purge channel which were separated by a dialysis membrane. The separation channel had a high-salt inlet; the high-salt electrolyte was gradually diluted by dialysis through the low-salt purge channel (figure 3b). They were able to focus and separate a binary protein mixture.

Inglis et al used a conductivity gradient inside a nanochannel which connected a high salt and a low salt reservoir (figure 3c). An electro-osmotic flow provided the necessary counterflow. Two proteins were separated and 1000-fold preconcentration was achieved.<sup>60</sup>

### *DFGF*

Dynamic field gradient focusing (DFGF) was introduced by Huang and Ivory.<sup>61</sup> They used an array of individually controllable electrodes which were placed inside the separation channel for detailed control of the electric field gradient (figure 3d). Tracey et al. described a preparative scale DFGF instrument prototype.<sup>62, 63</sup> Burke et al. used DFGF for simultaneous separation of negatively and positively charged proteins. Focused peaks could be positioned, the authors even demonstrated that the positions of focused proteins could be swapped by locally changing the electric field gradient during the experiment.<sup>64</sup>

### *TGF*

Temperature gradient focusing (TGF) was introduced by Ross and Locascio<sup>9</sup>, who used a device with external heating blocks (figure 3e). A Tris/borate buffer was used because the conductivity of this buffer depends relatively strongly on temperature (more strongly than analyte ionic mobilities, which

are also affected by temperature). This results in an electric field gradient on which analytes could be focused. A wide range of compounds could be focused, including labeled amino acids, proteins, DNA and polystyrene particles. 10 000 fold preconcentration was achieved. Ross and Locascio also showed that Joule heating in a narrow channel section can be used for TGF (figure 3f), an effect which was studied more extensively in other publications<sup>65-67</sup>. Another interesting method to introduce a temperature gradient is optothermal heating. Akbari et al. used a digital projector as a light source and heater which could be moved in order to position a focused fluorescein zone.<sup>68</sup>

Balss et al. used TGF to perform two different DNA hybridization assays. In a first assay, a DNA target was focused and peptide nucleic acids (PNA) were introduced in the bulk flow, resulting in PNA-DNA hybridization. In a second assay, bulk flow was varied to move focused PNA-DNA duplexes through the temperature gradient in order to measure their melting temperature<sup>69</sup>. To overcome the limitation that only a few components can be simultaneously focused and separated on a temperature gradient, Hoebel et al. introduced scanning TGF in which the bulk flow is varied to obtain sequential focusing and elution of a larger number of compounds<sup>70</sup>.

## *EC*

Electrocapture (EC) devices use a capillary or tubing containing two Nafion junctions. The Nafion junctions are connected to reservoirs which contain a high and a low voltage electrode. A pressure-driven flow was applied to the capillary. Applying a voltage leads to concentration polarization across the Nafion junctions, resulting in ion enrichment at the upstream junction and

ion depletion at the downstream junction. On the resulting conductivity gradients analytes can be focused (figure 3g). Adjusting the flow rate leads to selective release of compounds. EC has been reviewed by Shariatgorji et al.<sup>71</sup> The technique has mainly been applied to proteins, peptides and DNA and has been used for preconcentration, separation, salt and detergent removal, buffer replacement and inline reactions. Importantly, EC could be coupled to mass spectrometry (MS)<sup>72, 73</sup>. To our knowledge, no other EFGF technique has been successfully hyphenated with MS yet. To date, EC also appears to be the only commercialized EFGF method<sup>74</sup>.

### *BEF*

Bipolar electrode focusing (BEF) was introduced by Dhopeskarwar et al.<sup>75</sup>, who used a simple linear channel containing an electrically floating bipolar electrode. When a voltage was applied over the channel, local ion depletion occurred at the bipolar electrode location. On the resulting conductivity gradient analytes could be focused (figure 3h). The ion depletion zone appears to be caused by electrode reactions<sup>76</sup>. Interestingly, if the bipolar electrode was connecting two parallel microchannels, a faradaic form of concentration polarization occurred, with ion enrichment in the cathodic channel<sup>6</sup>. This configuration is very similar to the H-shaped concentration polarization devices discussed below. Up to 500 000 fold concentration enrichment was reported with this device. In a similar dual channel configuration, cations and anions could be separated and enriched simultaneously<sup>77</sup>.

### *Concentration polarization; micro/nanofluidic CP devices*

Concentration polarization (CP) is a well-known phenomenon from membrane technology, which has gained considerable attention in the last 10 years from researchers of micro- and nanofluidic separations. Since 2005, when Wang et al.<sup>4</sup> developed an elegant implementation of the principle in a micro/nanofluidic device, chip-based CP devices have attracted much attention. A detailed review of CP theory has been published recently<sup>78</sup>, simultaneously with a review of micro/nanofluidic CP devices<sup>79</sup>.

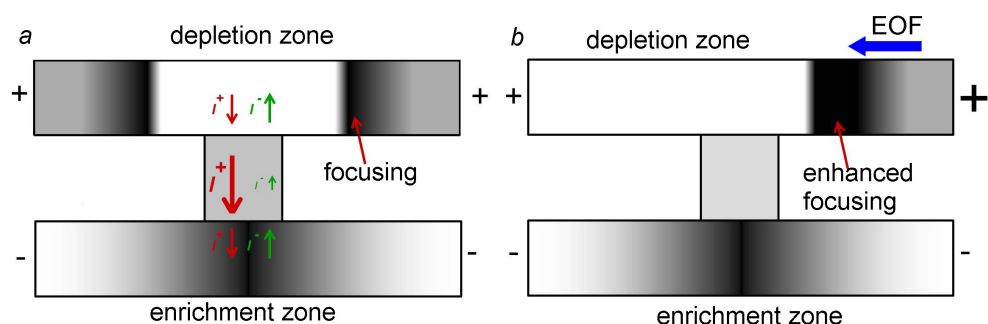


**Figure 4.** Phenomena in concentration polarization devices. a) Formation of depletion and enrichment zones due the imbalance of cation versus anion flux inside the nanochannel. b) Inducing a tangential EOF results in analyte trapping at the upstream border of the depletion zone.

CP is a phenomenon that can occur across nanopores and nanochannels. Upon applying a voltage across a nanochannel, ions (both cations and anions) accumulate at one entrance of the nanopore while being depleted at the opposite entrance. This effect can be ascribed to the surface charge of the material of which the nanochannel is made. Often used materials like glass, silicon and PDMS have a negative surface charge, particularly at high pH's, due to deprotonation of silanol groups (equilibrium of  $\text{SiOH}$  and  $\text{SiO}^-$ ).



Because in a nanochannel the walls are very close to one another, surface charges can become dominant, resulting in coion exclusion and counterion enrichment inside the nanochannel (figure 4). While electrical current through a microchannel is carried equally (in a sense) by anions and cations, it must be carried mostly by cations inside a nanochannel with a negative surface charge. In other words, cation flux inside the nanochannel is higher than in the adjacent microchannel or reservoir; while anion flux is lower. A simple summation of ion fluxes reveals that both cations and anions are enriched at the cathodic side of the nanochannel and depleted at the anodic side (in the case of a negative surface charge). Thus, enrichment and depletion zones are formed (figure 4a)<sup>80, 81</sup>.

In the aforementioned publication of Wang et al<sup>4</sup>, an H-shaped channel geometry was used, comprising a nanochannel which connected two parallel microchannels. CP across the nanochannel induced depletion zone formation in one of the microchannels. A tangential electric field induced an electroosmotic flow (EOF) through this microchannel, carrying charged analytes. Due to the conductivity difference at the depletion zone border, the analytes can be trapped very efficiently (figures 3i, 4b). Over 10 000 000 concentration factors were reported<sup>4</sup>. With a similar device, Kim et al. reported similar concentration factors for protein preconcentration.<sup>5</sup> Though this latter author casted some doubt on this result because it would require extraordinarily high flow velocities, it is evident that very efficient preconcentration could be achieved. Wang et al. and Kim et al. also demonstrated a zone electrophoresis separation after preconcentration. Many methods have been published to produce similar devices<sup>79</sup>. These devices have been used for enzyme assays<sup>82-84</sup>, immunoassays<sup>85-88</sup>, inline labeling<sup>89</sup> and

desalination<sup>90</sup>. Moreover, massive parallelization of the device also has been achieved<sup>88, 91</sup>. Interestingly, the ion depletion effect also can be induced in a single channel by placing a Nafion patch. Electric field lines going through the Nafion induce depletion zone formation, providing a focusing gradient (figure 3k)<sup>7, 92</sup>. Alternatively, elastomeric valves in PDMS devices also can be employed, in “closed” state, leaving a nanogap between the valve membrane and the channel wall, which can be used to induce CP and preconcentration effects (figure 3j, see also chapter 3)<sup>93, 94</sup>.

### **ITP and EFGF intertwined**

#### *EFGF processes in ITP*

In ITP, focusing occurs in conjunction to gradient effects, supporting the view that ITP is a form of EFGF. Diffusion effects create overlap between adjacent zones, resulting in an electric field gradient on which analytes with intermediate mobility will be focused.

With regard to focusing effects, many authors refer to ITP as a stacking method. However, as a concentration mechanism, stacking should be discerned from focusing: during focusing ion velocities change of sign, while in stacking ion velocities change in magnitude but not of sign. In ITP, stacking indeed plays a role, but focusing is the principal mechanism for concentration and separation of analytes.

Figure 5 shows a scheme of a conventional ITP separation in which one analyte has reached plateau concentration while three other analytes are in peak mode. The corresponding electric field is also shown. Clearly, two gradients are present: one between the TE and the analyte plateau, and one

between the analyte plateau and the LE. The peak mode analytes are focused on these gradients.

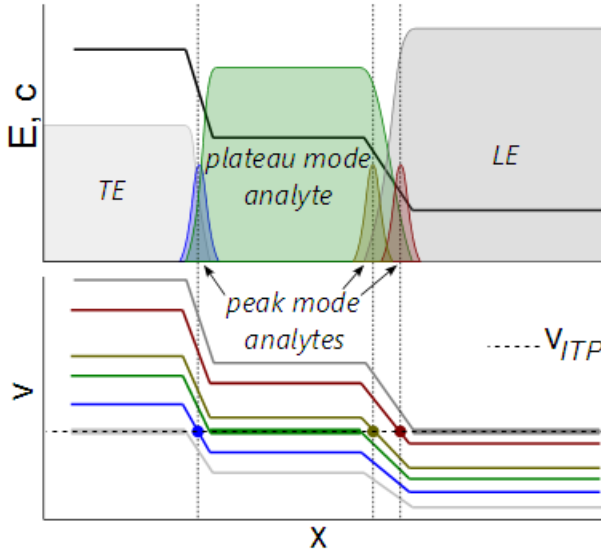


**Figure 5.** Profiles of electric field ( $E$ ), ion concentrations ( $c$ ) and ion velocity profiles ( $v$ ) in an ITP separation containing a LE, a TE, a plateau mode analyte and three peak mode analytes. Focusing occurs at locations where analyte velocity is equal to the ITP velocity. Focusing locations of peak mode analytes are indicated by vertical dotted lines.

When comparing figure 2 and figure 5 the similarities between EFGF and ITP become evident. In both situations, ions are focused at the points where their velocities are equal to the gradient velocity, the locations of these points differing depending on the ionic mobility. The most significant difference between the figures is that one of the analytes in figure 5 reaches a plateau. Plateau concentration ions have a line instead of a single point on which the ion velocity is equal to the isotachopheric velocity  $v_{ITP}$  (which is the equivalent of  $v_{gradient}$ ). For peak mode ions the only difference is that multiple gradients are present.

The two peaks in figure 5, which are situated between the analyte plateau and the LE are focused at slightly different positions. Due to the self-correcting mechanism of ITP, the gradients on which peak mode ions are focused are often very steep. Multiple ions on a single gradient therefore usually can not be resolved as individual peaks. However, Khurana et al. used the slow reaction kinetics of carbonate ions with an amine-containing TE to create a shallow gradient between the TE and the LE on which multiple DNA molecules could be separated in resolved peaks<sup>95</sup>.

#### *ITP processes in EFGF methods*

In an EFGF experiment, analyte ions are focused on a fixed position on a gradient. This implies that upon completion of the focusing process all focused analytes have the same velocity. In other words, gradient focusing results in something to which the term iso-tacho-phoresis may be applied very literally. For analytes focused on a gradient the isotachophoretic condition holds. We have seen that from this condition a number of notable characteristics can be derived: each co-ion will form a pure, sharply defined zone with a plateau concentration and with an electric field which is adjusted to the ionic mobility of the co-ion concerned. Therefore it can be predicted that in EFGF analytes will form adjacent plateau-shaped zones similar to conventional ITP. Just as in conventional ITP, such plateau zones will only form if sufficient analyte is present. If analytes are present in low quantities only, EFGF will be similar to peak mode ITP.

A significant difference between current-day EFGF and ITP methods is that EFGF does not require a discontinuous electrolyte system with a LE and a TE. Using a LE and a TE is the most common method to impose the

isotachophoretic condition on a separation. There is however no reason to assume that this is the only method. Gradient focusing also has an isotachophoretic outcome, simply because immobilization on a gradient results in equal velocities for the focused analytes. Moreover, several crucial ITP parameters do not depend on TE parameters. The dependence of plateau concentrations on LE (and not TE) concentration has already been pointed out. Additionally, analyte zone speed and width are (at least in peak mode ITP) independent of TE conductivity.<sup>48</sup>

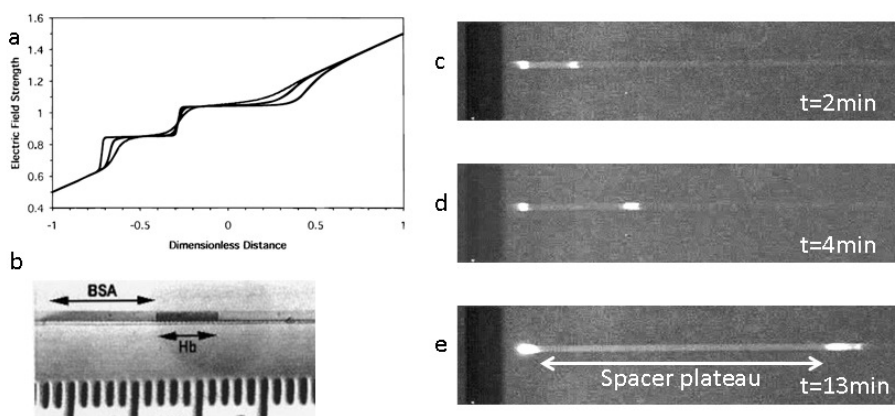


**Figure 6.** Indications of ITP processes in several EFGF methods: a) Koepler simulated the electric field yielding a stair-like pattern that is typical for ITP (reproduced with permission from ref 55); b) Greenlee found sharply defined contiguous analyte plateau zones in CGF (reproduced with permission from ref 59); c-e) In BEF, Laws found a separation of two focused zones by a continuously growing zone, indicating the insertion of a spacer (reproduced with permission from ref 99).

Important hallmarks of ITP have been described already in early papers on EFGF methods. Koepler and Ivory<sup>55</sup> performed modeling of classical EFGF and showed that the electric field gradient evolved into a stair-like profile if sufficiently high concentrations of two model analytes were provided (figure 6a). A stair-like electric field gradient is very characteristic for ITP. However,

in their analysis the corresponding analyte zones did not clearly have a plateau shape, though clearly deviating from a Gaussian profile. Nevertheless, in the experimental section of the same paper, an absorbance trace of separated myoglobins shows an analyte zone with a plateau-like shape.

In conductivity gradient focusing, Greenlee and Ivory observed wide contiguous bands of BSA and hemoglobin. The border between these bands was very sharply defined and the concentration throughout the bands appeared to be constant (figure 6b). The authors noted that such bands are characteristic for ITP, but viewed the isotachophoretic effect as undesired<sup>59</sup>.

Lin et al<sup>96</sup> studied finite sample effects in TGF (i.e. situations in which sample concentration is large enough to affect the electric field distribution) using a model based on a generalized Kohlrausch regulation function. Experimental results were used to verify some of their observations. In TGF, plateau-shapes are not expected for concentration profiles, since the temperature gradient significantly affects analyte mobility. However, the velocity profiles in the simulations of Lin et al. showed a plateau-shaped zone which broadened over time. The study of Lin et al. did not include multiple analyte ions, which we predict to reveal multiple ITP-like zones.

For EC, Astorga-Wells et al.<sup>97</sup> compared flow velocities and measurements of local electric fields. If the background electrolyte is migrating with equal, but opposite velocity with respect to the flow velocity, the ratio  $v_{\text{flow}}/E$  should be equal to the ionic mobility of the background electrolyte ions (see also eq 2). At low flow velocities, this was indeed the case for several background electrolytes, which points at stable zones of immobilized background electrolyte. Moreover, the upstream local electric field was independent of the externally applied voltage (using equal flow velocities), which is evidence of

local electric field adjustment to the isotachophoretic condition: ions in plateau mode must have a uniform value of the ratio  $v_{\text{flow}}/E$ . At higher flow velocities, the concentration polarization effect broke down and the focusing condition was no longer present. In the same research, separation of analytes into adjacent zones was observed, although it was not clear whether these zones were peaks or plateaus. The authors explained their findings as being consistent with ITP.

In BEF, Hlushkou et al.<sup>98</sup> observed both in experiments and simulations that a focusing analyte (bodipy disulfonate) reached a plateau concentration independent of the starting concentration. This plateau concentration was about five times lower than the electrolyte concentration (1 mmol/L TrisHCL). Simulated profiles of the electric field distribution revealed a growing plateau, which extended the electric field gradient. Although the authors do not mention ITP effects as a possible explanation, we do think their results are consistent with ITP. In another paper on BEF, Laws et al.<sup>99</sup> used up to three fluorescent analytes, which they were able to separate. Although some of these separations appeared to occur in peak mode, one of the video's in the supplementary information of that paper clearly showed a rapidly broadening weakly fluorescent zone, which spaced some other analytes apart (figure 6 c-e). The length of this zone (>5 mm) stretched well beyond the predicted range of the electrode-induced electric field gradient. The fluorescence intensity in this zone appeared to be approximately constant. The authors did not comment on this zone in their paper, but we strongly suspect that it has an isotachophoretic nature. Finally, in a recent publication describing BEF focusing of the cationic species  $[\text{Ru}(\text{bpy})_3]^{2+}$ , the formation of a plateau-shaped analyte zone was also observed<sup>100</sup>.

### *dzITP*

The clearest case of an ITP separation induced by EFGF is perhaps depletion zone isotachopheresis (dzITP). dzITP was recently developed in our lab using conventional H-shaped micro/nanofluidic CP devices (figure 7a)<sup>101</sup>. At the upstream border of the depletion zone, analytes were focused and, if present in sufficient concentrations, plateau zones were readily formed (figure 7b). Discrete and continuous injections were performed for up to four fluorescent analytes and were separated in ITP zones. Using a non-fluorescent spacer, it was possible to elute a focused 6-carboxyfluorescein zone towards the upstream reservoir, while keeping fluorescein focused at a stable position at the depletion zone border (figure 7c). Moreover, positioning of the dzITP zones was possible by controlling the length of the upstream part of the depletion zone by means of voltage actuation. In a second paper on dzITP, we demonstrated the tunability of the ionic mobility window<sup>102</sup>. Focused compounds could be released along the depletion zone in the downstream part of the channel. Similar to a valve that can be opened to several extends, the flux of released compound could be controlled. This was used for both pulsed and continuous release. In continuous mode, a balance of fluxes of released and supplied compound established filter action. A marker compound was partially released, defining the ionic mobility cut-off. Undesired compounds are coreleased while compounds in the desired ionic mobility window are trapped behind the marker compound zone. This principle was applied to selectively enrich 6-carboxyfluorescein over lower-mobility fluorescein despite having a 250x lower starting concentration; to achieve this, acetate was used as a non-fluorescent spacer to establish the ionic mobility cut-off between fluorescein and 6-carboxyfluorescein (figure



7d). Additionally, for dilute raw urine fluorescein was used as a marker compound while simultaneously acting as an underspeeding tracer for indirect detection.

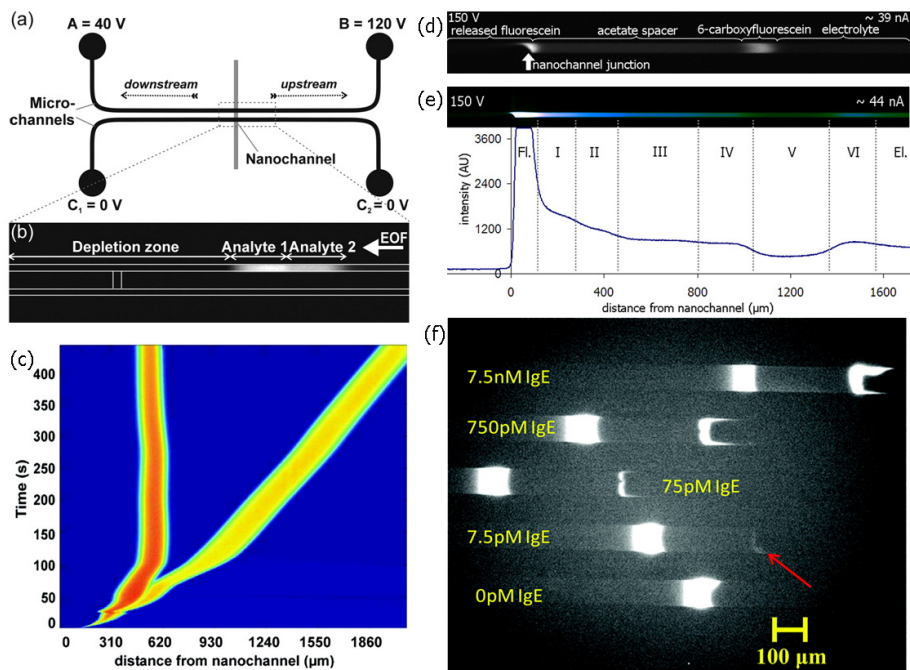


**Figure 7.** Functionality of dzITP. a) Schematic representation of a H-shaped concentration polarization device as used for depletion zone isotachopheresis. b) dzITP-separated zones at the border of a depletion zone. c) Spatiotemporal plot of a dzITP separation using a discrete injection of fluorescein and 6-carboxyfluorescein and a continuous injection of acetate. The acetate acts as a non-fluorescent spacer, eluting focused 6-carboxyfluorescein while fluorescein remains trapped at the border of the depletion zone. Images a-c reproduced with permission from ref. 101. d) selective enrichment of 6-carboxyfluorescein over fluorescein by ionic mobility filtering. e) Selective trapping and indirect detection of urine compounds using fluorescein as a marker. FL: fluorescein. EL:electrolyte. The Roman numerals I-VI indicate putative analyte zones. Images d and e reproduced with permission from ref. 102. f) Fluorescent aptamer assay for detection of several concentrations of IgE. The left fluorescent band arises from unbound aptamer, the band on the right arises from IgE-bound aptamer. The bands are spaced by non-fluorescent BSA protein. Image reproduced with permission from ref. 86.

This way, several urine constituents within a specific ionic mobility window were efficiently enriched and separated into distinct zones (figure 7e). Cheow et al<sup>86</sup> used dzITP in ultrasensitive IgE and HIV-1 RT assays, using fluorescent aptamers for detection. BSA was used as a non-fluorescent spacer between bound and unbound aptamer, improving detection (figure 7f).

## **Implications and perspectives**

### *Unification of ITP and EFGF*

In this review we have presented an argument for the unification of the concepts of ITP and EFGF. The bottomline of this argument is that ITP and EFGF are both founded on the isotachophoretic principle: all focused ions migrate with the same velocity in a completed separation. From the isotachophoretic principle many hallmarks of ITP can be derived, all of which have been observed in simulations and/or experimental research of EFGF methods. This includes the existence of analyte plateau concentrations independent of analyte starting concentrations but dependent on leading electrolyte concentration, adjustment of local electric field to the isotachophoretic condition, the formation of contiguous analyte bands, and the observation of plateaus in electric field and analyte velocity. Moreover, typical ITP tricks like the use of spacers and tracers can be applied to EFGF methods.

A possible counterargument is that EFGF methods generally do not use a discontinuous electrolyte system, comprising a LE and a TE in conventional ITP. However, the use of a LE/TE system should be regarded as one of the many ways in which the isotachophoretic condition can be imposed on a separation. Focusing gradients can be a fully-fledged alternative to a TE zone.

To underscore the role of ITP processes in EFGF, it will be useful to speak of peak mode and plateau mode EFGF, similar to peak mode and plateau mode ITP. Plateaus give a maximum to preconcentration, lead to alterations of the gradient profile, but also extend the separation beyond the original range of the gradient (figure 8) and give the possibility to apply many ITP tricks.

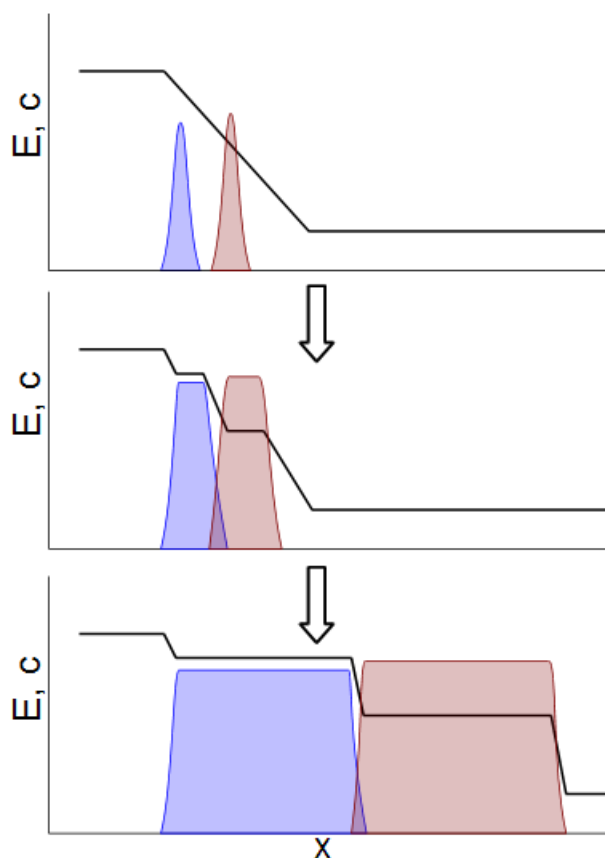


**Figure 8.** Transition from peak mode to plateau mode in EFGF. In peak mode (above), the electric field gradient is hardly affected by the focusing analytes. During the transition (middle), plateaus will form in the electric field gradient. After prolonged focusing in plateau mode, the analyte plateaus can grow far beyond the range of the original gradient (below).

#### *Advantages and disadvantages of EFGF*

EFGF techniques have several crucial advantages over conventional ITP, providing extra versatility which may make an EFGF technique a method of first choice. First, EFGF methods generally are single-electrolyte methods (CGF is an exception). This makes injection procedures more straightforward,

saves preparation and consumption of electrolyte solutions and will make EFGF more accessible to untrained personnel.

Second, EFGF can be induced at predefined and stable positions. This is also possible in ITP, but that requires special counterflow protocols. In DFGF and BPE, the focusing locations are simply determined by the placement of electrode(s), in TGF by the placement of heater elements, in EC and dzITP by the location of the nanochannel or nanoporous membrane, etc. Monitoring of the focusing and separation process is more straightforward with these methods.

Third, in many EFGF methods zone positioning is possible. This can be done by varying the counterflow, resulting in a shift of focusing positions. In TGF positioning also can be done by changing the location of the heater element, in DFGF by changing the voltage differences between the individual electrodes, and in dzITP by varying the position of the depletion zone border. Zone positioning allows repeated and on-demand detection, specific reactions and interactions with zones containing certain coatings and gels, and manipulations with local physical perturbations such as a magnetic field. Fourth, in several EFGF methods, including classical EFGF, DFGF, CGF and TGF, shallow gradients can be created, which is useful for resolving individual peaks with close mobilities. In conventional ITP this is often problematic.

Finally, in EFGF methods the ionic mobility window can be tuned during the experiment, for example by changing the counterflow velocity, or by varying the differences in electric field, or (as in dzITP filtering) by adjusting the balance between supply and release fluxes.

This provides enormous versatility in the selectivity of EFGF methods, which can be used for enrichment and purification strategies, as well as for

sequential trapping and analysis of different classes of compounds based on ionic mobilities.

EFGF methods have also a few disadvantages compared to conventional ITP. Perhaps the most important disadvantage is that EFGF methods require dedicated instrumentation, while conventional ITP can be performed in a simple CE capillary. Conventional ITP is compatible with commercial CE apparatuses while for EFGF methods hardly any commercial equipment exists (with the exception of EC<sup>74</sup>). With regard to miniaturization, on-chip ITP does not require the special components needed for EFGF methods like membranes, electrodes, heating elements or nanochannels. A second disadvantage, which affects only a limited range of applications, is that trailing-side injections are often difficult or even not possible in EFGF methods. In counterflow methods, the flow can strongly oppose trailing-side injections. Moreover, analyte velocity often only locally changes of sign. Consequently, trailing-side injected analytes are not transported towards the focusing region. Trailing-side injections may be crucial for some assays based on conventional ITP, for example when extracting high-mobility nucleic acids from low-mobility protein inhibitors.<sup>103</sup> Such assays might have poor feasibility with many EFGF-induced ITP methods.

#### *Synergism of ITP in EFGF*

The insight that EFGF methods have ITP nature leads to the realization of several important ITP phenomena in EFGF. An important aspect is that ITP can form zones that are pure with respect to co-ions. The insight that such zones also can be formed by EFGF may be useful for purification applications. A powerful ITP trick is the use of spacers. The baseline separation that may be

obtained by the use of a spacer is not only very useful for detection, but also for (bio)chemical assays. For example, undesired reactions may be prevented. Additionally, a reaction may be monitored by quantifying the amount of reaction product that is transferred across a spacer zone. Indirect detection by non-focusing tracers, such as the counterspeeder and underspeeder concept originally developed for ITP, is also applicable to EFGF. Another important lesson from ITP is that zones can grow indefinitely if sufficient compound is present. Similarly, in EFGF zones may grow beyond the range of the original gradient (figure 8). So if in EFGF plateau zones are allowed, peak capacity is not limited by the range of the gradient, but rather by the length of the separation channel upstream from the gradient.

Table 1 lists a number of features that are demonstrated or predicted in ITP and EFGF methods. Most demonstrated features have been discussed in the previous sections, and have been referenced if not so. The predicted features have been extrapolated from observations of similar features in other EFGF methods and may require adjustments of existing methods. In some cases a feature might not be available due to intrinsic limitations of a method. From table 1, a number of important observations can be made. First, all features demonstrated in conventional ITP have also been demonstrated in one or more EFGF methods. CP devices (including dzITP) stand out in this regard. Second, as discussed in the previous section, EFGF methods have several features not being available with conventional ITP, providing important extra functionality and simplicity of use. Third, once the predicted features are realized, these features might be combined at will, making each EFGF method a very versatile toolbox for bioanalysis.

**Table 1** Predicted and demonstrated features of ITP/EFGF methods

Feature	(transient) ITP	Classical EFGF	CGF	DFGF	TGF	BEF	EC	CP devices & dzITP
Analyte plateau zones	<b>d</b>	<b>d</b>	<b>d</b>	p	p	<b>d</b>	p	<b>d</b>
>10 000 fold preconcentration	<b>d</b>	<b>d</b>	p	p	<b>d</b>	<b>d</b>	p	<b>d</b>
Separation of proteins and peptides	<b>d</b>	<b>d</b>	<b>d</b>	<b>d</b>	<b>d</b>	p	<b>d</b>	<b>d</b>
Separation of nucleic acids	<b>d</b>	p	p	p	<b>d</b>	p	<b>d</b>	p
Separation of small molecules/ions	<b>d</b>	<b>d</b>	p	p	<b>d</b>	<b>d</b>	p	<b>d</b>
Dynamic control of analyte zone position		p	p	<b>d</b>	<b>d</b>	<b>d</b> <sup>103</sup>		<b>d</b>
Dynamic control of ionic mobility window		<b>d</b>	p	p	<b>d</b>	<b>d</b> <sup>104</sup>	<b>d</b>	<b>d</b>
Use of spacer compounds	<b>d</b>	p	p	p	p	p	p	<b>d</b>
Indirect analyte detection using tracers	<b>d</b>	p	p	p	p	p	p	<b>d</b>
Single electrolyte		<b>d</b>		<b>d</b>	<b>d</b>	<b>d</b>	<b>d</b>	<b>d</b>
Desalting	<b>d</b> <sup>105</sup>		p			p	<b>d</b>	<b>d</b>
Enzyme assays	<b>d</b> <sup>106</sup>	p	p	p	p	p	<b>d</b> <sup>107</sup>	<b>d</b>
Immunoassays	<b>d</b> <sup>108</sup>	p	p	p	p	p	p	<b>d</b>
Nucleic acid hybridization assays	<b>d</b>	p	p	p	<b>d</b>	p	p	p
Hyphenation with CE	<b>d</b>	p	p	p	p	p	<b>d</b> <sup>109</sup>	<b>d</b>
Hyphenation with MS	<b>d</b>	p	p	p	p	p	<b>d</b>	p

**d** = demonstrated, p = predicted

## Opportunities and outlook

With so many potential advantages for sensitivity and selectivity, ITP/EFGF methods will have many breakthrough applications in diverse fields of biology, including -omics studies, biomarker discovery, drug discovery and diagnostics. So far, all methods described above have been implemented either as a microfluidic setup, a capillary setup, or preparative scale setup. We expect particular benefit from the microfluidic and capillary setups in distinctive application fields.

For capillary ITP/EFGF setups we foresee highest impact in hyphenated settings. The use of transient ITP to enhance CE separations has already been proven a powerful technique. Increased usability is expected as the LE/TE buffer system is replaced with a single electrolyte system, simplifying sample preparation and injection procedures. In addition, the intrinsic concentration and clean-up capabilities of such a system may add to the reproducibility and sensitivity of CE separations. Another promising application will be direct hyphenation with mass spectrometry (MS). Electrocapture and concentration polarisation devices have shown powerful performance in desalting of samples, an operation that is highly important to prevent ion suppression in electron-spray mass spectrometry. Furthermore, dzITP has shown that focused analyte bands can be selectively released, enabling transport to the electrospray emitter on a band-by-band basis. This will also enhance sensitivity of MS-based detection. The clearest demonstration of this potential so far has been demonstrated in electrocapture<sup>72</sup>. EFGF methods will raise the quality of ITP separations and become an attractive complement or even an alternative for current day CE-MS, HPLC-MS and direct infusion MS techniques.

For microfluidic setups, the biggest opportunities lie in the field of molecular interaction assays. For such type of assays, the fact that one can trap molecular species in solution reduces surface interactions that are a typical disturbance in solid-phase immobilized assays. The fact that molecular compounds of lower mobility or opposite charge can be flushed through focused analyte zones dramatically increases binding and interaction efficiencies. Similar opportunities exist for multiple reagents that are concentrated in overlapping peak mode zones. Quantification through



measurement of zone growth enables real-time determination of binding constants and enzyme activity. A promising example is the aptamer dzITP assay presented by Cheow et al.<sup>86</sup> When adding functionality like selective ionic mobility filtering and the use of spacers and tracers, a molecular interaction platform of unprecedented versatility is obtained. We envision many impactful biochemical assays, including protein-protein and protein/nucleic acid interaction assays for determining binding constants; enzyme activity assays, amongst which protein kinase-inhibitor assays are important as many kinases play a significant role in cancer and other diseases; immunoassays; metabolite-protein interaction platforms for drug discovery purposes; and nucleic acid hybridization assays. These assays, being made sensitive and specific, do not necessarily require complicated instrumentation like MS or NMR, but will become available as stand-alone benchtop instruments for rapid diagnostics suitable for clinical settings. By integrating microelectronics and miniaturized detection technology, ITP/EFGE methods will be available as hand-held analyzers<sup>iii</sup> that may be used for water and food quality monitoring, homeland security and point-of-care diagnostics.

## **Conclusion**

A large number of EFGE and ITP techniques have been developed to-date and a wide range of applications and functionality have been demonstrated. In this review we have presented arguments and strong evidence from literature for the unification of both techniques, implying that EFGE and ITP functionality might be integrated on a single platform. This combined toolbox includes amongst others ultra-efficient and selective preconcentration, separation, tunable analyte focusing windows, requirement of a single

electrolyte only, and the ability to desalt and clean-up samples. Among the most promising applications are hyphenation with CE and MS for -omics studies and biomarker discovery, as well as a wide range of molecular interaction assays for drug screening and clinical diagnostics.

## References

1. B. Jung, R. Bharadwaj and J. G. Santiago, *Analytical Chemistry* **78** (7), 2319-2327 (2006).
2. D. Bottenus, T. Z. Jubery, Y. Ouyang, W.-J. Dong, P. Dutta and C. F. Ivory, *Lab on a Chip* **11** (5), 890-898 (2011).
3. J. Wang, Y. Zhang, M. R. Mohamadi, N. Kaji, M. Tokeshi and Y. Baba, *Electrophoresis* **30** (18), 3250-3256 (2009).
4. Y.-C. Wang, A. L. Stevens and J. Han, *Analytical Chemistry* **77** (14), 4293-4299 (2005).
5. S. M. Kim, M. A. Burns and E. F. Hasselbrink, *Analytical Chemistry* **78** (14), 4779-4785 (2006).
6. R. K. Anand, E. Sheridan, K. N. Knust and R. M. Crooks, *Analytical Chemistry* **83** (6), 2351-2358 (2011).
7. M. Kim, M. Jia and T. Kim, *Analyst* (2013).
8. P. H. Humble, R. T. Kelly, A. T. Woolley, H. D. Tolley and M. L. Lee, *Analytical Chemistry* **76** (19), 5641-5648 (2004).
9. D. Ross and L. E. Locascio, *Analytical Chemistry* **74** (11), 2556-2564 (2002).
10. Z. K. Shihabi, *Journal of Chromatography A* **902** (1), 107-117 (2000).
11. J. L. Beckers and P. Boček, *Electrophoresis* **21** (14), 2747-2767 (2000).
12. D. M. Osbourn, D. J. Weiss and C. E. Lunte, *Electrophoresis* **21** (14), 2768-2779 (2000).
13. M. Urbánek, L. Křivánková and P. Boček, *Electrophoresis* **24** (3), 466-485 (2003).
14. R.-L. Chien, *Electrophoresis* **24** (3), 486-497 (2003).
15. C.-H. Lin and T. Kaneta, *Electrophoresis* **25** (23-24), 4058-4073 (2004).
16. M. C. Breadmore, *Electrophoresis* **28** (1-2), 254-281 (2007).
17. Z. Malá, A. Šlampová, P. Gebauer and P. Boček, *Electrophoresis* **30** (1), 215-229 (2008).
18. S. L. Simpson Jr, J. P. Quirino and S. Terabe, *Journal of Chromatography A* **1184** (1-2), 504-541 (2008).

19. M. C. Breadmore, J. R. E. Thabano, M. Dawod, A. A. Kazarian, J. P. Quirino and R. M. Guijt, *Electrophoresis* **30** (1), 230-248 (2009).
20. M. C. Breadmore, M. Dawod and J. P. Quirino, *Electrophoresis* **32** (1), 127-148 (2011).
21. L. Kartsova and E. Bessonova, *Journal of Analytical Chemistry* **64** (4), 326-337 (2009).
22. Z. Malá, P. Gebauer and P. Boček, *Electrophoresis* **32** (1), 116-126 (2011).
23. B. C. Giordano, D. S. Burgi, S. J. Hart and A. Terray, *Analytica chimica acta* (2012).
24. Y. Chen, W. Lü, X. Chen and M. Teng, *Central European Journal of Chemistry*, 1-28 (2012).
25. A. Šlampová, Z. Malá, P. Pantůčková, P. Gebauer and P. Boček, *Electrophoresis* (2012).
26. C.-C. Lin, J.-L. Hsu and G.-B. Lee, *Microfluidics and Nanofluidics* **10** (3), 481-511 (2011).
27. K. Sueyoshi, F. Kitagawa and K. Otsuka, *Journal of separation science* **31** (14), 2650-2666 (2008).
28. M. C. Breadmore, A. I. Shallan, H. R. Rabanes, D. Gstoettenmayr, A. S. Abdul Keyon, A. Gaspar, M. Dawod and J. P. Quirino, *Electrophoresis* **34** (1), 29-54 (2013).
29. C. J. Holloway and I. Trautschold, *Fresenius' Journal of Analytical Chemistry* **311** (2), 81-93 (1982).
30. J. Petr, V. Maier, J. Horáková, J. Ševčík and Z. Stránský, *Journal of separation science* **29** (18), 2705-2715 (2006).
31. G. Garcia-Schwarz, A. Rogacs, S. S. Bahga and J. G. Santiago, *Journal of Visualized Experiments* (61) (2012).
32. P. Gebauer and P. Boček, *Electrophoresis* **18** (12-13), 2154-2161 (1997).
33. P. Gebauer and P. Boček, *Electrophoresis* **21** (18), 3898-3904 (2000).
34. P. Gebauer and P. Boček, *Electrophoresis* **23** (22-23), 3858-3864 (2002).
35. P. Gebauer, Z. Malá and P. Boček, *Electrophoresis* **28** (1-2), 26-32 (2007).
36. P. Gebauer, Z. Malá and P. Boček, *Electrophoresis* **30** (1), 29-35 (2009).
37. P. Gebauer, Z. Malá and P. Boček, *Electrophoresis* **32** (1), 83-89 (2011).
38. Z. Malá, P. Gebauer and P. Boček, *Electrophoresis* (2012).
39. J. G. Shackman and D. Ross, *Electrophoresis* **28** (4), 556-571 (2007).
40. C. Ivory, *Separation Science and Technology* **35** (11), 1777-1793 (2000).
41. R. T. Kelly and A. T. Woolley, *Journal of separation science* **28** (15), 1985-1993 (2005).
42. M. M. Meighan, S. J. R. Staton and M. A. Hayes, *Electrophoresis* **30** (5), 852-865 (2009).

43. C. A. Vyas, P. M. Flanigan and J. G. Shackman, *Bioanalysis* **2** (4), 815-827 (2010).
44. F. Kohlrausch, *Annalen der Physik* **298** (10), 209-239 (1897).
45. V. Hruška and B. Gaš, *Electrophoresis* **28** (1-2), 3-14 (2007).
46. T. K. Khurana and J. G. Santiago, *Analytical Chemistry* **80** (1), 279-286 (2007).
47. R. D. Chambers and J. G. Santiago, *Analytical Chemistry* **81** (8), 3022-3028 (2009).
48. T. K. Khurana and J. G. Santiago, *Analytical Chemistry* **80** (16), 6300-6307 (2008).
49. D. Kaniansky, M. Masár, J. Bielčíková, F. Iványi, F. Eisenbeiss, B. Stanislowski, B. Grass, A. Neyer and M. Jöhnck, *Analytical Chemistry* **72** (15), 3596-3604 (2000).
50. M. Bercovici, C. M. Han, J. C. Liao and J. G. Santiago, *Proceedings of the National Academy of Sciences* **109** (28), 11127-11132 (2012).
51. D. Bottenus, T. Z. Jubery, P. Dutta and C. F. Ivory, *Electrophoresis* **32** (5), 550-562 (2011).
52. S. S. Bahga and J. G. Santiago, *Analyst* **138** (3), 735-754 (2013).
53. A. A. Kazarian, E. F. Hilder and M. C. Breadmore, *Journal of separation science* **34** (20), 2800-2821 (2011).
54. W. S. Koegler and C. F. Ivory, *Journal of Chromatography A* **726** (1-2), 229-236 (1996).
55. W. S. Koegler and C. F. Ivory, *Biotechnology Progress* **12** (6), 822-836 (1996).
56. J. Liu, X. Sun, P. B. Farnsworth and M. L. Lee, *Analytical Chemistry* **78** (13), 4654-4662 (2006).
57. Q. Wang, S.-L. Lin, K. F. Warnick, H. D. Tolley and M. L. Lee, *Journal of Chromatography A* **985** (1-2), 455-462 (2003).
58. D. N. Petsev, G. P. Lopez, C. F. Ivory and S. S. Sibbett, *Lab on a Chip* **5** (6), 587-597 (2005).
59. R. D. Greenlee and C. F. Ivory, *Biotechnology Progress* **14** (2), 300-309 (1998).
60. D. W. Inglis, E. M. Goldys and N. P. Calander, *Angewandte Chemie International Edition* **50** (33), 7546-7550 (2011).
61. Z. Huang and C. F. Ivory, *Analytical Chemistry* **71** (8), 1628-1632 (1999).
62. N. I. Tracy, Z. Huang and C. F. Ivory, *Biotechnology Progress* **24** (2), 444-451 (2008).
63. N. I. Tracy and C. F. Ivory, *Electrophoresis* **29** (13), 2820-2827 (2008).
64. J. M. Burke, Z. Huang and C. F. Ivory, *Analytical Chemistry* **81** (19), 8236-8243 (2009).
65. S. M. Kim, G. J. Sommer, M. A. Burns and E. F. Hasselbrink, *Analytical Chemistry* **78** (23), 8028-8035 (2006).
66. Z. Ge, C. Yang and G. Tang, *International Journal of Heat and Mass Transfer* **53** (13-14), 2722-2731 (2010).

67. G. J. Sommer, S. M. Kim, R. J. Littrell and E. F. Hasselbrink, *Lab Chip* **7** (7), 898-907 (2007).
68. M. Akbari, M. Bahrami and D. Sinton, *Microfluidics and Nanofluidics* **12** (1), 221-228 (2012).
69. K. M. Balss, D. Ross, H. C. Begley, K. G. Olsen and M. J. Tarlov, *Journal of the American Chemical Society* **126** (41), 13474-13479 (2004).
70. S. J. Hoebel, K. M. Balss, B. J. Jones, C. D. Malliaris, M. S. Munson, W. N. Vreeland and D. Ross, *Analytical Chemistry* **78** (20), 7186-7190 (2006).
71. M. Shariatgorji, J. Astorga-Wells and L. Ilag, *Anal Bioanal Chem* **399** (1), 191-195 (2011).
72. J. Astorga-Wells, H. Jörnvall and T. Bergman, *Analytical Chemistry* **75** (19), 5213-5219 (2003).
73. S. Vollmer, J. Astorga-Wells, T. Bergman and H. Jörnvall, *International Journal of Mass Spectrometry* **259** (1-3), 73-78 (2007).
74. [http://www.epizell.com/service\\_electrocapture.html](http://www.epizell.com/service_electrocapture.html).
75. R. Dhopeshwarkar, D. Hlushkou, M. Nguyen, U. Tallarek and R. M. Crooks, *Journal of the American Chemical Society* **130** (32), 10480-10481 (2008).
76. R. K. Perdue, D. R. Laws, D. Hlushkou, U. Tallarek and R. M. Crooks, *Analytical Chemistry* **81** (24), 10149-10155 (2009).
77. K. N. Knust and R. M. Crooks, *Lab on a Chip* (2012).
78. T. A. Zangle, A. Mani and J. G. Santiago, *Chemical Society Reviews* **39** (3), 1014-1035 (2010).
79. S. J. Kim, Y. A. Song and J. Han, *Chemical Society Reviews* **39** (3), 912-922 (2010).
80. Q. Pu, J. Yun, H. Temkin and S. Liu, *Nano Letters* **4** (6), 1099-1103 (2004).
81. R. B. Schoch, J. Han and P. Renaud, *Reviews of Modern Physics* **80** (3), 839 (2008).
82. J. H. Lee, Y.-A. Song, S. R. Tannenbaum and J. Han, *Analytical Chemistry* **80** (9), 3198-3204 (2008).
83. J. H. Lee, B. D. Cosgrove, D. A. Lauffenburger and J. Han, *Journal of the American Chemical Society* **131** (30), 10340-10341 (2009).
84. A. Sarkar and J. Han, *Lab on a Chip* **11** (15), 2569-2576 (2011).
85. Y.-C. Wang and J. Han, *Lab on a Chip* **8** (3), 392-394 (2008).
86. L. F. Cheow and J. Han, *Analytical Chemistry* **83** (18), 7086-7093 (2011).
87. J. H. Lee and J. Han, *Microfluidics and Nanofluidics* **9** (4), 973-979 (2010).
88. S. H. Ko, S. J. Kim, L. F. Cheow, L. D. Li, K. H. Kang and J. Han, *Lab on a Chip* **11** (7), 1351-1358 (2011).
89. C. Wang, J. Ouyang, D.-K. Ye, J.-J. Xu, H.-Y. Chen and X.-H. Xia, *Lab on a Chip* **12** (15), 2664-2671 (2012).

90. S. J. Kim, S. H. Ko, K. H. Kang and J. Han, *Nature Nanotechnology* 5 (4), 297-301 (2010).
91. J. H. Lee, Y.-A. Song and J. Han, *Lab on a Chip* 8 (4), 596-601 (2008).
92. S. H. Ko, Y.-A. Song, S. J. Kim, M. Kim, J. Han and K. H. Kang, *Lab on a Chip* 12 (21), 4472-4482 (2012).
93. C. H. Kuo, J. H. Wang and G. B. Lee, *Electrophoresis* 30 (18), 3228-3235 (2009).
94. J. Quist B. Trietsch, P. Vulto, T Hankemeier (submitted).
95. T. K. Khurana and J. G. Santiago, *Lab Chip* 9 (10), 1377-1384 (2009).
96. H. Lin, J. G. Shackman and D. Ross, *Lab on a Chip* 8 (6), 969-978 (2008).
97. J. Astorga-Wells, S. Vollmer, T. Bergman and H. Jörnval, *Analytical Chemistry* 79 (3), 1057-1063 (2007).
98. D. Hlushkou, R. K. Perdue, R. Dhopeswarkar, R. M. Crooks and U. Tallarek, *Lab Chip* 9 (13), 1903-1913 (2009).
99. D. R. Laws, D. Hlushkou, R. K. Perdue, U. Tallarek and R. M. Crooks, *Analytical Chemistry* 81 (21), 8923-8929 (2009).
100. E. Sheridan, D. Hlushkou, K. N. Knust, U. Tallarek and R. M. Crooks, *Analytical Chemistry* 84 (17), 7393-7399 (2012).
101. J. Quist, K. G. H. Janssen, P. Vulto, T. Hankemeier and H. J. van der Linden, *Analytical Chemistry* 83 (20), 7910-7915 (2011).
102. J. Quist, P. Vulto, H. van der Linden and T. Hankemeier, *Analytical Chemistry* 84 (21), 9065-9071 (2012).
103. A. Rogacs, Y. Qu and J. G. Santiago, *Analytical Chemistry* (2012).
104. R. K. Anand, E. Sheridan, D. Hlushkou, U. Tallarek and R. M. Crooks, *Lab Chip* 11 (3), 518-527 (2010).
105. E. Sheridan, K. N. Knust and R. M. Crooks, *Analyst* 136 (20), 4134-4137 (2011).
106. V. Shkolnikov, S. S. Bahga and J. G. Santiago, *Physical Chemistry Chemical Physics* (2012).
107. G. Bruchelt, M. Buedenbender, K.-H. Schmidt, B. Jopski, J. Treuner and D. Niethammer, *Journal of Chromatography A* 545 (2), 407-412 (1991).
108. J. Astorga-Wells, T. Bergman and H. Jörnval, *Analytical Chemistry* 76 (9), 2425-2429 (2004).
109. C. C. Park, I. Kazakova, T. Kawabata, M. Spaid, R.-L. Chien, H. G. Wada and S. Satomura, *Analytical Chemistry* 80 (3), 808-814 (2008).
110. J. Astorga-Wells and H. Swerdlow, *Analytical Chemistry* 75 (19), 5207-5212 (2003).
111. G. Kaigala, M. Bercovici, M. Behnam, D. Elliott, J. Santiago and C. Backhouse, *Lab on a Chip* 10 (17), 2242-2250 (2010).

# 3

## Single-Electrolyte Isotachophoresis Using a Nanochannel-Induced Depletion Zone

*Published in Analytical Chemistry, 2011, 83 (20), pp 7910–7915*

Isotachophoretic separations are triggered at the border of a nanochannel-induced ion-depleted zone. This depletion zone acts as a terminating electrolyte and is created by concentration polarization over the nanochannel. We show both continuous and discrete sample injections as well as separation of up to four analytes. Continuous injection of a spacer compound was used for selective analyte elution. Zones were kept focused for over one hour, while shifting less than 700  $\mu\text{m}$ . Moreover, zones could be deliberately positioned in the separation channel and focusing strength could be precisely tuned employing a three-point voltage actuation scheme. This makes depletion zone isotachophoresis (dzITP) a fully controllable single-electrolyte focusing and separation technique. For on-chip electrokinetic methods, dzITP sets a new standard in terms of versatility and operational simplicity.

Isotachophoresis (ITP) is a powerful electrokinetic technique for the concentration, separation, purification, and quantification of ionic analytes, especially when downscaled to microfluidic devices.<sup>1, 2</sup> In 1998, Walker et al. were among the first to demonstrate on-chip ITP using Raman spectroscopy to detect herbicides.<sup>3</sup> Kanianski et al. coupled ITP to capillary electrophoresis (CE) on a chip and showed isotachopherograms of up to 14 analytes.<sup>4</sup> Several

reports describe over 10,000-fold concentration.<sup>5-7</sup> Jung et al. even reported millionfold sample stacking using transient ITP.<sup>8</sup> Miniaturized ITP is applicable to a broad range of samples, including toxins from tap water,<sup>9</sup> explosive residues,<sup>10</sup> proteins,<sup>11</sup> DNA from PCR samples,<sup>12, 13</sup> nucleic acids from whole blood,<sup>14</sup> and small RNA molecules from cell lysate.<sup>15</sup> Hybridization of RNAs with molecular beacons by ITP<sup>16</sup> was applied to bacterial rRNAs from urine,<sup>17</sup> demonstrating the potential of on-chip ITP for biochemical assays. A major recent achievement was the integration of an ITP chip and laser-induced-fluorescence (LIF) detection into a single handheld device.<sup>18</sup> Nevertheless, ITP has still to come to its full potential, as until now it has not been widely used for bioanalytical applications.<sup>19-21</sup> A major limitation is that ITP requires a sample to be injected between a leading electrolyte and a terminating electrolyte. Compared to, e.g., capillary electrophoresis (CE), which uses a single electrolyte only, handling and method development is not straightforward. Another limitation of conventional ITP is that analyte zone positions are difficult to control. This is due to the different conductivities of the ITP zones, resulting in continuous changes of electric field distributions during electromigration. Several stationary ITP strategies have been developed to alleviate this limitation. One such strategy employs a hydrodynamic counterflow, but this has the disadvantage of dispersion due to a parabolic flow profile.<sup>22</sup> A more elegant strategy is balancing the electrophoretic motion of the ITP zones by an opposite electro-osmotic flow (EOF).<sup>23-26</sup> However, with this method it is still complicated to change analyte zone positions in a controlled manner without changing pH or electrolyte concentrations.



In this paper we overcome the mentioned limitations by a radically different approach which combines the strengths of on-chip ITP with the merits of nanofluidic concentration devices.<sup>27, 28</sup> These devices, which have been extensively reviewed by Kim et al.,<sup>29</sup> are in fact miniaturized variants of electrocapture devices. Electrocapture is a powerful method which utilizes capillaries with perm-selective membrane junctions for trapping and selective release of ionic compounds.<sup>30, 31</sup> In nanofluidic concentration devices, at least two parallel microchannels are connected by a nanochannel, over which an electric field is applied (Figure 1a). Asymmetric distribution of anions and cations<sup>32, 33</sup> makes the nanochannel perm-selective, leading to concentration polarization.<sup>34-36</sup> This causes the formation of a depletion zone in the anodic microchannel. A tangential EOF through this microchannel transports analytes toward the border of the depletion zone, where they are trapped (Figure 1b). Various groups have investigated devices based on similar principles,<sup>37-43</sup> showing that this has become a very active research field within a short time. Potential applications include immunoassays,<sup>44-47</sup> enzyme assays,<sup>44, 48, 49</sup> massive parallelization,<sup>50, 51</sup> and desalination.<sup>52</sup> Here we employ a depletion zone to induce isotachophoretic separations. To our knowledge, this is the first time such separations are demonstrated in nanofluidic concentration devices. Depletion zone isotachopheresis (dzITP), as we coin this novel approach, is performed with a single electrolyte only. A three-point voltage actuation scheme gives complete control over the position of the zones and the sharpness of their borders, utilizing the fact that the method is quasistatic. The simplicity and versatility of our method makes it a powerful new tool in the electrokinetic focusing and separation toolkit.

## Experimental Section

### *Chemicals*

Lithium carbonate was obtained from Acros Organics (Geel, Belgium), disodium fluorescein was obtained from Riedel-de Haën (Seelze, Germany), 6-carboxyfluorescein was obtained from Sigma-Aldrich (Steinheim, Germany), and sodium acetate was obtained from Merck (Darmstadt, Germany). FITC-labeling of glutamate and leucine was performed as follows. To 0.5 mmol of amino acid an aqueous solution of potassium hydroxide, 1 g/ml, was added in a 1:1 weight:volume ratio, followed by addition of 1 ml of ethanol. Under vigorous stirring on ice, a suspension of FITC in ethanol (1 mol/L) was added to the amino acid in a molar ratio of 1:1; together with 1 ml 0.5 mol/L potassium hydroxide and 0.5 mL ethanol. This mixture was left on ice to react for 2 h in the dark under continued stirring. Purification of the reaction product was performed using a Gilson preparative HPLC system (Gilson, Inc., Middleton, USA) equipped with a Phenomex Gemini C18 column, 15x21 mm, 5 micron (Phenomenex, Torrance, USA) using an acetonitrile/water (10 mmol/L ammonium acetate, pH=8) gradient. Purity of compounds was established with LC-UVMS and CZE-LIF and found to be > 99%. After freeze-drying, each purified FITC-amino acid was dissolved in dimethyl sulfoxide (DMSO), 1.0 mmol/L, and stored at -80°C awaiting experiments.

In all experiments, 2.0 mmol/L lithium carbonate, pH 10.6, was used as the background electrolyte. Solutions were prepared fresh before experiments.

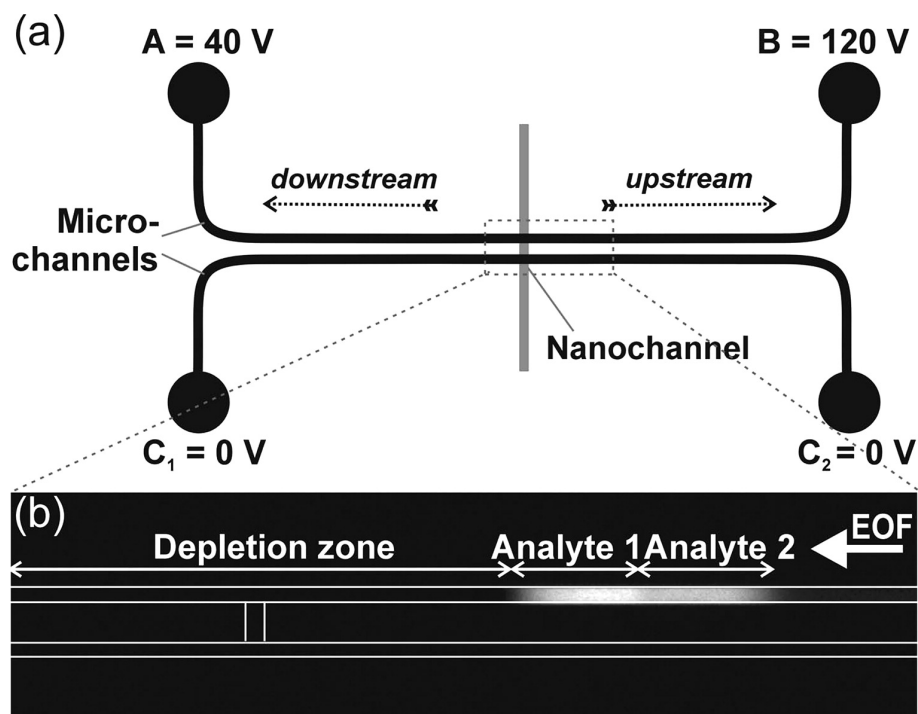


**Figure 1.** (a) Chip layout consisting of two microchannels and one nanochannel. An example of three-point voltage actuation is provided: A is the downstream voltage and B the upstream voltage, while the lower channel is connected to ground, as represented by voltages  $C_{1,2} = 0$  V. Downstream and upstream directions are indicated by dashed arrows. (b) Example of dzITP separated zones. The channel contains a depletion zone that extends mostly in the downstream channel. Analytes focus at the border of the depletion zone and order themselves in clearly distinguishable zones. Lines that indicate micro- and nanochannels were drawn onto the CCD images.

### Chip Fabrication

Chips were fabricated in Pyrex wafers using standard lithography techniques and deep reactive ion etching (DRIE). Photoresists (SU 8-10 and ma-P 1275) and developers (mr-Dev 600 and ma-D 331) were obtained from Microresist Technologies (Berlin, Germany). N-methylpyrrolidone (NMP) was obtained

from Rathburn Chemicals (Walkerburn, Scotland). AbsorbMax<sup>TM</sup> film, fuming nitric acid (100%) and hexamethyldisilazane (HMDS) were obtained from Sigma-Aldrich (Steinheim, Germany). Chips containing micro- and nanochannels were fabricated in 4" Pyrex<sup>®</sup> wafers (Si-Mat, Kaufering, Germany). The wafers were spin coated with SU 8-10; the wafer was first accelerated to 500 rpm in 5 seconds to allow resist spreading, directly followed by an acceleration to 2000 rpm in 5 seconds, which was maintained for 30 seconds. After spin coating, the resist was allowed to settle for 8 hours at room temperature, after which the resist was prebaked using a hotplate by controlled heating to 95°C in 8 minutes, followed by ambient cool down. The resist was exposed at 6 mW/cm<sup>2</sup> for 25 seconds in a Suss MA 45 mask aligner (Karl Suss KG, München-Garching, Germany) in which a Hoya UV<sub>34</sub> filter (LG optical, Churchfield, UK) was installed to prevent SU 8 T-topping. During exposure AbsorbMax film was attached to the back side of the wafer, to prevent undesired reflections. The microchannel pattern was transferred using a 5" chromium mask (Delta Mask, Enschede, The Netherlands). A post-exposure bake was done by controlled heating to 95°C in 8 minutes, followed by ambient cool down. Development was done for 3 minutes in mr-Dev 600 developer followed by washing in isopropanol and demineralized water. Using the developed SU 8 resist as a mask, microchannels were etched into the glass wafers by a 1 hour deep reactive ion etching (DRIE) step. DRIE was performed in an Oxford Plasmalab 90+ parallel plate reactor (Oxford Instruments, Abingdon, United Kingdom) using an argon/SF<sub>6</sub> plasma. Gas flows were 20 sccm for argon and 25 sccm for SF<sub>6</sub>. After establishing a stable plasma at 10 mTorr, pressure was set at 2 mTorr. Forward power was 200W. After etching, the SU 8 resist was stripped by placing the wafers in NMP for several hours at

70°C, followed by removal of remaining particles in a fuming nitric acid bath. The wafers were rinsed in water, spin-dried, and baked for 5 minutes at 110°C for dehydration. The wafers were spin coated with HMDS followed by a curing bake at 150°C for 5 minutes. Next, ma-P resist was spin coated at 1000 rpm for 30 seconds preceded by 10 seconds of acceleration. The resist was prebaked for 5 minutes at 95°C. Transfer of the nanochannel pattern was performed by an exposure step as performed as described above. Development was done with ma-D 331 developer for 5 minutes. To etch the nanochannels, DRIE was performed with same parameters as described above, except for the etch time, which was 100 seconds. The ma-P resist was stripped with acetone. Micro- and nanochannel depths were measured with a Dektak 150 profilometer (Veeco, Tucson, AZ) and by scanning electron microscopy using a FEI NovaTM NanoSEM apparatus (FEI, Hillsboro, OR). Each etched wafer was bonded with a second pyrex wafer. In these wafers, fluidic access holes were ultrasonically drilled using a diamond bit. Both wafers were subsequently cleaned in acetone, piranha acid and nitric acid, followed by a 1 minute dip in KOH. A pre-bond was realized upon application of manual pressure, after which direct bonding was performed in an oven (Model P320, Nabertherm GmbH, Lilienthal, Germany). The temperature was ramped to 600°C in 3 h, which temperature was maintained for 4 h, followed by cooling to room temperature with a rate of 50°C/h. After bonding, wafers were not diced, a whole wafer was used from which a single chip was selected. The microchannels had 1.7 µm depth and 20 µm width. Microchannel lengths between fluid reservoirs and the nanochannel were 0.91 cm. The nanochannel that connected the two microchannels was 60 nm deep, 25 µm wide, and 50 µm long.

### *Chip Preparation*

The chip was prefilled with ethanol to eliminate air trapping, after which the chip was flushed at least 15 min with 100 mmol/L NaOH, 15 min with demineralized water, and 15 min with background electrolyte (2.0 mmol/L lithium carbonate). Fluid replacement and flushing was accomplished by leaving the fluid reservoir at one end of a microchannel empty. A combination of capillary action and evaporation of fluid generated a flow which was sufficient to replace all fluid in a microchannel in approximately 3 min. Reservoirs were washed 3 times after fluid replacement. After flushing, all channels and reservoirs were filled with the background electrolyte (2.0 mmol/L lithium carbonate).

### *Setup and Microscopy*

Access holes were extended with fluidic reservoirs (volume 100  $\mu$ L) using a custom-build interface that was attached to the chip surface using a vacuum. The fluidic reservoirs were electrically connected using gold electrodes. Two power supplies (ES 0300 045, Delta Elektronika BV, Zierikzee, The Netherlands) were controlled via the analog outputs of an NI USB 6221 data acquisition system using LabVIEW 8.2 software (National Instruments, Austin, TX). For fluorescence microscopy, an Olympus IX71 microscope (Olympus, Zoeterwoude, The Netherlands) was used in combination with an Hamamatsu Orca-ER digital camera and Hokawo version 2.1 imaging software (Hamamatsu Photonics, Nuremberg, Germany). The magnification was 40 $\times$ . To minimize photobleaching, low lamp intensities were combined with 1.0 s integration times.

### *Data Processing*

Spatiotemporal plots (Figure 2) were composed using MATLAB, by adjoining fluorescence profiles obtained from image sequences that were recorded during the experiments. Fluorescence profiles were obtained by averaging 50 image lines and correcting them for background signal. False colors were assigned to represent fluorescence intensity. Raw CCD images were used in Figure 3. Fluorescence profiles were obtained from the CCD images and were smoothed by averaging over 5 pixels. Slope values were determined at the inflection points of the smoothed profiles and normalized with respect to the maximum intensity value of the corresponding analyte zone. Locations of the edges of the zones were obtained by determining the position of the inflection point relative to the upstream edge of the nanochannel.

## **Results and Discussion**

### *Device Operation*

Figure 1a,b shows the general device operation for dzITP. The upper channel in Figure 1a,b is the separation channel; this is the channel where isotachophoretic zones are formed during the experiment. Three-point voltage actuation is utilized: to each of the access holes of the separation channel a voltage source is connected, while the other channel is connected to ground. Upon voltage application, concentration polarization takes place: an ion depletion zone forms in the separation channel, while in the other channel an ion enrichment zone forms (not shown here, see ref 29). Asymmetric voltage application over the separation channel yields an EOF through this channel. The channel arm between the higher voltage and the nanochannel is referred to as the “upstream channel”, while the arm between

the lower voltage and the nanochannel is referred to as the “downstream channel” (see Figure 1a). Downstream, the depletion zone continues to grow until the fluid reservoir is reached. This process sometimes appears to lead to fluctuations during the first 30–60 s of an experiment. In the upstream direction, depletion zone growth becomes balanced by the opposing EOF. When the downstream depletion zone reaches the outlet, the electrical resistance in this channel reaches a more stable value, resulting in a near-stable position for the upstream depletion zone border. At this border, analytes are focused based on a difference in ion density (for detailed theory, see Zangle et al.<sup>35</sup>). Meanwhile, analyte concentration and separation into adjacent zones is achieved according to isotachophoretic principles (see Figure 1b). The depletion zone serves here as a terminating electrolyte, and the background electrolyte takes the function of the leading electrolyte. They define the ionic mobility window of analytes that can be focused. The upper boundary of this mobility window is defined by the mobility of the leading ion in the background electrolyte: analytes with higher mobilities will be transported toward the reservoir. The lower boundary depends on the electric field in the depletion zone, which is very high. For example, Kim et al. measured a 30-fold amplified electric field in the depletion zone.<sup>53</sup> Only analytes with very low mobilities are transported through this barrier by EOF. As the current setup is based on a glass chip, the channels have a negative surface charge. Consequently, only anions are focused and separated at the depletion zone border. In order to enable focusing and separation of cations, the surface charge of the device should be reversed by applying a surface coating or by choosing a different substrate.



### *Discrete and Continuous Injections*

dzITP is demonstrated for both discrete and continuous injections (see Figure 2a,b). Fluorescein, 50  $\mu\text{mol/L}$ , and 6-carboxyfluorescein, 50  $\mu\text{mol/L}$ , were used as analytes; applied voltages were 120 V (upstream) and 40 V (downstream). For discrete injections, only the separation channel was filled with sample, while remaining channels and fluid reservoirs contained background electrolyte only. This resulted in a 309 pL injection volume, as calculated from the microchannel dimensions. Figure 2a shows that isotachophoretic separation continues until all analytes from the discrete sample are focused, after which the zone widths become constant. Over time, bending points can be observed in the growth rate of the analyte zones, as indicated by the arrows in Figure 2a. These bending points correspond to the exhaustion of fluorescein (arrow I) and 6-carboxyfluorescein (arrow II). Lower mobility compounds are exhausted at an earlier stage than compounds of higher mobility, the reason being that lower mobility compounds have a lower electrophoretic drift to counter the EOF, resulting in a higher net velocity. In continuous injections, the analytes were also placed in the upstream fluid reservoir, providing a practically inexhaustible supply of analytes. Therefore, zone broadening was continuous (see Figure 2b). Clearly, no bends due to analyte exhaustion were present. Zone broadening speed of the lower mobility compound (fluorescein) is higher than that of the higher mobility compound (6-carboxyfluorescein), again due to a higher net velocity. Continuous injections are therefore most advantageous for the extraction and focusing of low-concentration, low-mobility analytes, while discrete injections are useful in the quantitative analysis of multiple analytes.

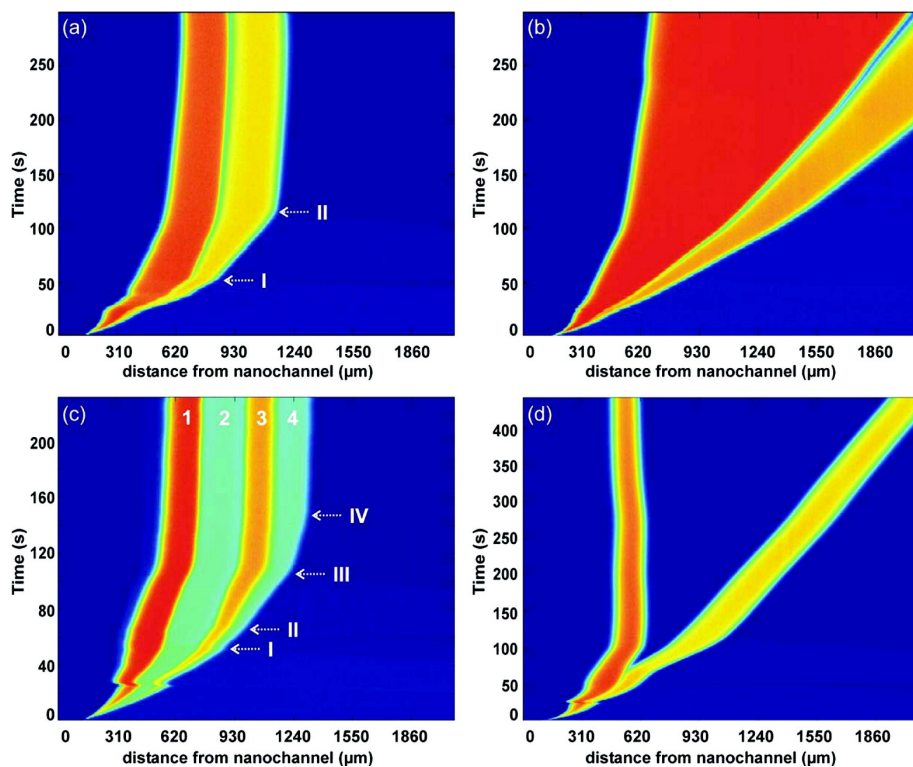


**Figure 2.** Spatiotemporal plots of dzITP separations. (a) Discrete injection of fluorescein and 6-carboxyfluorescein. Arrows I and II indicate exhaustion of fluorescein and 6-carboxyfluorescein, respectively. (b) Continuous injection of fluorescein and 6-carboxyfluorescein. (c) Discrete injection and separation of four compounds: fluorescein (1), FITC-leucine (2), 6-carboxyfluorescein (3), and FITC-glutamate (4). Arrows I-IV indicate exhaustion of these respective analytes. (d) Discrete injection of fluorescein and 6-carboxyfluorescein combined with a continuous injection of acetate.

### *Four-Compound Separation*

Figure 2c shows concentration and separation of four compounds. A discrete sample containing fluorescein, 6-carboxyfluorescein, FITC-leucine, and FITC-glutamate, 40 μmol/L each, was injected. External voltages were 120 V (upstream) and 40 V (downstream). Within 100 s, four zones of clearly

distinguishable fluorescence intensity were formed. Standard addition was used to assign the four zones to each of the four analytes: a doubled concentration of the respective analyte led approximately to a doubling of the width of the corresponding zone ( Figure 3). Here, too, bends in the profile coincide with the exhaustion of each of the respective analytes.

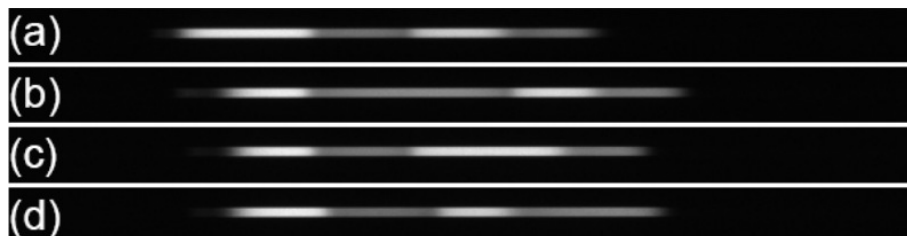


**Figure 3.** Analyte zone identification by standard addition. In each experiment, the four analytes (fluorescein, FITC-leucine, 6-carboxyfluorescein and FITC-glutamate) were present in concentrations of 30  $\mu\text{mol/L}$ , except for the analyte to be identified, which had a concentration of 60  $\mu\text{mol/L}$ . Discrete injections were performed. From left to right, the four zones were identified as follows: a) first zone: fluorescein; b) second zone: FITC-leucine; c) third zone: 6-carboxyfluorescein; d) fourth zone: FITC-glutamate

### *Spacer Compounds*

A combination of a continuous and a discrete injection is shown in Figure 2d. The upstream fluid reservoir was filled with electrolyte containing 100  $\mu\text{mol/L}$  sodium acetate as a spacer compound, but no analytes. The separation channel was filled with electrolyte containing 30  $\mu\text{mol/L}$  of both fluorescein and 6-carboxyfluorescein as analytes, but no spacer compound. External voltages were 120 V (upstream) and 40 V (downstream). Initially, fluorescein and 6-carboxyfluorescein are focused in adjacent zones. After 70 s, acetate, which has an ionic mobility in between that of fluorescein and 6-carboxyfluorescein, arrives and spaces the two compounds. The fluorescein zone remains focused at the depletion zone border, while the 6-

carboxyfluorescein zone is pushed away in upstream direction by the continuously broadening acetate zone. Spacer addition enables baseline separation of fluorescent compounds enabling more precise identification and quantification. Furthermore, a single compound or a specific group of compounds can be selectively transported away from the depletion zone and can eventually be eluted from the system, while other compounds remain at their near-stationary position at the border of the depletion zone. Advantageously, all compounds remain focused during this process. Thus, spacer addition is a powerful method for purification and transport.

### *Positional Stability*

A crucial feature of dzITP is the positional stability of the depletion zone border. A near-stationary condition is reached after a rather short period, typically on the order of 100 s (see Figure 2), in which depletion rate and EOF velocity reach a balance. A discrete injection experiment was performed with 50  $\mu\text{mol/L}$  of both fluorescein and 6-carboxyfluorescein; external voltages were 120 V (upstream) and 40 V (downstream). In this experiment, the depletion zone border shifted less than 700  $\mu\text{m}$  in 1 h. A previous report on nanofluidic concentration devices indicated a near-zero shift after 3 h of actuation<sup>28</sup>, although under different experimental conditions, indicating that the result reported here could be further optimized. However, the near-stability of the isotachophoretic separations demonstrated here greatly enhances monitoring of focusing and separation processes by microscopy without  $x/y$  control of the microscope stage. Additionally, the experimental time range is much larger than for nonstationary ITP methods, allowing higher concentration factors to be achieved.

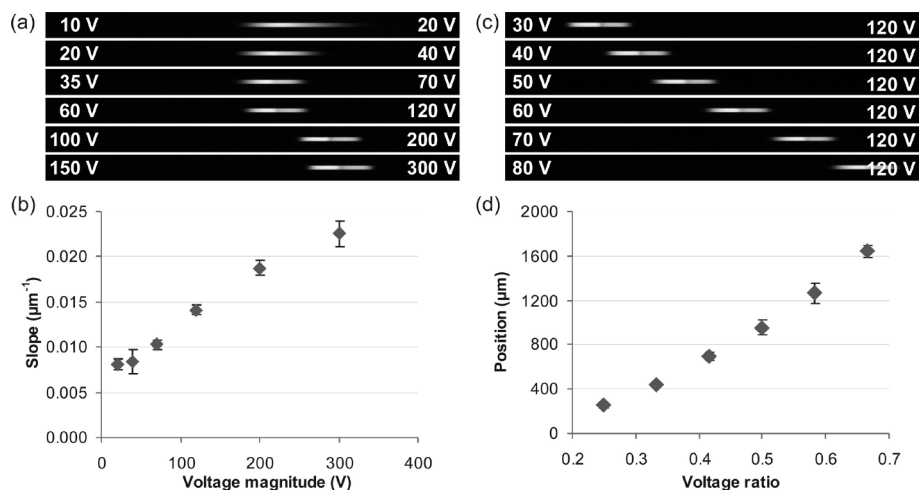


**Figure 4.** Three-point voltage actuation. (a) Focusing and separation of fluorescein and 6-carboxyfluorescein at several voltage magnitudes. (b) Dependence of focusing strength on the voltage magnitude. Focusing strengths are represented by the steepness of the slopes between the fluorescein plateau and the depletion zone; voltage magnitudes are represented by the upstream voltage. (c) Fluorescein and 6-carboxyfluorescein zones at different ratios between upstream and downstream voltages. (d) Distances of the edge between the depletion zone and the fluorescein zone from the nanochannel. Measurements were triplicated and randomized.

### Three-Point Voltage Actuation

In Figure 4 we demonstrate the versatility that is provided by a three-point voltage actuation approach. In Figure 4a,b the magnitude of the upstream and downstream voltages was varied, while maintaining the ratio between them. This enables tuning of the extent to which analytes are focused. For low voltages the two zones are barely distinguishable, while for high voltages sharp edges of the zones can be observed. Figure 4b shows normalized slope values in fluorescence intensity per micrometer. The results suggest a linear trend between voltage magnitude and zone sharpness. Analyte zone positions are not greatly influenced by a change of the voltage magnitude as long as the

ratio between upstream and downstream voltages is kept constant. In principle, this enables a free choice of the maximum field strength and resulting focusing strength. However, small shifts in analyte zone positions are observed at higher voltage magnitudes. We measured maximum shifts of  $364 \pm 21 \mu\text{m}$ .

In Figure 4c,d the voltage ratio is varied by means of the downstream voltage. The zones can be shifted over a range of 1.4 mm by varying the voltage ratio between 0.25 and 0.67 (downstream voltage: upstream voltage). Zone positions appear to relate rather linearly to the voltage ratio. Separations are maintained, although at increasing ratios defocusing occurs. The 1.4 mm zone shift is accompanied by a decrease of slope values on the order of  $0.006 \mu\text{m}^{-1}$ . Complete control over analyte zone position and sharpness is a crucial and unique advantage of dzITP over conventional ITP methods. In conventional methods, a single stable position can be obtained by EOF balancing, but during the experiment this position can not be easily changed without changing parameters like pH or electrolyte concentrations. Contrarily, in dzITP this is easily done by tuning the upstream and downstream voltage magnitudes. Real-time image analysis of fluorescent markers can be used as feedback input for three-point voltage actuation, enabling automated zone positioning control. Moreover, great benefit is offered to experimental readout, as analyte zones can be scanned in a precisely controllable manner by steering them along a sensor.

### *Synergy of dzITP*

Table 1 summarizes the synergy that emerges from the combination of ITP and nanofluidic concentration devices, as provided by dzITP. Except for the

requirement of multiple electrolytes, dzITP has all key characteristics of ITP: focusing toward plateau concentrations and separation into adjacent zones that are ordered according to ionic mobility. Spacer compounds can be used to segregate adjacent zones. From nanofluidic concentration devices, dzITP takes the single-electrolyte advantage, as well as positional stability. Three-point voltage actuation adds to this synergy the possibility of precise control of focusing strength and zone positioning.

**Table 1.** Comparison of dzITP with Conventional ITP Methods and Nanofluidic Concentration Devices (NCD). v = intrinsic or standard possibility; – = not possible or not demonstrated in literature; m = possible with modification.

<b>property</b>	<b>ITP</b>	<b>NCD</b>	<b>dzITP</b>
analyte focusing	v	v	v
separation of ions	v	–	v
spacer insertion	v	–	v
single electrolyte	–	v	v
near-stationary	m	v	v
voltage-controlled zone positioning	–	–	v

## Conclusion and Outlook

In this paper we have demonstrated isotachophoretic separations employing a nanochannel-induced depletion zone as a trailing electrolyte. dzITP requires only a single electrolyte to be injected and can be performed easily with both discrete and continuous injections. We demonstrated separations of up to four compounds in clearly distinguishable zones within 100 s. A spacer was inserted to improve baseline separation of fluorescent compounds, and to induce selective transport of analytes while maintaining sharply focused zones. Moreover, full control over analyte position and zone sharpness was demonstrated using the unique three-point voltage control of dzITP.

Scanning of analyte zones using three-point voltage actuation will enable simple integration of sensors such as surface-enhanced Raman spectroscopy (SERS), surface plasmon resonance (SPR), and conductimetry or electrochemical detection. As dzITP is much easier to use than conventional ITP, integration into a microfluidic platform for everyday laboratory use will be very attractive, as exemplified by the Agilent 2100 Bioanalyzer for on-chip capillary electrophoresis. Integration in hand-held analysis devices, as has been recently done for conventional ITP,<sup>18</sup> may find interesting applications in water quality monitoring, explosive detection, point-of-care screening, etc. Future research focuses on coupling of the technique to sampling and detection modules. We see great potential for dzITP in our metabolomics research, particularly for the extraction, preconcentration, and quantification of low-abundant metabolites from small complex biological samples. Thanks to its unique combination of voltage-controlled versatility and single-electrolyte simplicity, dzITP holds the promise to become a core component in the electrokinetic chip-based platforms of the future.

## References

1. L. Chen, J. E. Prest, P. R. Fielden, N. J. Goddard, A. Manz and P. J. R. Day, *Lab on a Chip* **6** (4), 474-487 (2006).
2. S. M. Kenyon, M. M. Meighan and M. A. Hayes, *Electrophoresis* **32** (5), 482-493 (2011).
3. P. A. Walker, M. D. Morris, M. A. Burns and B. N. Johnson, *Analytical Chemistry* **70** (18), 3766-3769 (1998).
4. D. Kaniansky, M. Masár, J. Bielčíková, F. Iványi, F. Eisenbeiss, B. Stanislawski, B. Grass, A. Neyer and M. Jöhnck, *Analytical Chemistry* **72** (15), 3596-3604 (2000).
5. D. Bottenus, T. Z. Jubery, Y. Ouyang, W.-J. Dong, P. Dutta and C. F. Ivory, *Lab on a Chip* **11** (5), 890-898 (2011).
6. D. Bottenus, T. Z. Jubery, P. Dutta and C. F. Ivory, *Electrophoresis* **32** (5), 550-562 (2011).



7. J. Wang, Y. Zhang, M. R. Mohamadi, N. Kaji, M. Tokeshi and Y. Baba, *Electrophoresis* **30** (18), 3250-3256 (2009).
8. B. Jung, R. Bharadwaj and J. G. Santiago, *Analytical Chemistry* **78** (7), 2319-2327 (2006).
9. M. Bercovici, G. V. Kaigala, C. J. Backhouse and J. G. Santiago, *Analytical Chemistry* **82** (5), 1858-1866 (2010).
10. J. E. Prest, M. S. Beardah, S. J. Baldock, S. P. Doyle, P. R. Fielden, N. J. Goddard and B. J. T. Brown, *Journal of Chromatography A* **1195** (1-2), 157-163 (2008).
11. H. Huang, F. Xu, Z. Dai and B. Lin, *Electrophoresis* **26** (11), 2254-2260 (2005).
12. D. Liu, Z. Ou, M. Xu and L. Wang, *Journal of Chromatography A* **1214** (1-2), 165-170 (2008).
13. D. Liu, M. Shi, H. Huang, Z. Long, X. Zhou, J. Qin and B. Lin, *Journal of Chromatography B* **844** (1), 32-38 (2006).
14. A. Persat, L. A. Marshall and J. G. Santiago, *Analytical Chemistry* **81** (22), 9507-9511 (2009).
15. R. B. Schoch, M. Ronaghi and J. G. Santiago, *Lab on a Chip* **9** (15), 2145-2152 (2009).
16. A. Persat and J. G. Santiago, *Analytical Chemistry* **83** (6), 2310-2316 (2011).
17. M. Bercovici, G. V. Kaigala, K. E. Mach, C. M. Han, J. C. Liao and J. G. Santiago, *Analytical Chemistry* **83** (11), 4110-4117 (2011).
18. G. V. Kaigala, M. Bercovici, M. Behnam, D. Elliott, J. G. Santiago and C. J. Backhouse, *Lab on a Chip* **10** (17), 2242-2250 (2010).
19. L. Suntornsuk, *Anal Bioanal Chem* **398** (1), 29-52 (2010).
20. A. García-Campaña, L. Gámiz-Gracia, F. Lara, M. Olmo Iruela and C. Cruces-Blanco, *Anal Bioanal Chem* **395** (4), 967-986 (2009).
21. F. E. Ahmed, *Journal of Chromatography B* **877** (22), 1963-1981 (2009).
22. M. Urbánek, A. Varenne, P. Gebauer, L. Křivánková and P. Gareil, *Electrophoresis* **27** (23), 4859-4871 (2006).
23. M. C. Breadmore, *Journal of Chromatography A* **1217** (24), 3900-3906 (2010).
24. M. C. Breadmore, *Electrophoresis* **29** (5), 1082-1091 (2008).
25. M. C. Breadmore and J. P. Quirino, *Analytical Chemistry* **80** (16), 6373-6381 (2008).
26. G. I. Abelev and E. R. Karamova, *Molecular Immunology* **26** (1), 41-47 (1989).
27. S. M. Kim, M. A. Burns and E. F. Hasselbrink, *Analytical Chemistry* **78** (14), 4779-4785 (2006).
28. Y.-C. Wang, A. L. Stevens and J. Han, *Analytical Chemistry* **77** (14), 4293-4299 (2005).
29. S. J. Kim, Y.-A. Song and J. Han, *Chemical Society Reviews* **39** (3), 912-922 (2010).

30. J. Astorga-Wells, S. Vollmer, S. Tryggvason, T. Bergman and H. Jörnvall, *Analytical Chemistry* **77** (22), 7131-7136 (2005).
31. S.-R. Park and H. Swerdlow, *Analytical Chemistry* **75** (17), 4467-4474 (2003).
32. A. Plecis, R. B. Schoch and P. Renaud, *Nano Letters* **5** (6), 1147-1155 (2005).
33. K. G. H. Janssen, H. T. Hoang, J. Floris, J. de Vries, N. R. Tas, J. C. T. Eijkel and T. Hankemeier, *Analytical Chemistry* **80** (21), 8095-8101 (2008).
34. T. A. Zangle, A. Mani and J. G. Santiago, *Analytical Chemistry* **82** (8), 3114-3117 (2010).
35. T. A. Zangle, A. Mani and J. G. Santiago, *Chemical Society Reviews* **39** (3), 1014-1035 (2010).
36. Q. Pu, J. Yun, H. Temkin and S. Liu, *Nano Letters* **4** (6), 1099-1103 (2004).
37. Q. Yu and Z. Silber-Li, *Microfluid Nanofluid* **11** (5), 623-631 (2011).
38. K.-D. Huang and R.-J. Yang, *Electrophoresis* **29** (24), 4862-4870 (2008).
39. H. Yu, Y. Lu, Y.-g. Zhou, F.-b. Wang, F.-y. He and X.-h. Xia, *Lab on a Chip* **8** (9), 1496-1501 (2008).
40. X. Mao, B. R. Reschke and A. T. Timperman, *Electrophoresis* **31** (15), 2686-2694 (2010).
41. B. Scarff, C. Escobedo and D. Sinton, *Lab on a Chip* **11** (6), 1102-1109 (2011).
42. D. Wu and A. J. Steckl, *Lab on a Chip* **9** (13), 1890-1896 (2009).
43. K. Zhou, M. L. Kovarik and S. C. Jacobson, *Journal of the American Chemical Society* **130** (27), 8614-8616 (2008).
44. J. H. Lee, Y.-A. Song, S. R. Tannenbaum and J. Han, *Analytical Chemistry* **80** (9), 3198-3204 (2008).
45. J. Lee and J. Han, *Microfluid Nanofluid* **9** (4-5), 973-979 (2010).
46. L. F. Cheow, S. H. Ko, S. J. Kim, K. H. Kang and J. Han, *Analytical Chemistry* **82** (8), 3383-3388 (2010).
47. Y.-C. Wang and J. Han, *Lab on a Chip* **8** (3), 392-394 (2008).
48. J. H. Lee, B. D. Cosgrove, D. A. Lauffenburger and J. Han, *Journal of the American Chemical Society* **131** (30), 10340-10341 (2009).
49. A. Sarkar and J. Han, *Lab on a Chip* **11** (15), 2569-2576 (2011).
50. S. H. Ko, S. J. Kim, L. F. Cheow, L. D. Li, K. H. Kang and J. Han, *Lab on a Chip* **11** (7), 1351-1358 (2011).
51. J. H. Lee, Y.-A. Song and J. Han, *Lab on a Chip* **8** (4), 596-601 (2008).
52. S. J. Kim, S. H. Ko, K. H. Kang and J. Han, *Nat Nano* **5** (4), 297-301 (2010).
53. S. J. Kim, L. D. Li and J. Han, *Langmuir* **25** (13), 7759-7765 (2009).

# 4

## Tunable Ionic Mobility Filter for Depletion Zone Isotachophoresis

*Published in Analytical Chemistry, 2012, 84 (21), pp 9065–9071*

We present a novel concept of filtering based on depletion zone isotachophoresis (dzITP). In the micro/nanofluidic filter, compounds are separated according to isotachophoretic principles and simultaneously released selectively along a nanochannel-induced depletion zone. Thus, a tunable low-pass ionic mobility filter is realized. We demonstrate quantitative control of the release of fluorescent compounds through the filter using current and voltage actuation. Two modes of operation are presented. In continuous mode, supply, focusing and separation are synchronized with continuous compound release, resulting in trapping of specific compounds. In pulsed mode, voltage pulses result in release of discrete zones. The dzITP filter was used to enhance detection of 6-carboxyfluorescein 4-fold over fluorescein, even though it had 250x lower starting concentration. Moreover, specific high-mobility analytes were extracted and enriched from diluted raw urine, using fluorescein as an ionic mobility cut-off marker and as a tracer for indirect detection. Tunable ionic filtering is a simple but essential addition to the capabilities of dzITP as a versatile toolkit for biochemical assays.

Filtration is popular amongst sample pretreatment methods as it is fast and simple to implement. Filtration works by placing a barrier in a flow that

allows some compounds to pass while other compounds are trapped behind it. Although most filtration methods are primarily based on size exclusion, several electrokinetic techniques also can be used. For example, in isotachopheresis (ITP) ionic compounds can be trapped very selectively in an ionic mobility window defined by a terminating and a leading electrolyte.<sup>1</sup> Compounds outside the ionic mobility window will not be trapped, making filtration possible.<sup>2</sup> Moreover, impressive concentration factors of trapped compounds can be achieved, up to a million.<sup>3</sup> ITP is therefore highly amenable to extract and enrich components from complex biological samples. Notwithstanding its many strengths, the fact that a conventional ITP separation is defined by multiple electrolytes makes it a complex method, especially if fraction recovery or ionic mobility window tuning is desired during experiments.

Counter flow gradient focusing methods are another group of electrokinetic technologies capable of filtration. They rely on a force balance of fluid flow and electrophoresis, which is obtained by inducing an electric field gradient in the fluid flow. Analytes become immobilized at the point where their electrophoretic velocity is equal to the flow velocity.<sup>4</sup> Filter action can be established when some compounds have either too high or too low ionic mobility to be immobilized on the electric field gradient. The electric field gradient can be established in many different ways. For example, in electric field gradient focusing (EFGF) a converging channel is used.<sup>5</sup> With EFGF, undesired low mobility compounds could be removed while desired protein was concentrated.<sup>6</sup> In temperature gradient focusing (TGF), the sensitivity of electrolyte conductivity towards temperature is used to establish an electric field gradient.<sup>7</sup> TGF has been used to focus small molecules at specific

positions, while excluding proteins from the channel using a counterflow.<sup>8</sup> A similar exclusion effect was used by Meighan et al, who concentrated and differentiated proteins in bulk solution near the entrance of a channel.<sup>9</sup>

The integration of nanofluidic components into microfluidic networks has opened up many interesting new perspectives. In some cases, electrostatic or size-based exclusion has been used as a filtering principle<sup>10</sup>. An approach which is less prone to clogging and more interesting from an electrokinetic perspective is the use of a nanochannel-induced ion-depleted zone. Such a depletion zone can be formed by concentration polarization, a process that occurs upon application of an electric field over perm-selective conducts (that is, inside a nanochannel the surface charge of the walls permits counterions, but excludes co-ions).<sup>11, 12</sup> The depletion zone can be maintained at a stable position adjacent to the nanochannel entrance, even if placed in a fluid flow. The high electric field in the depletion zone blocks charged compounds from passing, making such devices suited for highly efficient analyte trapping<sup>13</sup> and water purification<sup>14</sup> applications. Experiments with electrocapture devices, which use nanoporous membranes for depletion zone formation, have indicated that they can be used as a filter that separates between ionic mobilities<sup>15</sup>. Apart from nanoporous channels and membranes, depletion zones also can be formed by several other means, bipolar electrodes being most notable<sup>16</sup>.

Recently we introduced depletion zone isotachophoresis (dzITP), using a nanochannel-induced depletion zone at the border of which analytes were focused and separated into adjacent zones<sup>17</sup> (chapter 3). As the depletion zone replaces the terminating electrolyte that is used in conventional ITP, dzITP is a single-electrolyte isotachophoretic method, which is an important

simplification. Moreover, dzITP exhibits great versatility, because analyte zones can be precisely positioned by tuning the balance between fluid flow through the separation channel and depletion zone growth. dzITP has been used to study complexation of aptamers and proteins<sup>18</sup>. Here, we greatly leverage the versatility of dzITP by introducing a novel filtering principle that selects compounds based on ionic mobility. The dzITP filter does not depend on physical or chemical properties of the filter substrate, like pore size, nor is it based on a force balance of fluid flow and analyte (electro)migration, in contrast to the electrokinetic technologies mentioned above. Instead, it primarily depends on a balance of fluxes. A limited, controlled stream of compounds is released along the depletion zone. The depletion zone can thereby be imagined as a tunable valve that can be opened or closed in order to control the release of focused compounds. Selectivity is obtained as dzITP orders compounds into distinct zones before they can pass the depletion zone. Since low-mobility compounds are focused closest to the depletion zone, the dzITP filter is a low-pass filter. Ionic mobility cut-offs are tunable by synchronization of isotachophoretic focusing, separation and release of one or multiple zones. Two modes of operation for dzITP filtering are demonstrated. In continuous mode, supply and release of compounds are balanced in order to establish an ionic mobility cut-off, preferably aided by a partially released marker compound. Compounds with lower mobilities than the marker compound are co-released with the marker compound; compounds with higher mobilities are trapped in isotachophoretic zones behind the marker compound zone. In pulsed mode, the flow is temporarily increased to allow one or more individual zones to be released aided by visual feedback control. The device was used for specific enrichment of low-

abundant 6-carboxyfluorescein over highly abundant fluorescein, using continuous release and a spacer compound. Moreover, dzITP filtering was employed for trapping and indirect detection of specific metabolites from urine using fluorescein as a mobility cut-off marker. These experiments demonstrate the applicability of dzITP filtering for real-time monitored pretreatment and analysis of complex biological samples.

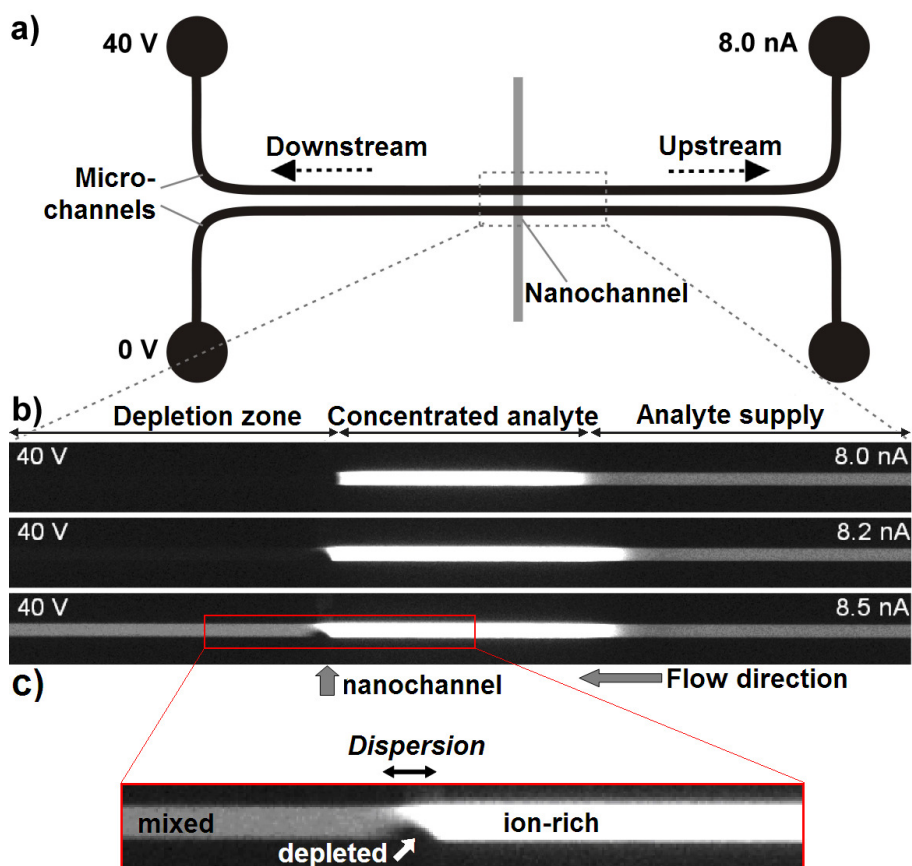


**Figure 1.** a) Device layout with an example of applied voltages and currents. b) CCD images showing the part of the separation channel near the nanochannel junction. With increasing currents, a focused zone of fluorescein becomes increasingly released. c) Inset showing two laminar streams: depleted fluid from the nanochannel and ion-rich fluid from the dzITP-separation. The two fluid streams are mixed rapidly downstream from the nanochannel.

## Experimental Section

### *Chemicals*

Lithium carbonate was purchased from Acros Organics (Geel, Belgium), disodium fluorescein was purchased from Riedel-de Haën (Seelze, Germany), 6-carboxyfluorescein was purchased from Sigma-Aldrich (Steinheim, Germany). FITC-leucine and FITC-glutamate were synthesized as described in chapter 1. 2.0 mmol/L lithium carbonate, pH 10.5, was used as the background electrolyte, unless indicated otherwise.

### *Chip Preparation*

Chips were fabricated in Pyrex wafers using standard lithography techniques and dry etching with an SF<sub>6</sub>/Ar plasma. Details of the chip fabrication procedure can be found in chapter 3. The chips had microchannels with 1.7  $\mu\text{m}$  depth and 20  $\mu\text{m}$  width. The length of the microchannels was 0.9 cm, as measured between the nanochannel junction and the fluid reservoirs. The nanochannels were 60 nm deep, 25  $\mu\text{m}$  wide, and 50  $\mu\text{m}$  long. Before experiments, chip filling was done with ethanol to prevent bubble formation, after which the chips were flushed with electrolyte. Fluid replacement and flushing of channels was done as described in chapter 3. For continuous injections, channels and reservoirs were filled with the same solution containing both electrolyte and sample. For discrete injections, the separation channel was filled with solution containing electrolyte and sample, while the upstream reservoir contained electrolyte only.



### *Setup and Microscopy*

Fluidic reservoirs (40  $\mu$ L) were created by attaching a custom-build interface to the access holes of the chip using a vacuum. Gold electrodes were used for electrical connections. Voltages were controlled by one or two power supplies (ES 0300 045, Delta Elektronika BV, Zierikzee, The Netherlands), which in turn were controlled by an NI USB 6221 data acquisition system using LabVIEW 8.2 software (National Instruments, Austin, TX). Current actuation was performed with a Keithley 2410 source meter unit (Keithley, Cleveland, OH). In most experiments, current actuation was performed via the electrode connected to the upstream (sample) reservoir, while the downstream reservoir was connected to a constant voltage. In these experiments, only one of the reservoirs of the bottom channel was connected to ground (see figure 1a). However, in the pulsed mode experiments (figure 4), both the upstream and downstream reservoir were connected to voltage sources, while both reservoirs of the bottom channel were connected to ground. For imaging, we used a fluorescence microscope (Olympus IX71, Olympus, Zoeterwoude, The Netherlands) to which a Hamamatsu Orca-ER digital camera was mounted, which was controlled by Hokawo version 2.1 imaging software (Hamamatsu Photonics, Nueremberg, Germany). The integration time for an image was 0.5 s (1 s in figure 3), and the magnification was 40x. Raw CCD images were used in the figures. The false-color image in figure 6 was processed in Hokawo 2.1, to obtain this image, an EXFO X-Cite 120 Fluorescence Illumination System (Lumen Dynamics Group, Mississauga, Canada) was used to increase sensitivity. Fluorescence intensity values were corrected for background signal.

### *Urine Analysis*

Fresh urine sample was obtained from an adult, healthy volunteer and immediately processed for analysis. The sample was 100x diluted in 2.0 mmol/L lithium carbonate containing 100  $\mu\text{mol/L}$  of fluorescein and subsequently injected into the device, without any further sample preparation.

## **Results and Discussion**

### *Analyte Release*

The filtering principle is based on the fact that analytes in dzITP zones can be released along the depletion zone into the downstream part of the separation channel. This is shown in figure 1. A depletion zone is formed in the separation channel upon voltage and current actuation. The analyte, 150  $\mu\text{mol/L}$  of fluorescein, is focused at the upstream border of the depletion zone and forms an isotachophoretic zone. 2.5 mM lithium carbonate was used as the electrolyte. As described in chapter 3, the analyte zone could be positioned at varying distances from the nanochannel by changing the ratio between the voltages and/or currents at the upstream and downstream fluid reservoirs. This positioning is a result of a shifting balance between nanochannel ion pumping capacity and electro-osmotic flow (EOF). Increasing the currents at the upstream reservoir results in increased EOF; therefore the fluorescein zone is positioned closer to the nanochannel. Upon sufficient increase of the EOF, the depletion zone cannot be maintained any longer in the upstream channel<sup>20</sup>. Therefore, compounds are released along the depletion zone into the downstream channel, which enables filter operation. In figure 1b, three situations are shown. When 8.0 nA is applied,

the depletion zone border, as indicated by the concentrated fluorescein zone, is positioned at a small distance from the nanochannel junction. Upon a small relative increase of the EOF (by increasing the current to 8.2 nA) a small stream of non-depleted liquid from the upstream channel, which carries some of the concentrated fluorescein, starts to flow into the downstream channel. If the current is further increased to 8.5 nA, the contribution of the fluorescein-rich fluid stream becomes much larger (figure 1c). In fact, at the nanochannel junction two laminar streams can be discerned, one containing ion-rich fluid from the upstream channel and one containing ion-depleted liquid resulting from the concentration polarization process over the nanochannel (figure 1c). Downstream from the nanochannel, the two streams rapidly mix through dispersion, forming a homogeneous dilution of the released fluorescein.

The graph in figure 2 shows how the intensity of released fluorescein in the downstream channel depends on the applied current. A zone of concentrated fluorescein was established by conventional dzITP and subsequently released using different currents on the sample reservoir, while maintaining a constant voltage of 40V at the downstream reservoir. The results of three experimental series using the same conditions are shown, to indicate reproducibility. An important value which can be derived from the graph is the threshold current. Above this threshold, analyte starts to be released.

In the graph, threshold currents can be estimated for each experimental series by interpolation of the point where fluorescence intensity becomes zero. These estimated values vary in the order of 2.5%. Even though between the experimental series the variation in threshold currents is quite small, the corresponding variations in fluorescence intensity are significant. The reason

is that in the filter regime the amount of analyte that is released is quite sensitive to small changes in electric fields. There are several potential causes for small variations in threshold currents, most importantly a shift in electrolyte distribution within the nano/microchannel network. Additional effects include conductivity and pH changes due to  $\text{CO}_2$  dissolution from the atmosphere and variations in the zeta potential of the micro- and nanochannel walls. To obtain better reproducibility, applied current settings should therefore be corrected for the threshold current.

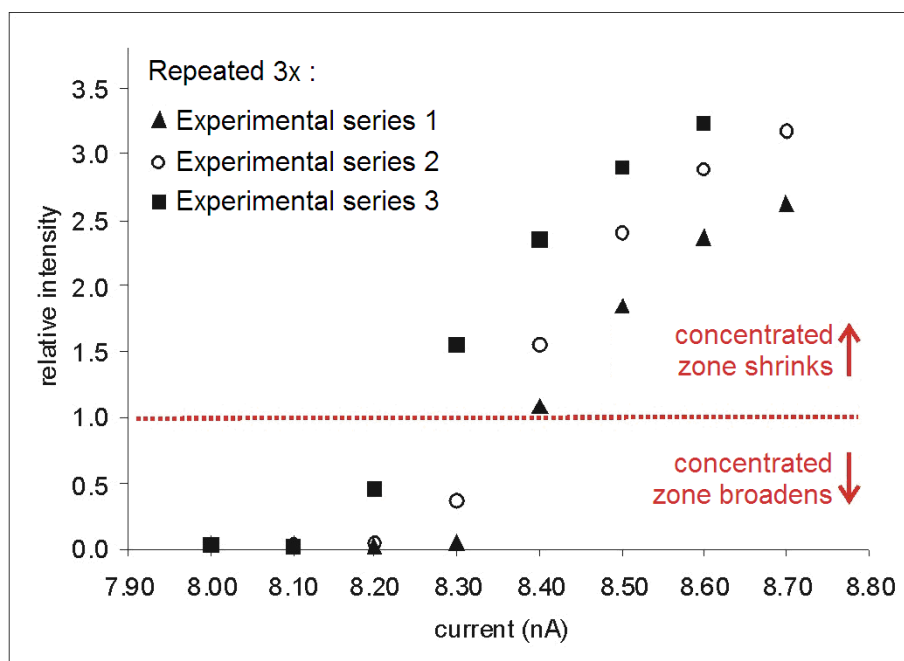


**Figure 2.** Graph of fluorescence intensity in the downstream channel relative to the intensity of non-concentrated analyte upstream in the channel as a function of the applied current. The red dashed line indicates equal concentration zone growth and release. Below this line the zone is broadening, above it is shrinking. The results of three experimental series with identical experimental conditions show that results are reproducible within 200pA.

The values for the fluorescence intensities in the downstream channel in figure 2 are calculated relative to the intensity in the channel region upstream from the concentrated zone. Therefore, if the relative intensity is equal to one, supply and release of analytes are equal. This particular regime is indicated by the red dashed line in figure 2. At higher values, more analyte is released than supplied and concentrated analyte zones will shrink and ultimately disappear. At lower values, release is smaller than supply and concentrated zones continue to grow. Thus, the growth rate of the concentrated fluorescein zone is indicative for the balance of the supply and release fluxes. This is used for continuous filtering as described in the following sections.

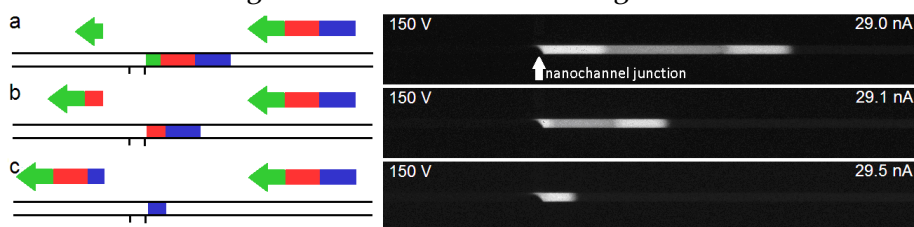


**Figure 3.** Schematic representation (left) and experimental results (right) showing continuous operation of the dzITP filter. The filter is tuned by balancing release (left arrows) and supply (right arrows) of analytes, determining which analytes pass through the filter and which are trapped in isotachophoretic zones. Analytes are fluorescein, FITC-leucine and 6-carboxyfluorescein. a) Fluorescein is partly released, the other analytes are completely retained. b) Fluorescein is completely released, FITC-leucine partly. c) Fluorescein and FITC-leucine are completely released, 6-carboxyfluorescein partly.

### *Continuous Filtering*

Figure 3 shows how the dzITP filter is operated in order to collect compounds above a certain mobility cut-off, while continuously releasing other compounds. In this experiment, fluorescein, 6-carboxyfluorescein and FITC-leucine, each 50  $\mu\text{mol/L}$ , were injected continuously by placing the sample solution in the upstream reservoir. A depletion zone was established and

subsequently the current that was applied through the upstream reservoir was tuned just above the threshold current (figure 3a). This resulted in continuous release of analyte along the depletion zone. The flux of released analyte was smaller than the supply flux of fluorescein. Therefore, fluorescein was only partly released and the concentrated zone of fluorescein continued to broaden. The other two analytes focused in zones behind the fluorescein zone and therefore were not released at all. This condition can be written as

$$0 < J_{\text{release}} < J_{\text{fluorescein}} \quad (1)$$

where  $J_{\text{release}}$  and  $J_{\text{fluorescein}}$  are the fluxes (in mol/s) of released analyte and supplied fluorescein, respectively. When increasing the current, more fluorescein was released than supplied; therefore no fluorescein zone was formed. Additionally, part of the FITC-leucine was released. Since release of FITC-leucine was only partial, a FITC-leucine zone was still formed, behind which all 6-carboxyfluorescein was collected in a second zone (figure 3b). This filtering condition can be written as

$$J_{\text{fluorescein}} < J_{\text{release}} < (J_{\text{fluorescein}} + J_{\text{FITC-leucine}}) \quad (2)$$

In this filtering regime still a narrow bright band can be observed at the depletion zone border, presumably this is due to limited stacking of fluorescein. However, full release of fluorescein is evidenced by the fact that this band does not broaden over time. Moreover, the FITC-leucine zone is growing less rapidly, which is evidence for partial release of FITC-leucine. A third regime is shown in figure 3c, in which all FITC-leucine (together with all fluorescein) and part of the 6-carboxyfluorescein is released. Here, the filtering condition is

$$(J_{\text{fluorescein}} + J_{\text{FITC-leucine}}) < J_{\text{release}} < (J_{\text{fluorescein}} + J_{\text{FITC-leucine}} + J_{\text{6-carboxyfluorescein}}) \quad (3)$$

Finally, at sufficiently high current, no filtering and no analyte zone formation is observed yielding the condition

$$J_{\text{release}} > (J_{\text{fluorescein}} + J_{\text{FITC-leucine}} + J_{\text{6-carboxyfluorescein}}) \quad (4)$$

In this regime, the electrolyte is co-released with all the analytes. The continuous filtering mode can be automated by setting the zone width of a specific, continuously injected marker compound to a predefined value, using a real-time image analysis algorithm as a feedback for applied voltages and currents. The marker compound zone can maintain a stable width only if continuous marker compound supply is balanced by partial release of the marker compound. The ionic mobility of the marker compound then precisely defines the ionic mobility cut-off of the dzITP filter: isotachophoretic principles guarantee that all ions with lower mobilities than the marker compound will be co-released while all higher mobility compounds will be focused and separated adjacent to the marker zone.

dzITP filtering is based on release along the depletion zone, yielding a temporary two-stream profile of analyte-rich and ion-depleted fluid (see also figures 1 b and c), and resulting in a balance of fluxes. The depletion zone may therefore be compared to a valve that allows to tune the quantity of compound that is to be released. This mechanism is in contrast with release through the depletion zone (or any other region with increasing electric field), in which case filtering can be achieved by tuning the force balance between fluid flow and opposite electrophoretic drift. The latter mechanism is quite common for gradient focusing methods, including EFGF and TGF. It has also been exploited in electrocapture devices, in which peptides and other compounds could be released sequentially across enrichment and depletion zones formed by concentration polarization<sup>15, 19</sup>.

### *Pulsed Filtering*

Figure 4 shows dzITP filtering in pulsed mode. A discrete amount of sample containing fluorescein (60  $\mu\text{mol/L}$ ), 6-carboxyfluorescein, FITC-leucine, and FITC-glutamate (each 30  $\mu\text{mol/L}$ ), was injected by filling the separation channel with electrolyte plus sample solution, while the upstream “sample” reservoir contained electrolyte without sample.

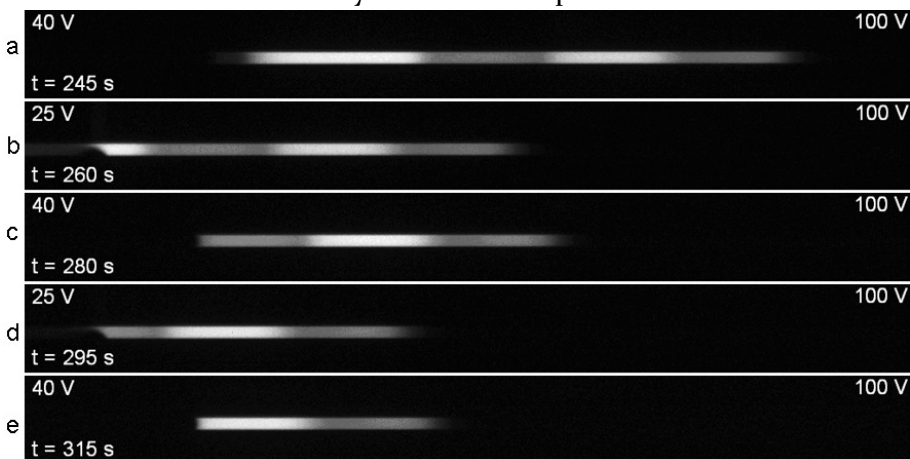


**Figure 4.** Pulsed operation of the dzITP filter. a) Completed dzITP-separation of a discrete injection of fluorescein, FITC-leucine, 6-carboxyfluorescein and FITC-glutamate. b) Release of the fluorescein zone. c) Retained zones after fluorescein release. c) Release of the FITC-leucine zone. d) Retained zones after fluorescein and FITC-leucine release.

First, a depletion zone was established in the upstream part of the channel, at the border of which the analytes were focused. Fluorescein focused closest to the depletion zone border, followed by FITC-leucine, 6-carboxyfluorescein and finally FITC-glutamate. During this stage, applied voltages were 120 V (upstream) and 40 V (downstream). After 3 minutes of voltage actuation, the dzITP separation was completed, resulting in the starting situation for the second stage, in which pulsed release of compounds was performed (figure 4a). The downstream voltage was temporarily lowered to 25 V. The analyte



zones were transported into the downstream direction until the nanochannel junction was reached, after which the first analyte zone (fluorescein) started to be released (figure 4b). All analyte zones would have been released if the downstream voltage were maintained at the lowered value. To prevent this, the downstream voltage was increased again to 40 V after the fluorescein zone was released. The depletion zone was re-established rapidly (sub-second scale) and the upstream depletion zone border slowly returned to its original position (~30 seconds). Behind the depletion zone border, the remaining analyte zones were retained (figure 4c). This procedure was subsequently repeated twice to release the FITC-leucine (figure 4d,e) and 6-carboxyfluorescein zones respectively.

In this experiment, the voltage actuation steps that ended the release of an individual zone was done manually, based on visual clues. Voltage actuation based on feedback from a sensor or from automatic image analysis might yield a more reliable procedure. It should be taken into account that in isotachophoretic separations there is always overlap between neighboring zones due to diffusion. Several approaches to this problem can be envisioned. First, if one desires “pure” analyte (for example, for identification during downstream analysis), only the heart of the corresponding zone can be selected, excluding other dzITP-separated compounds. Second, if one wants to ensure to select all of a certain zone, the “cuts” can be made in the centers of the neighboring zones. Finally, analytes can be released with regular time intervals to fractionate the dzITP-separation while accepting that a single compound might appear in multiple fractions, or that a single fraction contains multiple compounds.

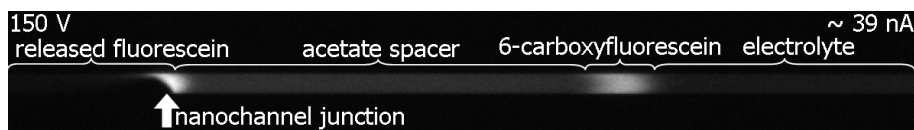


**Figure 5.** Selective enrichment of low-abundant 6-carboxyfluorescein over high-abundant fluorescein using acetate as a spacer compound. The image was obtained after 10 minutes of actuation

### *Selective enrichment*

dzITP filtering can be used to concentrate specific low-abundant analytes and to enrich them selectively over compounds of which the initial concentration is much higher. To demonstrate this, we continuously injected a sample mixture containing 100  $\mu\text{mol/L}$  fluorescein and 400 nmol/L 6-carboxyfluorescein. The mixture contained also 100  $\mu\text{mol/L}$  sodium acetate; the acetate ion has intermediate mobility between fluorescein and 6-carboxyfluorescein and therefore acted as a non-fluorescent spacer in isotachophoretic separations. Currents and voltages were tuned such that the acetate spacer zone was released partly, establishing the cut-off of the filter. Fluorescein, having a lower mobility, was co-released with acetate, while 6-carboxyfluorescein was trapped and concentrated at the upstream border of the acetate spacer zone (figure 5). The fluorescein traveling through the acetate zone is increased in concentration  $\sim 2.2$  times compared to its background concentration in the electrolyte, allowing indirect detection of the upstream acetate zone border where 6-carboxyfluorescein is to be focused. Already after 1 minute, the 6-carboxyfluorescein started to become visible as a peak. In 10 minutes, the intensity of the 6-carboxyfluorescein peak was increased 4-fold over the intensity of the fluorescein in the acetate zone and almost 10-fold over the fluorescence intensity in the background

electrolyte. Recalling that the starting concentration of 6-carboxyfluorescein was 250x lower than the fluorescein starting concentration, it is clear that dzITP filtering can be used for rapid enrichment of specific-low abundant compounds even in the presence of similar high-abundant compounds. This can be highly advantageous for biological samples, where the concentrations of analytes of interest can differ many orders of magnitude.

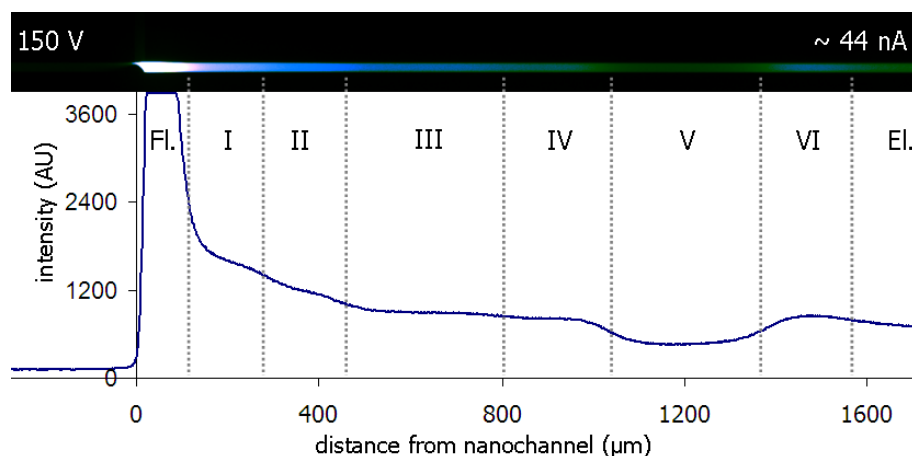


**Figure 6.** False-color CCD image showing dzITP filtration of urine after 5 minutes of actuation, using partly released fluorescein as a marker for ionic mobility cut-off and for indirect detection. The fluorescence profile of the CCD image shows six putative analyte zones, indicated by the Roman numerals I-VI. Fl. = fluorescein marker zone; El. = background electrolyte zone. The image was obtained after 6 minutes of actuation

### *Urine Sample*

Figure 6 shows a proof of principle for the application of the dzITP filter to a complex biological sample, using fluorescein as a marker compound. A continuous dzITP injection was performed. Without low-pass dzITP filtering, fluorescein and undesired low-mobility compounds would accumulate,

rapidly covering the complete read-out window. Therefore, the upstream current was tuned such that a fluorescein zone was established with an approximately stable width. Behind this fluorescein zone, compounds from the urine sample formed several other zones. The current had to be modulated slightly (45-43 nA) to keep release of fluorescein approximately constant, possibly due to changes in overall conductivity caused by broadening isotachophoretic zones. The zones are visualized by indirect detection. In isotachophoretic separations, each zone has its specific conductivity. While the continuously injected fluorescein migrates through these zones, its concentration is being adjusted to the local conductivity. The fluorescein thus is not only used as a marker, but also acts as tracer; it is a so-called “underspeeder”<sup>21</sup>. In the fluorescence profile in figure 6, six putative analyte zones are indicated. As in each isotachophoretic separation, the zones have overlap at the borders. The putative zone borders are therefore indicated at the inflection points between the zones in the fluorescence profile.

Theoretically, with this mode of indirect detection a stair-like fluorescence profile is expected, with increasing fluorescence intensities for each zone that is closer to the fluorescein zone. However, zone V in figure 6 has significantly lower fluorescence intensity. Possibly, this zone contains an analyte which quenches fluorescence.

The identity of the detected analytes is not known. However, the fluorescein marker and the carbonate electrolyte define a window of ionic mobilities, which contains only a limited number of metabolites out of the thousands of compounds in urine. These probably include only very small molecules or molecules that have, like fluorescein, at least a double negative charge. Notable metabolites that fulfill these conditions include acetate, aspartate,

glutamate and several citric acid cycle products. The carbonate electrolyte defines the upper limit of the mobility window and excludes some small ions, particularly chloride. Low-mobility compounds are co-released with the fluorescein.

It is probable that more than six urine metabolites are retained in the dzITP zones, however they might have insufficient starting concentrations and therefore are not forming individual zones, but rather are present as non-detectable peaks between the zones. For sample analysis it is therefore desirable to continue this continuous filtration step with a number of pulsed releases as described above. This way, fractions of enriched analytes can be sent to a detector located along the downstream channel for identification and quantification.

For our metabolomics research, the dzITP filter will be enabling, because it can be used to concentrate and fractionate many metabolites in the presence of at least two undesired classes of compounds in ultrasmall complex samples: proteins, which have lower mobility, and salts, which have higher mobility than most metabolites.

## **Conclusions**

We have developed a dynamic low-pass filter that separates compounds based on ionic mobility. The dzITP filter works by voltage or current-controlled release of compounds along a nanochannel-induced depletion zone. Isotachophoretic separation of compounds before the filter results in selectivity. In pulsed mode, dzITP-separated compounds are fractionated in plugs that are released sequentially along the depletion zone. In continuous mode, a certain (marker) compound is partially released, whereby the ionic

mobility of this compound defines the cut-off of the filter. Compounds with lower mobility are co-released, compounds with higher mobility are trapped in isotachophoretic zones. Importantly, this cut-off can be simply and rapidly tuned by voltage or current actuation. The dzITP filter has been demonstrated for the selective enrichment of low-abundant 6-carboxyfluorescein over highly abundant fluorescein. dzITP filtering was also applied to diluted raw urine sample, using fluorescein as a marker. Out of the thousands of compounds in urine, a small ionic mobility window was selected wherein five analyte zones were indirectly detected. The dzITP filter can thus enrich specific compounds from complex biological samples and enable real-time monitoring and detection.

## References

1. G. Garcia-Schwarz, A. Rogacs, S. S. Bahga and J. G. Santiago, *J. Visualized Exp* (61), e3890 (2012).
2. A. Persat and J. G. Santiago, *Analytical Chemistry* **83** (6), 2310-2316 (2011).
3. B. Jung, R. Bharadwaj and J. G. Santiago, *Analytical Chemistry* **78** (7), 2319-2327 (2006).
4. J. G. Shackman and D. Ross, *Electrophoresis* **28** (4), 556-571 (2007).
5. W. S. Koegler and C. F. Ivory, *Biotechnology Progress* **12** (6), 822-836 (1996).
6. S.-L. Lin, Y. Li, H. D. Tolley, P. H. Humble and M. L. Lee, *Journal of Chromatography A* **1125** (2), 254-262 (2006).
7. D. Ross and L. E. Locascio, *Analytical Chemistry* **74** (11), 2556-2564 (2002).
8. M. S. Munson, J. M. Meacham, L. E. Locascio and D. Ross, *Analytical Chemistry* **80** (1), 172-178 (2007).
9. M. M. Meighan, J. Vasquez, L. Dziubcynski, S. Hews and M. A. Hayes, *Analytical Chemistry* **83** (1), 368-373 (2010).
10. J. Han, J. Fu and R. B. Schoch, *Lab on a Chip* **8** (1), 23-33 (2008).
11. Q. Pu, J. Yun, H. Temkin and S. Liu, *Nano Letters* **4** (6), 1099-1103 (2004).
12. T. A. Zangle, A. Mani and J. G. Santiago, *Chemical Society Reviews* **39** (3), 1014-1035 (2010).

13. Y.-C. Wang, A. L. Stevens and J. Han, *Analytical Chemistry* **77** (14), 4293-4299 (2005).
14. S. J. Kim, S. H. Ko, K. H. Kang and J. Han, *Nat Nano* **5** (4), 297-301 (2010).
15. J. Astorga-Wells, S. Vollmer, T. Bergman and H. Jörnvall, *Analytical Chemistry* **79** (3), 1057-1063 (2007).
16. F. o. Mavr , R. K. Anand, D. R. Laws, K.-F. Chow, B.-Y. Chang, J. A. Crooks and R. M. Crooks, *Analytical Chemistry* **82** (21), 8766-8774 (2010).
17. J. Quist, K. G. H. Janssen, P. Vulto, T. Hankemeier and H. J. van der Linden, *Analytical Chemistry* **83** (20), 7910-7915 (2011).
18. L. F. Cheow and J. Han, *Analytical Chemistry* **83** (18), 7086-7093 (2011).
19. J. Astorga-Wells, S. Vollmer, S. Tryggvason, T. Bergman and H. J rnvall, *Analytical Chemistry* **77** (22), 7131-7136 (2005).
20. S. J. Kim, L. D. Li and J. Han, *Langmuir* **25** (13), 7759-7765 (2009).
21. R. D. Chambers and J. G. Santiago, *Analytical Chemistry* **81** (8), 3022-3028 (2009).





# 5

## PDMS Valves as Tunable Nanochannels for Concentration Polarization

*Published in Lab on a Chip 2013, 13, pp 4810-4815*

**Elastomeric microvalves in poly(dimethylsiloxane) (PDMS) devices are today's paradigm for massively parallel microfluidic operations. Here we report that such valves can act as nanochannels upon closure. When tuning nanospace heights between ~55 nm and ~7 nm, the nanofluidic phenomenon of concentration polarization could be induced. A wide range of concentration polarization regimes (anodic and cathodic analyte focusing and stacking) was achieved simply by valve pressure actuation. Electro-osmotic flow generated a counterpressure, therefore voltage actuation also could be used to actuate between concentration polarization regimes. 1000-fold preconcentration of fluorescein was achieved in just 100 s in the anodic focusing regime. After valve opening, a concentrated sample plug could be transported through the valve, though at the cost of some defocusing. Reversible nanochannels open new avenues for integrating electrokinetic operations and assays in large scale integrated microfluidics.**

During the last decade, many applications have been developed for microfluidic devices with integrated nanofluidic components<sup>1</sup>. One important property of nanofluidic components is perm-selectivity. Perm-selectivity results from the dominance of surface charge inside nanofluidic conducts, excluding co-ions and enriching counterions<sup>2, 3</sup>. This has led to the development of fluidic diodes<sup>4, 5</sup> and transistors<sup>6</sup>. An important accompanying

effect is concentration polarization: upon application of a voltage potential, ion enrichment and ion depletion zones arise at each entrance of the nanofluidic conduit respectively<sup>7, 8</sup>. In the case of a negative surface charge, for example in materials like glass, silicon and poly(dimethylsiloxane) (PDMS), a depletion zone is formed at the anodic entrance of the nanofluidic conduit. The sharp conductivity gradient at the border of the ion-depleted zone can be used for very efficient preconcentration of charged analytes ranging from proteins to nucleic acids and metabolites<sup>9, 10</sup>. Concentration factors exceeding a million have been reported<sup>9, 11</sup>. Based on this effect, we recently reported depletion zone isotachopheresis (dzITP), a simple and versatile method for focusing, separation and positioning of analytes<sup>12, 13</sup> (chapter 3 and 4). These effects have been employed in immuno- and enzyme assays<sup>10, 14</sup>. Other applications of on-chip concentration polarization include rapid mixing by electrokinetic instabilities of the depletion zone<sup>15</sup> and seawater desalination<sup>16</sup>. In a theoretical study of analyte preconcentration in micro-nano-micro structures, Plecis et al<sup>17</sup> have identified four different concentration polarization regimes. The four regimes correspond to the four interfaces where the balance between bulk flow (EOF) versus electrophoretic transport of analytes changes. In order of increasing bulk flow, cathodic stacking (CS) occurs at the cathodic entrance of a nanopore; cathodic counter gradient focusing (CCGF) occurs at the border of the enrichment zone; anodic counter gradient focusing (ACGF) occurs at the border of the depletion zone and anodic stacking (AS) occurs at the anodic entrance of the nanochannel. The model indicated that the ACGF regime is most efficient for analyte preconcentration. This must be explained by the facts that 1) the stacking regimes allow for analyte leakage through the nanochannel, while in the

focusing regimes all analytes are trapped; and II) the depletion zone interface has a much sharper electric field gradient than the enrichment zone interface. The ACGF regime and variants thereof are indeed very common in concentration polarization-based preconcentration devices.

To our knowledge, in literature no description can yet be found of a device that is able to reach all four concentration polarization regimes. We here propose to use elastomeric microvalves for tuning nanochannels to achieve various concentration polarization regimes. Such elastomeric microvalves are one of the most important and well-known inventions in the field of microfluidics, because they are easy to implement and offer the possibility to create large-scale integrated fluidic networks<sup>18</sup>. An elastomeric microvalve consists of a membrane between a fluidic channel and a control channel. When the control channel is pressurized, the membrane will deflect, displacing the fluid and closing off the fluidic channel<sup>19</sup>. Under certain conditions, upon closing the microvalve a nanometer-sized fluidic layer remains between the membrane and the wall of the fluidic channel. Because at sufficiently high pH's PDMS has a negative surface charge this effectively creates a perm-selective nanochannel. Kuo et al used this effect for a normally closed PDMS valve to trap DNA that upon opening could be released<sup>23</sup>.

In this paper we use elastomeric microvalves to create reversible and tunable nanospaces. Measurements of electrical resistance at different valve pressures indicate that in addition to full open or closure, nanospace height can be varied between ~55 nm and ~7 nm. Different concentration polarization regimes could be obtained by variation of the valve pressure and corresponding nanospace dimensions. Variation of voltages results in changes in electro-osmotic flow (EOF)-induced counterpressure, which also leads to

different concentration polarization regimes. Co-optimization of valve pressure and voltage resulted in a very efficient ACGF regime, by which a 1000-fold preconcentration of fluorescein was achieved in just 100 seconds. Preconcentrated sample could be released by opening the valve. Tunable PDMS nanochannels offer increased control over polarisation concentration phenomena that can be seamlessly integrated in large scale integrated microfluidics.

## **Experimental**

### *Chemicals.*

Lithium carbonate was obtained from Acros Organics (Geel, Belgium), disodium fluorescein was obtained from Riedel-de Haen (Seelze, Germany). Before each experimental series, solutions were prepared fresh from stock solutions.

### *Device fabrication and preparation.*

Chips were fabricated using well established multilayer soft lithography methods<sup>19, 20</sup>. Briefly, fluidic and pneumatic masters were fabricated by spin coating a 13µm film of ma-P 1275 (MicroResist Technology GmbH, Berlin, Germany) on glass substrates (Berliner Glas KGAA, Berlin, Germany) and prebaking for 2 minutes at 65°C, 115°C and 65°C consecutively. After exposure using a Karl Suss MA45 mask aligner (SÜSS MicroTec AG, Garching, Germany) and development with MAD 332 developer (MicroResist Technology GmbH, Berlin, Germany). To ensure rounded channels, wafers were reflow baked on a controlled hotplate by ramping to 114 °C in 15 minutes and baking for 20 min. Polydimethylsiloxane (Sylgard 184, Dow Corning,

Midland, MI) base and curing agents were mixed 10:1 (w:w), degassed and cast on masters and cured. PDMS membranes were prepared by spincoating the same PDMS on a glass substrate (2300 rpm, 75 s) and curing. After dicing and punching of access holes, the fluidic structures and membrane were bonded after oxygen plasma treatment (Femto Plasma System, Diener, Ebhausen, Germany) and bonded. Pneumatic structures containing the control channels were bonded to the other side of the membrane using the same process. The fluidic channels had  $160.7 \pm 3.1 \mu\text{m}$  width and  $13.4 \pm 0.9 \mu\text{m}$  height in the devices used for the resistance measurements. The control channel width (and therefore the unclosed valve membrane width) was  $133.3 \pm 2.7 \mu\text{m}$ . For the devices used in the concentration polarization experiments, the fluidic channel had  $108.5 \pm 2.7 \mu\text{m}$  width.

For channel filling, solutions were injected into the channels using a syringe. The control channel was dead-end filled with deionized water in order to prevent bubble formation caused by gas permeation through the valve membrane. The fluidic channel was flushed electrokinetically between concentration polarization experiments with identical solutions.

### *Setup and Microscopy*

For voltage actuation, an ES 0300 045 power supply (Delta Elektronika BV, Zierikzee, The Netherlands) was used, which was controlled by an NI USB 6221 data acquisition system using LabVIEW 8.2 software (National Instruments, Austin, TX). Currents were amplified using a Keithley 427 current amplifier (Keithley Instruments, Cleveland, OH) and were recorded using the NI USB 6221 device and LabVIEW. For current actuation, a Keithley 2410 sourcemeter unit was used. Microvalve pressure was regulated using a

Camozzi MC104 reducing valve (Camozzi spa, Brescia, Italy). On/off switching of the pressure was done using a solenoid valve (Isonic V1, Mead Fluid Dynamics inc, Chicago, IL) Microscopy was performed with an Olympus IX71 microscope (Olympus, Zoeterwoude, The Netherlands) to which an Hamamatsu Orca-ER digital camera was mounted, which was controlled by Hokawo version 2.1 imaging software (Hamamatsu Photonics, Nuremberg, Germany). The magnification was 40x.

The effect of valve pressure (0.5-3.0 bar) on concentration polarization was investigated using 2.0 mmol/L lithium carbonate, pH 10.5 as the electrolyte. 40  $\mu\text{mol/L}$  fluorescein was used as the analyte. A constant current of 100  $\mu\text{A}$  was applied. The same electrolyte conditions were used in the constant voltage experiments, in these experiments 20  $\mu\text{mol/L}$  fluorescein was used as the analyte; the valve pressure was 1.5 bar.

#### *Data processing.*

Charge coupled device (CCD) images were processed using the Hokawo version 2.1 software. All CCD images show a channel section with 2.1 mm length. Fluorescence intensity values were calculated in ImageJ (<http://rsb.info.nih.gov/ij/>) by averaging 20 image lines in the center of the fluidic channel and correcting for background signal.

## **Results**

### *Reversible perm-selective nanospace concept.*

Figure 1a depicts the concept of using a conventional elastomeric microvalve for concentration polarization purposes. The fluidic channel has a rounded

cross-section to allow uniform contact between the valve membrane and the channel wall upon pressurization of the control channel.

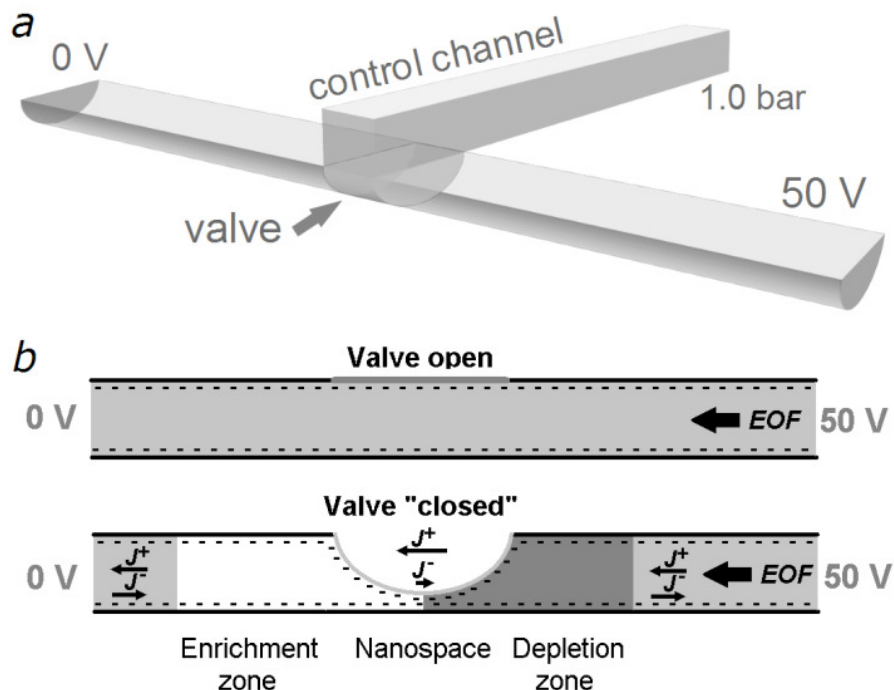


**Figure 1.** Schematic representations of the microvalve and the concentration polarization process with examples of applied voltages and pressures. a) 3d scheme of an elastomeric microvalve. The valve membrane is deflected by applying a pressure on the control channel. The fluidic channel is rounded to allow closure across the complete cross-section of the channel. b) Concentration polarization process across the nanospace which remains under the closed valve.  $J^+$  and  $J^-$  represent cation and anion fluxes respectively; due to the imbalance of these fluxes depletion and enrichment zones are formed after valve closure. Schematic representations of the microvalve and the concentration polarization process with examples of applied voltages and pressures. a) 3d scheme of an elastomeric microvalve. The valve membrane is deflected by applying a pressure on the control channel. The fluidic channel is rounded to allow closure across the complete cross-section of the channel. b) Concentration polarization process across the nanospace which remains under the closed valve.  $J^+$  and  $J^-$  represent cation and anion fluxes respectively; due to the imbalance of these fluxes depletion and enrichment zones are formed after valve closure.

Figure 1b shows how the surface charge of the PDMS (which results from deprotonation of SiOH groups) causes concentration polarization once a nanospace is formed upon partial closure of the valve. Negative surface charges on the PDMS surface are dominant in the nanospace, causing the current through the nanospace to be mostly carried by cations. Away from the nanospace, the fraction of the volume in the microchannel affected by the surface charge is too small to significantly achieve the same effect. The resulting imbalance in anion and cation transport leads to the formation of an ion-depleted zone at the anodic side of the valve, while at the cathodic side an enrichment zone is formed. At the border of these zones, analytes can be focussed or stacked.

#### *Nanospace tunability.*

The size of the nanospace can be tuned by controlling the pressure applied to the control channel. The electrical resistance of the nanospace is estimated by measuring currents immediately before and after valve closure, while applying a constant voltage of 40V (figure 2). In this experiment, concentration polarization effects were suppressed through the use of a 100 mmol/L HCl electrolyte. Resistance values for channel with closed valve were corrected with the resistance of the open channel in order to obtain the valve resistance. Resistance values vary from  $1.39 \pm 0.20 \text{ M}\Omega$  at 0.5 bar to  $46.13 \pm 5.31 \text{ M}\Omega$  at 3.0 bar. We observed that the area of the valve where the membrane was contacting the opposite wall also depended on the pressure. The width of this “closed” surface varied from  $\sim 25 \text{ }\mu\text{m}$  at 0.5 bar to  $\sim 85 \text{ }\mu\text{m}$  at 3 bar. When taking into account the width and the resistance of the closed valve versus the length and the resistance of the fluidic channel, and assuming uniform valve



closure, the nanospace height can be roughly estimated. The resistivity of the closed valve was  $\sim 250\times$  (at 0.5 bar) to  $\sim 2000\times$  (at 3 bar) higher than the resistivity of the fluidic channel. This leads to a rough estimate for nanospace heights from 55 nm at 0.5 bar down to 7 nm at 3.0 bar.

In some previous studies<sup>21, 22</sup>, much higher electrical resistances were reported. These values are expected to be strongly dependant on the device geometry including channel height, width and curvature, as well as membrane width, thickness and elasticity.

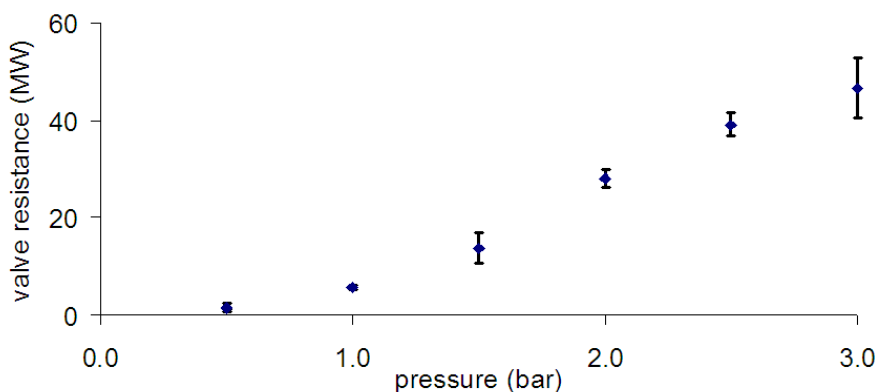


**Figure 2.** Graph of valve resistance versus valve pressure in a 100 mmol/L HCl solution. Measurements were triplicated and randomized.

### *Concentration polarization regimes through pressure-induced tunability.*

Figure 3 shows a number of concentration polarization phenomena at various pressures that correlate to the different concentration polarization regimes described by Plecis et al.<sup>17</sup>. At 0.5 bar, the fluorescein was efficiently concentrated directly at the edge of the closed valve membrane. After  $\sim 35$  seconds, however, more and more fluorescein leaked through the nanospace into the cathodic part of the channel, although concentration of fluorescein still occurred. This combination of analyte concentration and leakage through

a nanospace corresponds to the AS regime. At 1.0 and 1.5 bar, the ACGF regime was observed. In this regime the fluorescein focused most efficiently.



**Figure 3.** Concentration polarization regimes at different valve pressures in a 2.0 mmol/L lithium carbonate solution containing 40  $\mu\text{mol/L}$  fluorescein. A constant current of 100  $\mu\text{A}$  was applied. Images were taken 20 s after valve closure.

At 1.0 bar, a very small depletion zone was observed, which hardly grew. At 1.5 bar, a slowly growing depletion zone was present. At 2.0 bar, there is a transition between the ACGF and the CCGF regime. Some focusing takes place both at the cathodic and the anodic side, though very inefficient. From

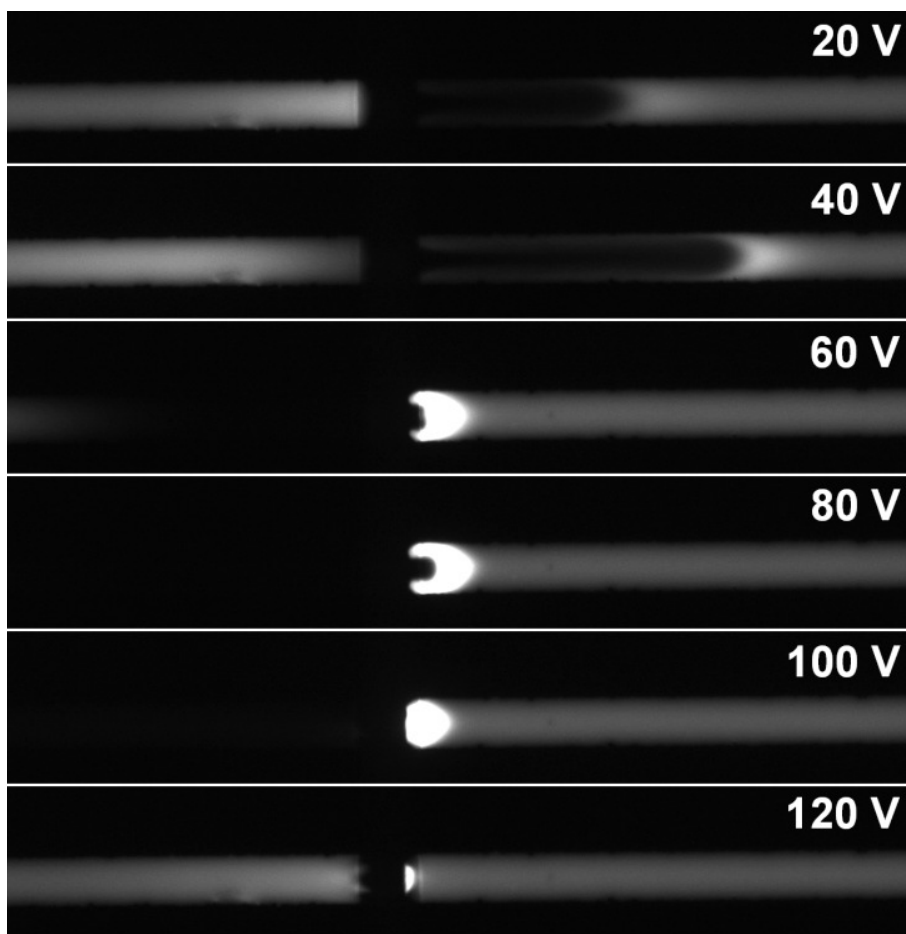
2.0 bar and higher, a rapidly growing depletion zone was observed. At the edges of the channel, clearly some fluorescein remains. It appears that the EOF, encountering the closed valve as a hydrostatic barrier, generates a hydrodynamic counterflow which strongly promotes depletion zone growth in the middle of the channel. At the edges, the rounded fluidic channel is very shallow, suppressing the hydrodynamic counterflow and allowing the non-depleted liquid to stay. Due to this effect, large depletion zones will be disadvantageous for preconcentration purposes because sample dispersion may become very significant. At 2.5 and 3 bar, we observe CCGF regimes. Plecis et al.<sup>17</sup> distinguished between stable and unstable CCGF; in unstable CCGF the focused peak shifts position away from the nanochannel. Stable CCGF occurs at lower flow rates and has more efficient focusing. The regime observed at 2.5 bar is clearly a case of unstable CCGF, while the regime at 3 bar is more similar to stable CCGF, as the concentrated sample peak moved much slower away from the valve. A CS regime is expected to occur at even higher valve pressures. Such pressures would however compromise the structural integrity of the device and could thus not be tested. Nevertheless, CS was observed when applying a low voltage, as discussed in the next section. The decrease in bulk flow due to increased hydraulic resistance is the most likely explanation of the observed differences in concentration polarization regimes.

By using different pressures for valve actuation, we have achieved at least three of the regimes described in the study of Plecis et al.<sup>17</sup>, namely the CCGF, the ACGF and the AS regime. Increasing pressures decrease the the nanospace under the nearly closed valve, which leads to: I) greater perm-selectivity, resulting in stronger concentration polarization and II) decreased bulk flow,

because the nearly closed valve acts as a hydrostatic barrier which counters EOF.

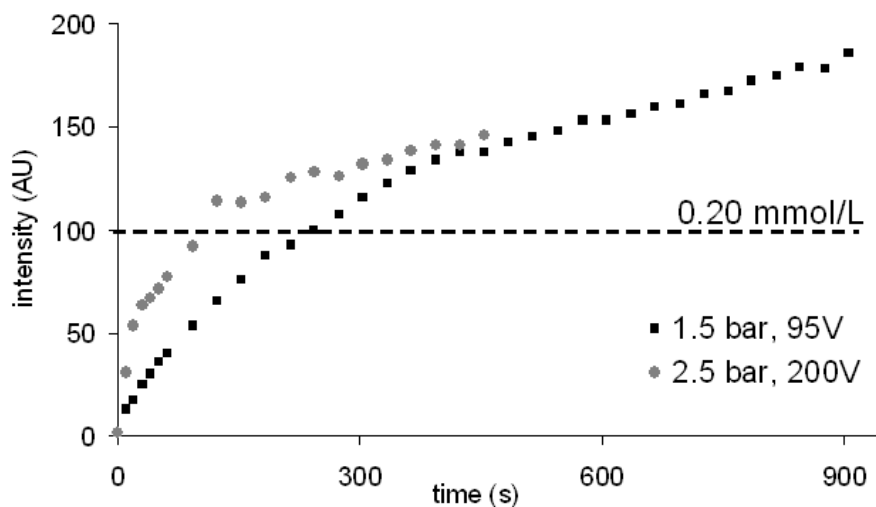
*Concentration polarization regimes at different voltages.*

Figure 4 shows a range of concentration polarization regimes under varying applied voltages. At 20V, we observe a CS regime, with highest fluorescein concentrations directly at the cathodic side of the closed valve membrane.



**Figure 4.** Concentration polarization regimes at different voltages in a 2 mmol/L lithium carbonate solution containing 20  $\mu\text{mol/L}$  fluorescein. Valve pressure was 1.5 bar. Images were taken 30 s after valve closure.

At 40V, CCGF is clearly observed. This is opposite to the findings in the simulations of Plecis et al, where increase of voltage leads to a shift of the cathodic concentration modes to the CS regime. An explanation for this is that the increased EOF induced pressure enlarges the nanospace height, which in turn allows for higher flow rate. At increased voltages, the relative contribution of the bulk flow becomes more significant. At 60 and 80 V, ACGF occurs. At 100V, small amounts of fluorescein are leaking through the nanospace, indicating the transition towards an AS regime. At 120V, AS is evident: all fluorescein is transferred through the nanospace, though some concentration is still occurring at the anodic side of the valve.



**Figure 5.** Graph of the increase of fluorescence intensity peak values during focusing of 200 nmol/L fluorescein in 2.0 mmol/L lithium carbonate. The results of two experiments are shown, using 1.5 bar valve pressure and 95 V (squares) and 2.5 bar and 200 V (circles). The dashed line represents the fluorescence intensity corresponding to 0.20 mmol fluorescein, indicating 1000-fold preconcentration.

*1000-fold preconcentration and analyte plug release.*

We determined preconcentration factors during ACGF focusing of a 200 nmol/L fluorescein solution. Figure 5 shows the development of the fluorescence intensity values in a focused peak. The dashed line corresponds to the intensity measured in a control solution of 0.20 mmol/L fluorescein, indicating the points at which 1000-fold preconcentration is achieved. In a first experiment, valve pressure was 1.5 bar and the external voltage was 95 V. In this experiment, 1000-fold concentration was achieved in about 270 seconds. In a second experiment, a higher valve pressure (2.5 bar) was applied in order to allow higher voltages. We found that at this valve pressure, 200V could be applied to achieve the ACGF regime, which would not be possible with lower valve pressures (at 1.5 bar the inefficient AS regime is dominant for voltages above 100 V, as discussed above). The higher voltage led to more efficient analyte trapping and 1000-fold preconcentration was achieved in only ~100 seconds.

As the depletion zone grows, an increasing amount fluorescein is trapped in the shallow regions alongside the depletion zone and is thus not benefiting the increase of peak intensity. Including a controlled feedback loop to stabilize the size and position of the depletion zone could significantly reduce this effect. While the total fluorescence signal showed linear increase ( $R^2=0.9965$  at 100V and  $R^2=0.9972$  at 200V), the increase in maximum fluorescence intensity slowed down over time. The discrepancy between a constant supply of analyte and a slowing increase in maximum fluorescence intensity can be explained by the observed peak broadening.

### *Valve opening.*

After preconcentration in the ACGF regime, fluorescein could be released by opening the valve (figure 6). A voltage of 200V was applied during valve opening, and valve pressure was 2.5 bar before valve opening. After valve opening, EOF transports the fluorescein zone towards the cathodic reservoir. As the focusing condition is no longer present, sample dispersion takes place, resulting in peak broadening and a decrease of peak concentration. 4 s after valve opening, the peak concentration was decreased about two-fold. Despite sample dispersion after valve opening, sample trapping in the ACGF regime is still highly advantageous as concentration factors can be several orders of magnitude higher.

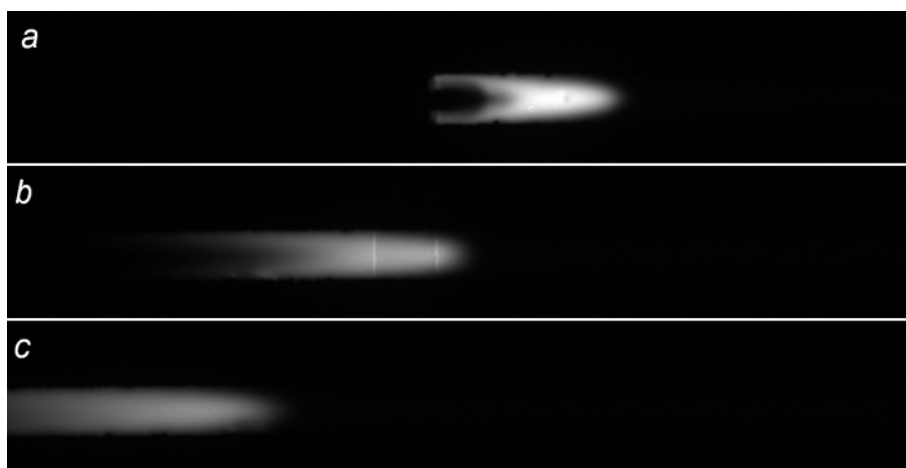


**Figure 6.** Transport and dispersion of a focused sample plug after valve opening; applied voltage was 200V. a) The concentrated sample plug just before valve opening. b) Sample plug 2 s after valve opening. c) Sample plug 4 s after valve opening.

## **Conclusions and perspectives**

PDMS microvalves have found widespread use and have been instrumental for many successful academic and commercial microfluidic applications. This

research provides evidence that such valves can be used as tunable reversible nanochannels. Measurements of electrical resistance across closed valves indicated the presence of a nanospace with heights in the order of 7 - 55 nm, dependent on the valve pressure. A wide range of concentration polarization regimes could be achieved just by tuning the microvalve pressure, while only requiring a single fluidic channel and a single electrolyte concentration. These regimes were very similar to the regimes predicted in previously published theoretical work. EOF-induced pressure appeared to have a significant effect on the size of the nanospace opening between the valve membrane and the channel walls, as concentration polarization regimes strongly depended on applied voltage. Efficient preconcentration of fluorescein was achieved and could be further improved by increasing both valve pressure and voltage, resulting in 1000-fold preconcentration in 100 s. After valve opening, the concentrated sample plug was transported past the valve, although this was accompanied by some dispersion of the sample plug.

Future studies should further optimize the design of elastomeric valves for nanochannel applications. Possibly a three-state valve can be made, which, dependent on applied pressure, is in open, nanospaced or completely closed state. In our devices, concentration polarization occurred only at relatively low electrolyte concentrations. Perm-selectivity may be improved by increasing the PDMS surface charge, for example using a coating, making the device compatible with a wider range of electrolytes and samples. An important next step is massive parallelization of the valve-based tunable nanochannels.

In biochemical assays that are performed in PDMS devices containing microvalves, our research will find several applications for efficient trapping



and preconcentration of charged components, improving reaction rates and detection limits.

## References

1. M. Napoli, J. C. T. Eijkel and S. Pennathur, *Lab on a Chip* **10** (8), 957-985 (2010).
2. A. Plecis, R. B. Schoch and P. Renaud, *Nano Letters* **5** (6), 1147-1155 (2005).
3. R. B. Schoch, J. Han and P. Renaud, *Reviews of Modern Physics* **80** (3), 839 (2008).
4. R. Karnik, C. Duan, K. Castelino, H. Daiguji and A. Majumdar, *Nano Letters* **7** (3), 547-551 (2007).
5. Z. S. Siwy, *Advanced Functional Materials* **16** (6), 735-746 (2006).
6. R. Karnik, R. Fan, M. Yue, D. Li, P. Yang and A. Majumdar, *Nano Letters* **5** (5), 943-948 (2005).
7. Q. Pu, J. Yun, H. Temkin and S. Liu, *Nano Letters* **4** (6), 1099-1103 (2004).
8. T. A. Zangle, A. Mani and J. G. Santiago, *Chemical Society Reviews* **39** (3), 1014-1035 (2010).
9. Y.-C. Wang, A. L. Stevens and J. Han, *Analytical Chemistry* **77** (14), 4293-4299 (2005).
10. S. J. Kim, Y. A. Song and J. Han, *Chemical Society Reviews* **39** (3), 912-922 (2010).
11. S. M. Kim, M. A. Burns and E. F. Hasselbrink, *Analytical Chemistry* **78** (14), 4779-4785 (2006).
12. J. Quist, K. G. H. Janssen, P. Vulto, T. Hankemeier and H. J. van der Linden, *Analytical Chemistry* **83** (20), 7910-7915 (2011).
13. J. Quist, P. Vulto, H. van der Linden and T. Hankemeier, *Analytical Chemistry* **84** (21), 9065-9071 (2012).
14. L. F. Cheow and J. Han, *Analytical Chemistry* **83** (18), 7086-7093 (2011).
15. S. Yu, T.-J. Jeon and S. M. Kim, *Chemical Engineering Journal* **197** (0), 289-294 (2012).
16. S. J. Kim, S. H. Ko, K. H. Kang and J. Han, *Nature Nanotechnology* **5** (4), 297-301 (2010).
17. A. Plecis, C. m. Nanteuil, A.-M. Haghiri-Gosnet and Y. Chen, *Analytical Chemistry* **80** (24), 9542-9550 (2008).
18. T. Thorsen, S. J. Maerkl and S. R. Quake, *Science* **298** (5593), 580-584 (2002).
19. M. A. Unger, H.-P. Chou, T. Thorsen, A. Scherer and S. R. Quake, *Science* **288** (5463), 113-116 (2000).

20. D. C. Duffy, J. C. McDonald, O. J. A. Schueller and G. M. Whitesides, *Analytical Chemistry* **70** (23), 4974-4984 (1998).
21. C.-Y. Chen, C.-H. Chen, T.-Y. Tu, C.-M. Lin and A. M. Wo, *Lab on a Chip* **11** (4), 733-737 (2011).
22. Y.-C. Wang, M. H. Choi and J. Han, *Analytical Chemistry* **76** (15), 4426-4431 (2004).

# 6

## Conclusions and Perspectives

Analysis of a wide range of biomolecules such as metabolites and peptides especially in small sample volumes is still a major challenge in analytical chemistry in general, and areas such as metabolomics especially. This thesis has presented novel concepts and methods for single-electrolyte isotachophoresis (ITP) using electric field gradient focusing (EFGF) in general and concentration polarization-based devices in particular. These concepts and methods can have a major impact on novel analytical workflows for the analysis of charged biomolecules.

In chapter 2, ITP and EFGF principles and methods have been reviewed. It has been argued that ITP and EFGF are identical types of methods because they share the isotachophoretic principle: all focused ions are moving with the same velocity. It is discussed that isotachophoretic phenomena are indeed ubiquitous in the wide range of EFGF methods that have been previously published. It is therefore proposed that the strengths of ITP and EFGF can therefore be combined to offer new opportunities in the sample preparation of small samples, and for the bioanalysis of complex samples in general.

Future challenges for ITP/EFGF methods include improvement of reproducibility and robustness, extensive characterizations, interfacing with appropriate detection technologies, such as mass spectrometry or detectors with a minimal size, downscaling and integration on microfluidic chip

platforms. This will result in ITP/EFGEF-based biochemical assays for diagnostics.

In chapter 3, depletion zone isotachopheresis (dzITP) in an H-shaped micro/nanofluidic glass devices has been described. By focusing analytes at the border of a nanochannel-induced depletion zone, isotachopheresis could be performed using a single electrolyte only. Three-point voltage actuation controlled the extent of focusing and the positioning of isotachopheretic analyte zones, a feature which may be useful for repeated scanning along a point sensor. As a single-electrolyte method, dzITP is an important simplification over conventional ITP. This could become particularly beneficial in designing simple to operate point-of-care devices.

In chapter 4, it has been shown that tunable ionic mobility filtering can be added to the functionality of dzITP. Through voltage- and/or current actuation, the release of compounds along the depletion zone has been controlled, the depletion zone being comparable to a valve that can be opened or closed at will. Both pulsed and continuous operation modes have been demonstrated. Using simultaneous dzITP filtering and focusing, a low-concentration compound was specifically enriched, while a second, high abundant compound was continuously released. Moreover, specific high-mobility compounds from diluted raw urine sample were trapped in isotachopheretic zones while low-mobility compounds were released. Fluorescein was used as a marker both for ionic mobility cut-off and for indirect detection. These experiments show the potential of dzITP for the

selective enrichment of low-abundant analytes in the presence of high concentrations of matrix compounds.

In chapter 5, a PDMS concentration polarization device was developed using an elastomeric microvalve to create a tunable reversible nanospace in a microchannel. Measurements of valve resistance indicated nanospace heights between ~7 and ~60 nm that could be obtained as dependent on valve pressure. By voltage and valve pressure regulation, a wide range of concentration polarization regimes was achieved. A more than 1000-fold preconcentrated compound was released by opening the valve. Though not demonstrated in this thesis, ITP separations might evolve when multiple compounds are focused at the border of a valve-induced depletion zone. In this way, PDMS microvalve devices might be used as single-channel dzITP devices.

From the insights and results reported in this thesis, it is clear that single-electrolyte isotachopheresis has enormous versatility. Efficient preconcentration, separation, filtering, compound selection, zone positioning, and indirect detection are all possible in a single method. It is expected that several operations may be added to this palette, including derivatization reactions, buffer replacement and desalting. These operations will not only be available for dzITP in both glass- and PDMS-based devices, but also to many of the other members of the large EFGF family.

The methods presented in this thesis are all chip-based. A key advantage is that in principle only very small sample volumes are needed. For discrete

dzITP injections as described in Chapter 2 and 3, injection volumes were 0.3 nL. Another important aspect is the potential for massive parallelization. It is expected to be possible to integrate hundreds of dzITP channels on a single chip. The very small footprint of the device is advantageous in this regard. For example, the device shown in Chapter 2 and 3 requires an area of 0.1 x 2.0 mm only (connections to fluidic reservoirs excluded). For discrete injections, a focused zone in dzITP may have a volume of less than 10 pL. We also envision on-chip integration of dzITP modules with other modules, for example reagent mixing or detection modules.

Future research should focus on dzITP assay development and on combining dzITP with electrospray ionization-mass spectrometry (ESI-MS). ESI-MS is a powerful tool for sensitive detection which provides rich information about chemical composition. Combined with ESI-MS and possibly with the great separation power of capillary zone electrophoresis, dzITP will greatly extend the coverage of comprehensive analyses of complex biological samples.

## Nederlandstalige samenvatting

Dit proefschrift gaat over de ontwikkeling van nieuwe methoden om (bio)chemische stoffen te scheiden en op te concentreren op basis van elektrische eigenschappen. Het uiteindelijke doel van deze methoden is om belangrijke stoffen met hoge gevoeligheid te kunnen detecteren in kleine hoeveelheden van complexe biologische monsters. Hierbij kan gedacht worden aan bijvoorbeeld ziektemarkers in bloed.

Hoofdstuk 1 geeft een korte inleiding en een motivatie waarom de technieken die in dit proefschrift beschreven staan van belang zijn voor het oplossen van belangrijke problemen op bioanalytisch gebied. Daartoe is onderzoek gedaan naar zowel theoretische concepten (hoofdstuk 2) als nieuwe technieken voor praktisch gebruik (hoofdstuk 3-5).

Stoffen die opgelost zijn in water hebben vaak een elektrische lading omdat zij ioniseren. Wanneer een elektrische spanning aangelegd wordt over een vloeistofkanaaltje dan zijn er allerlei trucs mogelijk waarmee deze ionen bijvoorbeeld gescheiden of geconcentreerd kunnen worden. In hoofdstuk 2 worden twee soorten van zulke methoden beschreven: isotachoforese (afgekort ITP) en "electric field gradient focusing"(afgekort EFGF). Opvallend is dat zowel ITP als EFGF in staat zijn om tegelijkertijd stoffen te scheiden en op te concentreren. Vooral dat laatste kunnen beide methoden heel efficiënt: concentratiefactoren van meer dan 10000 of zelfs een miljoen zijn herhaaldelijk in de wetenschappelijke literatuur gerapporteerd! Maar zo ingewikkeld als deze methoden klinken, zo moeilijk zijn ze ook te begrijpen. Daarom worden ze in hoofdstuk 2 uitgebreid uitgelegd. ITP is een methode

die twee verschillende zones van elektrolyten (ionenoplossingen) benut. Andere ionen worden tijdens een ITP-scheiding ingeklemd tussen deze zones en daar opgeconcentreerd. Als er genoeg aanwezig is, dan vormt zo'n stof een eigen zone. Is een ITP-scheiding eenmaal voltooid, dan ontstaat een trein van verschillende stoffen die achter elkaar met dezelfde snelheid zullen bewegen. De andere klasse van methoden, EFGF, bevat veel verschillende methoden. Wat ze met elkaar gemeen hebben is dat ze geladen stoffen onder invloed van een elektrisch veld tegen een vloeistofstroom in laten bewegen. Op het moment dat de stoffen een gradiënt in het elektrisch veld tegenkomen, zullen ze langzamer of juist sneller bewegen, totdat een punt bereikt wordt waarop de stoffen net zo hard gaan als de tegengestelde vloeistofstroom en staan ze op het oog stil. Op dat punt, dat voor iedere stof op een andere plaats kan liggen, worden deze stoffen gefocust en dus opgeconcentreerd. Er is nu een interessante theoretische ontdekking mogelijk: als een EFGF-scheiding voltooid is, dan staan al die geladen stoffen stil in de vloeistofstroom. Met andere woorden, ze bewegen allemaal met dezelfde snelheid, net als in ITP. Het moet dus mogelijk zijn om ook alle belangrijke kenmerken van ITP terug te vinden in EFGF-methoden. Wanneer de wetenschappelijke literatuur nagegaan wordt om te kijken wat er is waargenomen bij EFGF-methoden, dan worden inderdaad alle belangrijke ITP-verschijnselen teruggevonden. Het belangwekkende van deze ontdekking is dat heel veel trucs die ontwikkeld zijn voor ITP toegepast kunnen worden op EFGF, en andersom. Daardoor is het mogelijk om nieuwe bioanalytische methoden te ontwikkelen die ontzettend veelzijdig zijn.



Hoofdstuk 3 beschrijft de ontdekking van een nieuwe methode die de kenmerken van EFGF en ITP in zich verenigt. Depletiezone-isotachoforese (dzITP), zoals we deze nieuw door ons ontdekte methode genoemd hebben, wordt uitgevoerd in glazen chips met daarin een aantal vloeistofkanaaltjes die gevuld zijn met een elektrolyt. Er zijn twee parallel lopende microkanalen die verbonden zijn door een nanokanaal. Glasoppervlakken zijn geladen als ze in contact staan met een waterige oplossing. In een glas met water merk je daar niets van, maar in een nanokanaal zitten de glasoppervlakken zo dicht bij elkaar dat ze zorgen voor bijzondere eigenschappen: een nanokanaal in glas laat positief geladen ionen veel makkelijker door dan negatief geladen ionen. Wordt een elektrische stroom door het nanokanaal gestuurd, dan heeft dat tot gevolg dat aan de ene ingang van het nanokanaal ionen zich ophopen, terwijl ze aan de andere kant aan de vloeistof onttrokken worden. Zo een gebied waaraan ionen onttrokken zijn wordt een depletiezone genoemd. Aan de rand van de depletiezone is een sterke gradiënt in het elektrisch veld. Daar kan dus EFGF plaatsvinden: geladen stoffen kunnen sterk worden geconcentreerd aan de rand van de depletiezone. Als verschillende stoffen in hoge concentraties toevoegt worden, gebeurt er iets wat (zonder de kennis van hoofdstuk 2) onverwacht is: elk van de stoffen vormt een plateauvormige zone precies zoals in ITP. In tegenstelling tot gewone ITP zijn bij dzITP niet twee elektrolyten nodig, maar slechts één. Het andere elektrolyt wordt vervangen door de depletiezone. Dit kan ITP aanzienlijk eenvoudiger maken voor gebruik in diverse bioanalytische experimenten. Er zijn ook andere voordelen: in dzITP focussen stoffen zich op een stabiele positie, en bovendien kan die positie gevarieerd worden door simpelweg de gebruikte voltages te veranderen.

Hoofdstuk 4 laat zien dat de depletiezone in dzITP gebruikt kan worden als een soort filter. Dit kan gedaan worden door de toegepaste voltages of stroomsterkte te variëren, net als bij het positioneren van de dzITP-zones. Het filter kan helemaal afgesloten worden, dan hopen alle moleculen zich op achter het filter. Het kan ook gedeeltelijk afgesloten worden, dan kan een deel van de stoffen er langs, maar er ontstaat nog wel een ophoping van stoffen. Dit effect kan in dzITP gecombineerd worden met het feit dat verschillende stoffen zich scheiden in verschillende zones als ze opgehoopt worden. Dat leidt tot interessante mogelijkheden. Door afwisselend het scheidingskanaal geheel dan wel gedeeltelijk af te sluiten met een depletiezone kunnen de gescheiden zones om de beurt langs de depletiezone gestuurd worden. Wanneer stoffen continu aangevoerd worden, is het ook mogelijk om de filterafsluiting zodanig in te stellen dat de stoffen die zich vooraan zouden ophopen continu langs de depletiezone stromen, maar omdat niet alles erlangs kan hopen de "achterste" stoffen zich nog wel op. De filterwerking is dan als volgt: stoffen die langzaam tegen de stroom in migreren worden met de vloeistofstroom langs de gedeeltelijke afsluiting gesleurd, terwijl stoffen die snel tegen de stroom in migreren zich ophopen. Dit kan bijvoorbeeld gebruikt worden om een snel migrerende stof die een veel lagere concentratie heeft dan een andere, langzaam migrerende stof zolang op te hopen tot die juist een hogere concentratie had. Ook kan men een markerstof gebruiken die gedeeltelijk langs de depletiezone migreert. Stoffen die langzamer migreren dan de marker stromen langs de depletiezone, terwijl sneller migrerende stoffen selectief opgehoopt worden en gescheiden worden in aparte zones. Dit experiment werd uitgevoerd met een verdund urinemonster, waaruit een aantal stoffen selectief opgeconcentreerd konden worden.

In hoofdstuk 5 worden experimenten beschreven in chips die gemaakt zijn van PDMS. Dit is een rubberachtig, doorzichtig en flexibel materiaal. In deze chips kunnen kleppen gemaakt worden door twee kanalen elkaar te laten kruisen, gescheiden door een dun membraan. Door druk te zetten op één van de kanalen wordt het membraan in het andere kanaal gedrukt, zodat dit kanaal afgesloten wordt. Het is echter mogelijk, onder de juiste omstandigheden, dat het kanaal niet helemaal afgesloten wordt en er nog een vloeistoffilm aanwezig blijft onder het membraan. In dit geval wordt een nanokanaal gecreërd, en als er dan een elektrische stroom doorheen geforceerd wordt zou men daar de effecten van moeten zien, zoals de vorming van een depletiezone. Deze hypothese kon met diverse experimenten inderdaad bevestigd worden. De mate waarin een depletiezone zich vormt kan gevarieerd worden door de druk op de klep te veranderen. Stoffen kunnen geconcentreerd worden aan de rand van de depletiezone volgens de principes van EFGF. Een hoge druk op de klep gecombineerd met hoge voltages geeft de hoogste concentratiefactoren. Na het concentreren van een stof kan de klep weer geopend worden, zodat de stof verder gestuurd kan worden door de kanaalstructuur voor nadere analyse. Overigens worden PDMS chips met dergelijke kleppen gebruikt voor zogenaamde "labs op een chip" om bijvoorbeeld de DNA-volgorde in een enkele cel te bepalen. Het is interessant dat dezelfde kleppen nu dus ook gebruikt kunnen worden voor EFGF-functionaliteit.

Tenslotte worden er in hoofdstuk 6 nog enkele conclusies getrokken en worden er enkele lijnen uitgezet voor toekomstig onderzoek. dzITP is een veelbelovende, veelzijdige methode. Het zou interessant zijn om honderden

dzITP-scheidingen op een enkele chip te integreren voor massief-parallele analyses. Met dzITP kan ook de gevoeligheid en betrouwbaarheid van metingen met massaspectrometrie (een techniek om veel verschillende chemische stoffen te detecteren en te identificeren) zeer waarschijnlijk sterk verbeterd worden. Ook zou het heel goed toegepast kunnen worden in bioassays, voor snelle metingen van specifieke (biologische) stoffen. Met name in het laatste geval biedt dat perspectieven voor nieuwe mogelijkheden om ziektemarkers te meten in ziekenhuizen en huisartsenpraktijken.

## **Dankwoord**

Wetenschap is in de dagelijkse praktijk vaak een onwetenschappelijke bezigheid. Voor de menselijke geest is het spannend en inspannend om zich voortdurend op onbekend terrein te begeven. Dat levert je als promovendus een innerlijke strijd op. Je kunt er als een berg tegenop zien om een nieuw experiment te beginnen. Je kunt helemaal ontmoedigd zijn als resultaat na resultaat tegenvalt. Maar als er dan uiteindelijk toch positieve resultaten komen, als je echt iets nieuws ontdekt, als je de eerste op de wereld bent die bepaalde verschijnselen waarneemt of die een nieuwe techniek beheerst, dan geeft wetenschap vervulling. Dan geeft het bovendien veel vreugde om je ontdekkingen te delen met de mensen die zelf ook inspanningen geleverd hebben om je onderzoek te doen slagen. Nu mijn onderzoek tot een voltooid proefschrift heeft geleid, wil ik graag nogmaals degenen bedanken die hebben bijgedragen aan mijn promotietraject.

Thomas Hankemeier, je hebt al tijdens mijn bachelor- en masterstage veel vertrouwen in mij en in mijn onderzoek gesteld. Dat is door de jaren heen zo gebleven, en daar ben ik heel dankbaar voor. Ik ben ook erg blij dat je nadrukkelijk vervolg geeft aan mijn onderzoek nu ik weg ben uit Leiden. Hopelijk heeft je gans nog veel profijt van mijn teil!

Heiko van der Linden, je hebt me veel ondersteuning en adviezen in met name de eerste drie jaar gegeven. De inzichten en adviezen die je me gaf op de momenten dat ik mezelf moest overwinnen ervaar ik nog steeds als waardevol.

Paul Vulto, je bent een inspirator. Dankzij jouw enthousiasme konden we veel bereiken in het laatste deel van mijn promotietraject. Zonder jouw input had mijn publicatielijst er een stuk minder interessant uitgezien.

De andere collega's van Analytical Biosciences verdienen eveneens mijn dank. Van hen is Kjeld Janssen degene die het nauwst betrokken was bij mijn onderzoek. Kjeld, je enthousiasme voor isotachoforese heb je op mij overgedragen en mede dankzij jouw ideeën hebben we een nieuwe vorm van isotachoforese ontdekt met veel voordelen.

Naast bovengenoemde collega's heeft Bas Trietsch als medeauteur bijgedragen aan een deel van dit proefschrift. Bas, bedankt voor je mooie idee om met een PDMS-klep een nanokanaal te vormen, en voor het opzetten van de fabricage van de chips waarmee dit effect daadwerkelijk aangetoond kon worden.

Loes Beijersbergen en Bea Reeuwijk verdienen veel erkenning voor allerlei praktische ondersteuning. Het voert te ver om alle andere collega's bij name te noemen, maar in het algemeen wil ik iedereen bedanken voor de collegialiteit, de interessante discussies en allerlei hulp waar ik gebruik van kon maken.

Diverse studenten waren zodanig geïnteresseerd in dit onderzoek dat ze er tijdens hun bachelor- of masterstage aan wilden werken. Niels Wattel, Jan Steinz, Guus van Engelen, Zeynep Kosem, Cynric Viceisza en Zahid Maqbool, bedankt voor jullie inzet!

Technische ondersteuning kwam er van de Fijnmechanische Dienst, en met name van Raphael Zwier. Het checken van de lithografie met scanning elektronenmicroscopie en het plasma-etsen van glazen chips was mogelijk dankzij de ondersteuning van Marcel Hesselberth en Daan Boltjes. Stefan Schlautmann van de universiteit van Twente heeft ook tijd willen reserveren voor hulp met de microfabricage. Jiajiie Li was in de begintijd van mijn promotie een fijne collega, hij heeft voor dit onderzoek chips geproduceerd aan de universiteit van Twente. Allen erg bedankt!

Uiteraard is er behalve deze met name genoemde mensen een veel bredere kring van collega's, ondersteunend personeel, reviewers, samenwerkingen et cetera waaraan ik ook mijn dank verschuldigd ben. Bovendien zijn er de familieleden en vrienden die door de jaren heen hun belangstelling en steun getoond hebben. Bedankt!

Tenslotte: de spanning en de vreugde die je als onderzoeker ervaart vormen in mijn ogen een afbeelding van de strijd en de blijdschap van het christelijke geloof. In dat licht wil ik graag ook God danken voor Zijn genadegaven.





## Curriculum Vitae

Jos Quist was born 1984, July 6th, in Bergen op Zoom, The Netherlands and grew up in the nearby town of Tholen. After receiving an atheneum diploma at the Calvijn College in Goes in 2002, he started to study Biopharmaceutical Sciences at Leiden University. A Bachelor degree was awarded in 2005, and after completing his study in 2008, he received the degree Master of Science. During his studies, Jos did his main internship at the Analytical Biosciences group of prof. Thomas Hankemeier. He worked on sub-cellular sampling from *Xenopus* oocytes. In 2008, he started a PhD project on Single-Cell Metabolomics in the same group, as a part of the Netherlands Metabolomics Centre. His work resulted in the discovery of depletion zone isotachopheresis (dzITP), which raised much interest at several major conferences and resulted in two publications in leading journal Analytical Chemistry, the first of them being featured on the journal cover. A second discovery was the presence of nanofluidic effects at closed microvalves in PDMS chips, which was published in the journal Lab on a Chip. From 2012 to 2013, he worked 9 months as a postdoctoral researcher at the Netherlands Metabolomics Centre in Leiden, collaborating with Agilent Technologies with the aim of integrating dzITP on their Bioanalyzer platform. Currently, Jos is working with prof. Serge Lemay as a postdoctoral researcher in the Nanoionics group, MESA+ institute, Twente University, in collaboration with the SmartTip company. He is developing the FluidFM platform (a force microscope with integrated microfluidics) for single cell analysis.

## Publication List

J. Quist\*, K. G. H. Janssen\*, P. Vulto, H. J. van der Linden and T. Hankemeier. *Single-Electrolyte Isotachophoresis Using a Nanochannel-Induced Depletion Zone*. Analytical Chemistry, 2011, 83 (20), p 7910. Cover article.

J. Quist, K. G. H. Janssen, P. Vulto and T. Hankemeier. *Tunable Ionic Mobility Filter for Depletion Zone Isotachophoresis* Analytical Chemistry, 2012 84 (21), p 9065

J. Quist\*, S. J. Trietsch\*, K. G. H. Janssen, P. Vulto and T. Hankemeier. *Elastomeric Microvalves as Tunable Nanochannels for Concentration Polarization*. Lab on a Chip, 2013, 13, p 4810

J. Quist, P. Vulto, and T. Hankemeier. *Isotachophoretic Phenomena in Electric Field Gradient Focusing: Perspectives for Sample Preparation and Bioassays*. Analytical Chemistry, submitted.

\*Shared first authorship